

**COMPARATIVE STUDY ON GROUND VIBRATIONS PREDICTION BY
STATISTICAL AND NEURAL NETWORKS APPROACHES AT
TUNÇBILEK COAL MINE, PANEL BYH**

**A THESIS SUBMITTED TO
THE GRADUATE SCHOOL OF APPLIED AND NATURAL SCIENCES
OF
MIDDLE EAST TECHNICAL UNIVERSITY**

BY

SALAH AKEIL

**IN PARTIAL FULFILLMENT OF THE REQUIREMENTS FOR
THE DEGREE OF MASTER OF SCIENCE**

IN

MINING ENGINEERING

JUNE 2004

Approval of the Graduate School of Natural and Applied Sciences

Prof. Dr. Canan ÖZGEN
Director

I certify that this thesis satisfies all the requirements as a thesis for the degree of Master of Science.

Ü. Atalay

Prof. Dr. Ümit ATALAY
Head of the Department

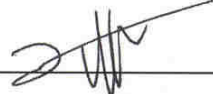
This is to certify that we have read this thesis and that in our opinion it is fully adequate, in scope and quality, as a thesis for the degree of Master of Science.

Aydın Bilgin

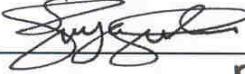
Assoc. Prof. Dr. H. Aydın BİLGİN
Supervisor

Examining Committee Members

Prof. Dr. Naci BÖLÜKBAŞI (METU, Mining)



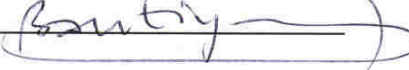
Prof. Dr. Tevfik GÜYAGÜLER (METU, Mining)



Prof. Dr. Celal KARPUZ (METU, Mining)



Prof. Dr. Bahtiyar ÜNVER (Hacettepe Univ., Mining)



Assoc. Prof. Dr. H. Aydın BİLGİN (METU, Mining)



I hereby declare that all information in this document has been obtained and presented in accordance with academic rules and ethical conduct. I also declare that, as required by these rules and conduct, I have fully cited and referenced all material and results that are not original to this work.

Name, Last name: Salah Akeil

Signature

A handwritten signature in black ink, appearing to be 'Salah Akeil', written in a cursive style.

ABSTRACT

COMPARATIVE STUDY ON GROUND VIBRATIONS PREDICTION BY STATISTICAL AND NEURAL NETWORKS APPROACHES AT TUNÇBILEK COAL MINE, PANEL BYH

Akeil, Salah

M.Sc., Department of Mining Engineering

Supervisor: Assoc. Prof. Dr. H. Aydin Bilgin

June 2004, 113 pages

In this thesis, ground vibrations induced by bench blasting from the Tunçbilek Coal Mine, Panel BYH, were measured to find out the site-specific attenuation and to assess the structural damage risk. A statistical approach is applied to the collected data, and from the data analysis an attenuation relationship is established to be used in predicting the peak particle velocity as well as to calculate the maximum allowable charge per delay. The values of frequencies are also analyzed to investigate the damage potential to the structures of Tunçbilek Township. A new approach to predict the peak particle velocity is also proposed in this research study. A neural network technique from the branch of the artificial intelligence is put forward as an alternative approach to the statistical technique.

Findings of this study indicate, according to USBM (1980) criteria, that there is no damage risk to the structures in Tunçbilek Township induced by bench blasting performed at Tunçbilek coal mine, Panel BYH. Therefore, it is

concluded that the damage claims put forward by the inhabitants of Tunçbilek township had no scientific bases. It is also concluded that the empirical statistical technique is not the only acceptable approach that can be taken into account in predicting the peak particle velocity. An alternative and interesting neural network approach can also give a satisfactory accuracy in predicting peak particle velocity when compared to a set of additional recorded data of PPV.

Keywords: Ground vibration, frequency, statistical approach, peak particle velocity, neural networks.

ÖZ

TUNÇBİLEK KÖMÜR MADENİ BYH PANOSUNDA YER SARSINTILARININ İSTATİSTİK VE YAPAY SİNİR AĞLARI YAKLAŞIMLARIYLA KARŞILAŞTIRMALI KESTİRİMİ

Akeil, Salah

Yüksek Lisans, Maden Mühendisliği Bölümü

Tez Yöneticisi : Doç. Dr. H. Aydın Bilgin

Haziran 2004, 113 sayfa

Bu çalışmada, Tunçbilek Kömür Madeni BYH panosunda yapılan basamak patlatmalarının yol açtığı yer sarsıntıları, sahaya özgü sönümlenmeyi bulmak ve yapılarda hasar olasılığını değerlendirmek amaçlarıyla ölçülmüştür. Derlenen verilere istatistik yaklaşım uygulanmış, her gecikmede ateşlenebilecek izin verilebilir en yüksek patlayıcı miktarlarını hesaplamak için olduğu kadar, en yüksek parçacık hızını kestirebilmek için istatistiksel veri analizinden bir sönümlenme ilişkisi belirlenmiştir. Tunçbilek beldesindeki yapılara hasar olasılığını araştırmak için ayrıca frekanslar da incelenmiştir. Bu çalışmada ayrıca en yüksek parçacık hızını kestirebilmek için yeni bir yaklaşım da önerilmiştir. İstatistik yöntemine seçenek bir yaklaşım olarak, yapay zeka bilim kolunun sinir ağı yöntemi ortaya konulmuştur.

Bu çalışmanın sonuçları, USBM (1980) (ABD Maden Bürosu) ölçütüne, Tunçbilek kömür madeni BYH panosunda yapılan basamak patlatmalarının

Tunbilek Beldesi'ndeki yapılar zerinde hi bir hasar olasılıđı yaratmadıđını gstermiřtir. Bu nedenle Tunbilek Beldesi'nde oturanların ileri srdkleri hasar iddialarının yanlıř olduđu sonucuna varılmıřtır. Ayrıca istatistik inceleme ynteminin, en yksek paracık hızı kestiriminde dikkate alınacak uygun tek yntem olmadıđı kanısına varılmıřtır. İlgin ve seenek bir yntem olan yapay sinir ađları yaklařımı, ek olarak llp kaydedilen deđerlerle karřılařtırıldıđında en yksek paracık hızının kestiriminde tatmin edici dođruluk sađlamaktadır.

Anahtar kelimeler: Yer sarsıntısı, frekans, istatistik yaklařım, en yksek paracık hızı, yapay sinir ađları yntemi

To My Family

ACKNOWLEDGEMENTS

I would like to express my deepest appreciation to my advisor Assoc. Prof. Dr. H. Aydin BILGIN for his kind supervision. Without his understanding, support, and guidance this thesis would not have been completed.

I offer my thanks to the examining committee members for serving on my master thesis committee.

Also, I thank the other department staff for their suggestions and guidance throughout both the lecture and thesis period.

Muharrem KILIÇ is gratefully acknowledged for his help during the field work and preparation of the thesis.

I also offer my sincere thanks to personnel of TKI, GLI, and Ozdoğan Construction Company for their help.

To my family and friends, I would like to express my great pleasure for their support.

TABLE OF CONTENT

ABSTRACT	iv
ÖZ	vi
DEDICATION.....	viii
ACKNOWLEDGEMENTS	ix
TABLE OF CONTENT.....	x
LIST OF TABLES	xiv
LIST OF FIGURES	xvi
LIST OF SYMBOLS	xviii

CHAPTER

1. INTRODUCTION	1
2. LITERATURE REVIEW	4
2.1 Principle of Fragmentation by Explosives	4
2.2 General Ground Vibration Characteristics	6
2.2.1 Principal of Ground Vibrations	6
2.2.2 Types of Vibration Waves	7
2.2.2.1 Body Waves	7
2.2.2.2 Surface Waves	9
2.3 Peak Component and True Vector Sum	11
2.4 Frequency Properties and Durations	12
2.5 Methods of Measuring Frequencies	13
2.6 Impact of Natural and Technological Factors on Seismic Effects of a Blast	14
2.6.1 Blasting conditions	14
2.6.2 Construction of explosive charge	15
2.6.3 Conditions of placing charges	15
2.6.4 Properties of rocks	16

2.7	Structure Response to Blast Excitation	17
2.7.1	Structure Components and Ground Vibration Parameters.....	18
2.7.2	Resonation and Amplification Factor.....	19
2.7.3	Distinction of blast-induced cracking from natural cracking	20
2.8	Blast-induced Air Overpressures	21
2.9	Human Response to Blast-induced Ground and Airborne Disturbances.....	21
2.10	Concept of Scaled Distance	22
2.11	Previous Investigations for Damage Criteria	24
2.11.1	Vibration Energy as Damage Criteria	24
2.11.2	Peak Particle Velocity as Damage Criteria	24
2.11.3	Peak Particle Velocity and Frequency as Damage Criteria	25
2.11.4	Peak Particle Velocity and Scaled Distance as Damage Criterion	29
2.12	Fundamentals of Neural Networks.....	31
2.12.1	Biological Basis of Neural Networks.....	31
2.12.2	Artificial Neurons.....	33
2.12.3	Artificial Neural Network.....	35
2.13	Backpropagation Neural Network.....	36
2.14	Error Back-propagation Algorithm.....	37
2.15	Neural Network Design and Architecture.....	43
2.15.1	Training Parameters.....	43
2.15.2	Data Scaling and Representation and Weight Initialization.....	43
3.	RESEARCH OBJECTIVES, SITE DESCRIPTION AND FIELD WORK.....	45
3.1	Research Objectives	45
3.2	Test Site Description	46

3.3	Regional Geological Settings	47
3.4	Rock Characterizations and Geological Observations at BYH Panel	49
3.5	Blasting Parameters.....	52
3.6	The Field Work	54
4.	STATISTICAL ANALYSES AND DISCUSSIONS.....	60
4.1	Measurement Results	60
4.2	The Adopted Site-specific Criterion	61
4.3	Statistical Analysis of Results.....	62
4.3.1	Round Blasts Events	62
4.3.2	Single Hole Events	68
4.4	Predictions of PPV at 50% and 95% Levels for Round Blasts	73
4.5	Maximum Allowable Charge for the Blasting Site	75
4.6	Frequencies Analysis	78
4.7	Frequency Distributions	80
4.8	The Optimum Delay Interval	82
5.	APPLICATION OF A NEURAL NETWORKS APPROACH IN PREDICTION OF PEAK PARTICLE VELOCITY	84
5.1	Introduction	84
5.2	Neural Network Methodology	84
5.3	The Neural Network Models for predicting the Peak Particle Velocity	85
5.4	Database for the Neural Network Model	86
5.5	Training Backpropagation Neural Network Model	86
5.6	Results and Discussions of Neural Network Models.....	88
5.6.1	One-Single Input Neural Network Model	88
5.6.2	Two Inputs Neural Network Model	90
5.7	Neural Network Approach versus Statistical Approach.....	96

6.	CONCLUSIONS AND RECOMMENDATION	99
6.1	Conclusions	99
6.2	Recommendation.	101
	REFERENCES	102
	APPENDIX A	108

LIST OF TABLES

TABLE

2.1	Langefors and Kihlstrom's Criterion	26
2.2	Guideline value of vibration velocity, DIN 4150, 1993	28
3.1	Physical and mechanical properties of Marl of Tunçbilek BYH Panel, from core samples	50
3.2	Rock mass properties of Tunçbilek BYH Panel	50
3.3	In-situ measurements of P-wave velocity, Tunçbilek BYH Panel	51
3.4	Blast design parameters applied at the mine	53
4.1	Coefficients of attenuation equation for all vibration components, round blasts.....	67
4.2	Coefficients of attenuation equation for all vibration components, single hole blasts.....	68
4.3	Prediction of peak particle velocity at 50% and 95% levels	73
4.4	Predicted and recorded values of peak particle velocity (PPV) at 50% average line and 95% upper bound line	74
4.5	Maximum allowable charge weight based on a given peak particle velocity at a given absolute distance for 50% average line	75
4.6	Maximum allowable charge based on a given peak particle velocity at a given absolute distance for 95% limit line	76
4.7	Comparisons of two methods used to determine frequencies: Zero- crossing and FFT methods	80
5.1	Neural network design and training parameters for all sessions one input model	88
5.2	Comparison between recorded peak particle velocities and predicted ones using one-single input neural network model	90

5.3	Neural network design and training parameters for all sessions, two input model	93
5.4	Comparison between recorded peak particle velocities and predicted ones using two inputs neural network model.....	95
5.5	Comparison between the predicted PPV's using statistical and neural network models and a set of recorded PPV.....	97
A.1	Vibration Data Pairs for round blasts measured at the mine site	109
A.2	Vibration Data Pairs for singlehole blasts measured at the mine site.....	113

LIST OF FIGURES

FIGURE

2.1	Sequence of events occurring in the rock mass after detonation	5
2.2	Typical coal mine blast vibration time histories.....	7
2.3	Characteristic of P-Wave in a solid medium	8
2.4	Characteristic of S-Wave in a solid medium	8
2.5	Characteristic of Rayleigh wave in a solid medium	9
2.6	Characteristic of Love waves in a solid medium	10
2.7	Vibration Components	10
2.8	Safe levels of blasting vibration for structures, USBM's Criterion,1980	27
2.9	Curves Representing the Vibration Velocity as A Function of the Frequency for DIN 4150, 1993	28
2.10	U.S. OSM's 1983 Recommendations	29
2.11	Schematic drawing of a typical neuron	32
2.12	Schematic representation of an artificial neuron	33
2.13	Activation function for neurons	34
2.14	Scheme of an artificial neural network	35
2.15	Graph of jagged error surface of error vs. weights	42
3.1	Map of Turkey shows Tunçbilek township of Tavşanlı county of Kütahya Province.....	46
3.2	General view of the mine's working area, BYH Panel	47
3.3	Integrated columnar section of rock units existing in The Tunçbilek coal mine BYH Panel	52
3.4	Blasting geometry applied at Tunçbilek Coal Mine, Panel BYH	54
3.5	Map of blast site, monitoring stations, and the Tunçbilek township.....	55
3.6	Instruments used in ground vibration measurements	56
3.7	Waveforms of a round-blast event	58

3.8	Measurement of the blasting parameters applied at the mine.....	59
4.1	Radial particle velocity versus scaled distance, round-blast (at 50% and upper 95% prediction limits).....	63
4.2	Vertical particle velocity versus scaled distance, round-blast (at 50% and upper 95% prediction limit)	64
4.3	Transverse particle velocity versus scaled distance, round-blast (at 50% and upper 95% prediction limit)	65
4.4	Peak particle velocity versus scaled distance, round-blast (at 50% and upper 95% prediction limit)	66
4.5	Peak particle velocity versus distance	67
4.6	Radial particle velocity versus scaled distance, single-hole blast (at 50% and upper 95% prediction limits)	69
4.7	Vertical particle velocity versus scaled distance, single-hole blast (at 50% and upper 95% prediction limits).....	70
4.8	Transverse particle velocity versus scaled distance, single-hole blast (at 50% and upper 95% prediction limits).....	71
4.9	Peak particle velocity versus scaled distance, single-hole blast (at 50% and upper 95% prediction limits)	72
4.10	Peak Particle Velocities versus Frequency (Zero-Crossing)	78
4.11	Peak Particle Velocities versus Dominant (FFT) Frequency (Hz) ...	79
4.12	Frequency distribution for radial component	80
4.13	Frequency distribution for vertical component	81
4.14	Frequency distribution for transverse component	81
5.1	Mean-square-error versus epochs for all training sessions	89
5.2	Neural network architecture for the best training model with single input	91
5.3	Mean-square-error versus epochs for all training sessions	93
5.4	Neural network architecture for the best training session with two inputs	94

LIST OF SYMBOLS

A:	Amplitude of ground vibration
F:	Frequency
T:	Time
FFT:	Fast Fourier Transform
PPV:	Peak Particle Velocity
PVS:	Peak Vector Sum
RPV:	Peak Radial Particle Velocity
VPV:	Peak Vertical Particle Velocity
TPV:	Peak Transverse Particle Velocity
F_R:	Radial component of frequency
F_V:	Vertical component of frequency
F_T:	Transverse component of frequency
W_d:	Total amount of explosive charge weight per time delay
D:	Absolute distance between blasting site and monitoring station
SD:	Scaled Distance
VOD:	Velocity Of Detonation
F_d:	Fundamental natural frequency
USBM:	United States Bureau of Mines
OSM:	Office of Surface Mining
K:	Ground transmission coefficient (intercept)
β:	Specific geological constant (slope)
Z.C.	Zero-crossing Frequency
NN:	Neural Network
MSE	Mean-square-error

CHAPTER 1

INTRODUCTION

The primary objective of blasting in mining is to break and move the rock. Whilst most blasts arguably achieve this objective reasonably efficiently, some of the energy applied to the rock by the detonating blast is inevitably converted into non-productive “waste” energy in the form of ground vibration and air blast. This energy leaves the vicinity of the blast and can travel a significant distance (as much as thousands of meters) before finally dissipating to negligible levels. In the meantime it can cause significant damage to rock structures and buildings, and disturbance to human occupants.

Ground vibrations are an integral part of the process of rock blasting and consequently they are unavoidable. With the general trend toward large blasts in mining and constructions projects, vibration problems and complaints have also increased. Consequently, lawsuit cases have developed between the mining industry and the general public at an accelerating rate. Complaints ranges from human disturbance to outright demolition of a residential structure, and although some of these claims are exaggerated, other legitimate. In spite of the many varying damage criteria established in the past, it is difficult to completely isolate vibration damage from damage caused by natural setting of the building, inadequate construction, old ages, etc. Even if a valid “fool proof” damage criterion were established, the critical problem remains to eliminate or considerably reduce all complaints resulting from ground vibrations and air blast, regardless of what the prevailing legal vibration limits are within a community. Therefore,

the effect of ground vibrations produced by blasting on building structures and human beings need to be predicted, monitored, and controlled by the blasting engineer as part of optimizing the job.

Many studies have been conducted to characterize the ground vibrations induced by blasting. The well-known ground vibration characteristics are the particle velocity magnitudes and frequencies. Dowding, 1985; Konya and Walter, 1991; and before that Siskind et al, 1980, demonstrated that magnitude of ground vibration is directly proportional to amount of charge per delay and inversely proportional to traveling distance of vibration waves. As a result of that, the concept of scaled distance was put forward in order to calculate the attenuation of particle velocity in the ground. Therefore, using the attenuation equation, derived from the relationship between the scaled distance and vibration magnitude, it is possible to predict the peak particle velocity as well as to find out the maximum allowable charge weight for the blasting site. Estimation of particle velocity and other components of ground vibration with reliable approach will give important facilities to the miners. Although many studies were carried out to isolate the environmental problems induced by blasting, as illustrated in the literature study in Chapter 2, a general reliable formula has not been established yet; rather a site-specific study is still needed in order to minimize the ground vibration impacts.

In the current study, ground vibrations induced by bench blasting from the Tunçbilek Coal Mine, Panel BYH, were measured to estimate the damage risk and to find out the site-specific attenuation. The research objectives and the site description are indicated in Chapter 3. The blasting operation, which is performed as a round-blast, is used to fragment the rock in order to facilitate the removal of overburden situated above the coal layers. In order to estimate the peak particle velocity and to produce a site-specific propagation equation as well as to estimate the maximum allowable charge for this site, field work and data collection were conducted over a period of four months. A

statistical approach is applied to the collected data, and from the data analysis an attenuation relationship is established to be used in predicting the peak particle velocity as well as to calculate the maximum allowable charge per delay. The frequencies are also analyzed to investigate the potential damage to the structures at Tunçbilek Township. The results and discussions are illustrated in Chapter 4.

In Chapter 5, a new approach to predict the peak particle velocity is proposed. A neural network technique from the branch of the artificial intelligence is put forward as an alternative approach to the statistical technique. The values predicted using the neural network and those calculated using the statistical model are compared with a set of recorded PPV values measured using Mini-Seis II Seismograph. Results showed that the neural network has the ability to predict the peak particle velocity with a satisfactory accuracy.

The main conclusions of the research and recommendations are given in Chapter 6.

CHAPTER 2

LITERATURE REVIEW

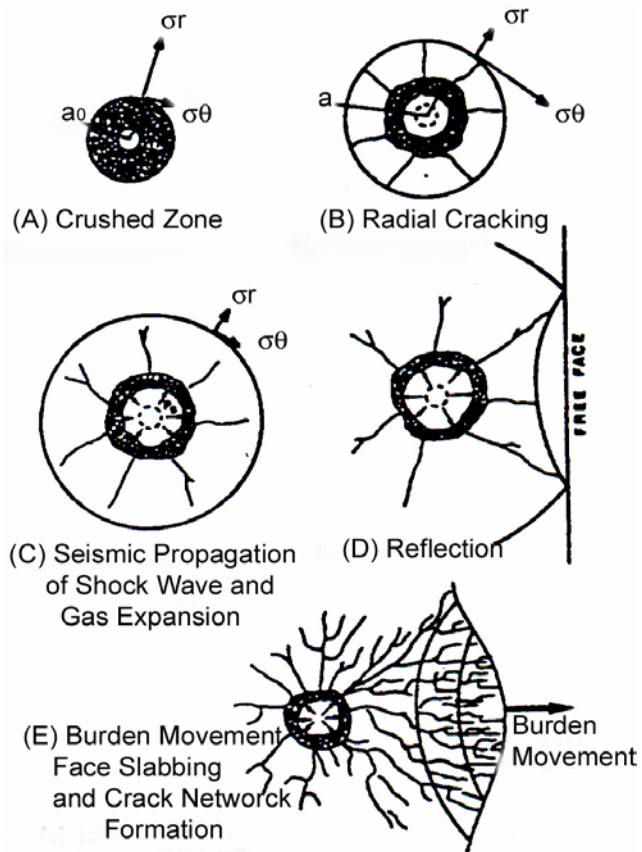
2.1 Principle of Fragmentation by Explosives

Understanding the basic principles of rock fragmentation by explosive charges is crucial for ground vibration assessment and optimizing successful blasting operation. According to Persson (1978), 1-20% of the energy of a detonated explosive charge, and also according to Langefors and Kihlstrom (1963), Duvall (1966) 5-15% is transferred to the surrounding rock as shock waves. The remaining part of the explosive energy released as very high pressure and temperature gaseous products of the reaction.

Kutter and Fairhurst (1971) indicated that there are three zones of varying destruction and deformation around the explosion. These zones are;

- the strong shock zone or hydrodynamic zone,
- the non-linear zone, and
- the elastic zone.

In the first zone, the radial compressive stresses generated from the shockwave exceed the dynamic compressive strength of the surrounding rock, and develop complete crushing as rock fail in compression, Figure 2.1. In the second zone, fracturing is due to the tangential stress. Since the tensile strength of the rock is not very high, the tangential tensile stresses create fractures. When the strain wave reaches the free surface of the rock, it is reflected and may cause spalling.



a_0 : Borehole radius

σ_r : Radial stress component

a : Equilibrium borehole pressure

σ_θ : Tangential stress comp.

Figure 2.1 Sequence of events occurring in the rock mass after detonation (Dowding and Aimone 1992).

Since the velocity of longitudinal waves is larger than the velocity of shear waves and as the strength of the rock in tension is much less than in compression, the reflected wave will break the rock in tension if it exceeds the tensile strength.

After the passage of the wave, the expanding explosion products start to penetrate into the radial cracks and exert high quasi-static pressure. High

temperature and high pressure borehole explosive gases can then flow into the system of the radial cracks generated and cause considerable additional extension of the number of these cracks (Olofsson, 1988). As the burden begins to move high compressive stresses within the rock begins to unload and generate more tensile stresses which complete the fragmentation process. The sequence of the event in the rock mass after the detonation is shown in Figure 2.1.

Generally speaking, the rock fracture during blasting is caused by the combined effects of shock and gas energies of an explosive and gas energy plays a relatively higher role during rock fragmentation depending upon the energy partitioning characteristics of the explosive. The remaining shock energy (spent after that rock fracturing) from the blast, in the absence of free faces travels as seismic waves in the ground (Singh, 1999).

2.2 General Ground Vibration Characteristics

2.2.1 Principal of Ground Vibrations

The ground vibration or seismic energy is usually described as a time-varying displacement, velocity, or acceleration of a particular point (particle) in the ground. Ground vibrations traveling through the ground may damage adjacent structures when they reach a certain magnitude. Some of the energy released from a blast propagates in all directions from the borehole as seismic waves with different frequencies. The energy from these seismic waves is damped by distance and the waves with the highest frequency are damped fastest. This means that the dominant frequencies from the blast are high at short distances and lower at large distances.

A typical particle velocity time history at a surface coal mine is shown in Figure 2.2. The most important parameters that describe the time history are peak amplitude, principal period ($= 1/\text{principal frequency}$) and duration of the

vibration. All these parameters are dependent on the blast sequence and transmission medium (Dowding 1985).

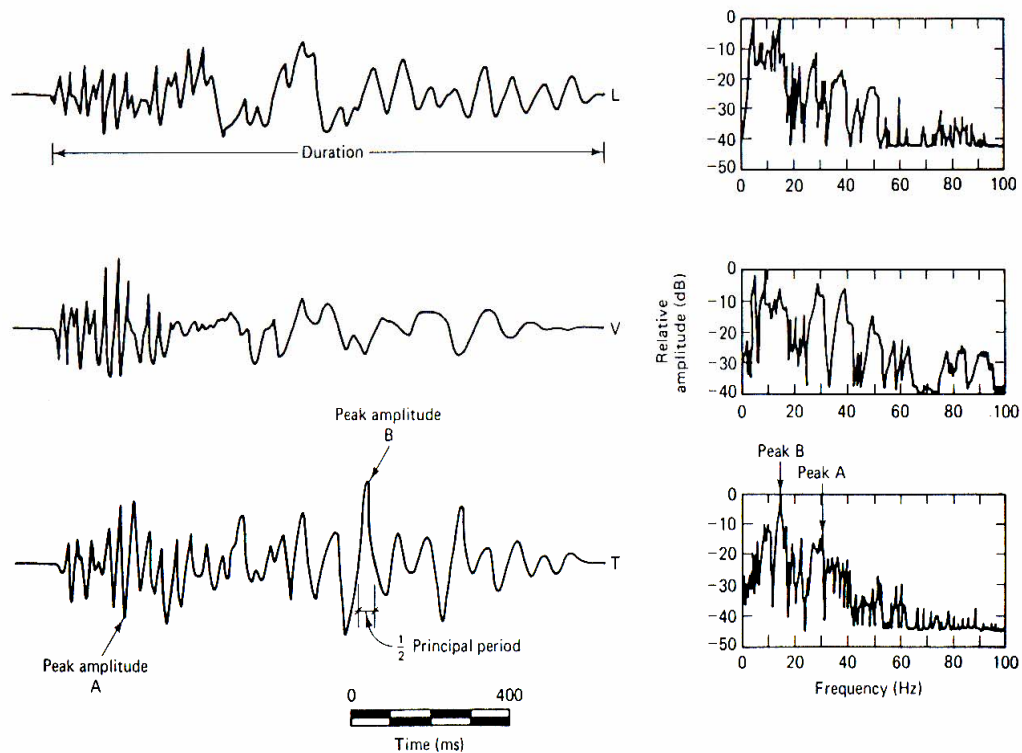


Figure 2.2 Typical coal mine blast vibration time histories (Dowding 1985).

2.2.2 Types of Vibration Waves

Interactions between the vibrations and the propagating media give rise to several types of waves. The main wave types can be divided into two varieties: body waves, and surface waves (Dowding 1985).

2.2.2.1 Body waves

Body waves are the waves that propagate through the body of the medium (rock or soil). They also can be subdivided into P-wave and S-wave;

P-wave

The P-wave is also called the primary compressional wave. It is the fastest wave through the ground. The particles in the wave move in the same direction as the propagation of the wave. Figure 2.3 shows the characteristics of P-wave in solid medium (Atlas 1987).

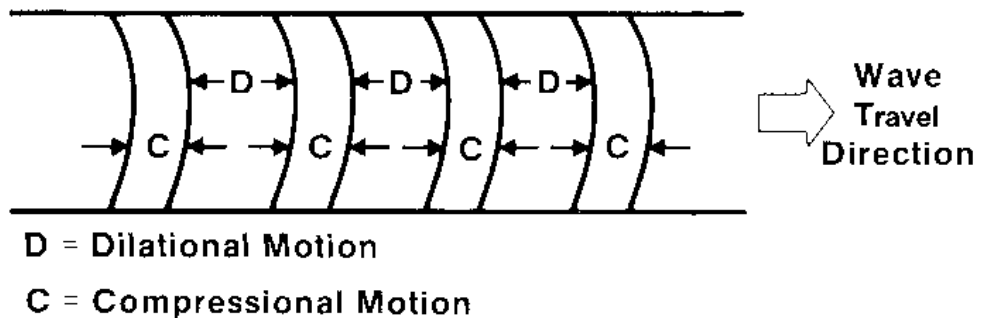


Figure 2.3 Characteristic of P-Wave in a solid medium (Atlas, 1987)

S-wave

The S-wave is also called the secondary or shear wave. It moves through the medium at the right angle to the wave propagation but slower than the P-wave. The S-wave is shown in Figure 2.4 as it propagates in a solid medium (Atlas 1987).

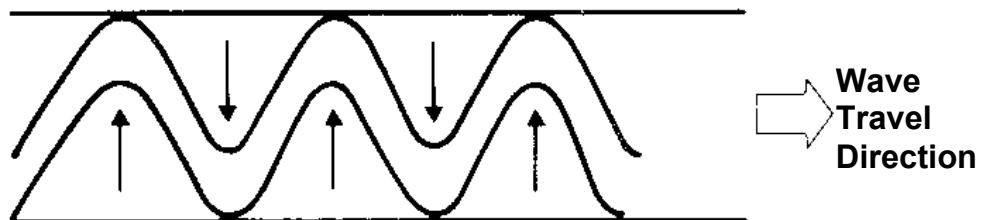


Figure 2.4 Characteristic of S-Wave in a solid medium (Atlas, 1987)

2.2.2.2 Surface Waves

Surface waves are the waves that are transmitted along a surface (usually the upper ground surface). The most important surface waves are the Rayleigh wave (R-wave) and Love wave.

R-wave

The R-wave propagates more slowly than the P-wave and S-wave and the particles move elliptically in the vertical plane and in the same direction as the propagation. Unlike the body wave's unidirectional particle motions, Rayleigh surface wave particle motion is two dimensional. These waves are similar to those produced by dropping a stone into a pool of water. As the water wave passes a piece of cork, the motion of the cork on water is described by a forward circle. Whereas, in rock a particle will follow a retrograde elliptical path, with the ratio of horizontal to vertical displacements equal to 0.7. Figure 2.5 shows the characteristics of Rayleigh waves in solid medium (Atlas 1987).

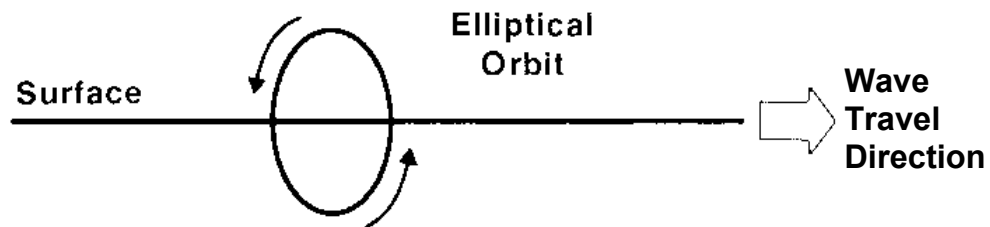


Figure 2.5 Characteristic of Rayleigh wave in a solid medium (Atlas, 1987)

Love wave

The Love wave is a surface wave with horizontal polarized particle motion. It is a transverse wave propagated in a low-velocity surface layer overlying a

medium in which elastic waves have higher velocities, as illustrated in Figure 2.6. The Love waves are faster than the Rayleigh waves and give particle motion that is transverse to that of propagation. Since their particle motion is always horizontal, love waves can never be recorded where a vertical geophone is used (Atlas, 1987).

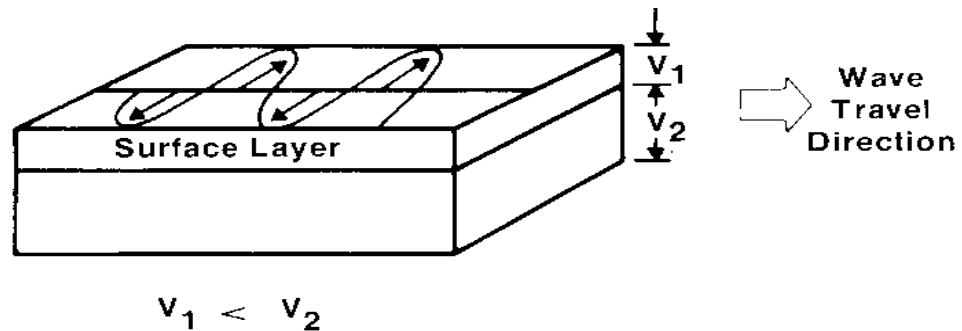


Figure 2.6 Characteristic of Love waves in a solid medium (Atlas, 1987)

To describe the motions completely, three perpendicular components of motion must be measured; the longitudinal, L, is usually oriented along a horizontal radius to the explosion. It follows, then, that the other two perpendicular components will be vertical, V, and transverse, T, to the radial direction, as shown in Figure 2.7, (Dowding 1985).

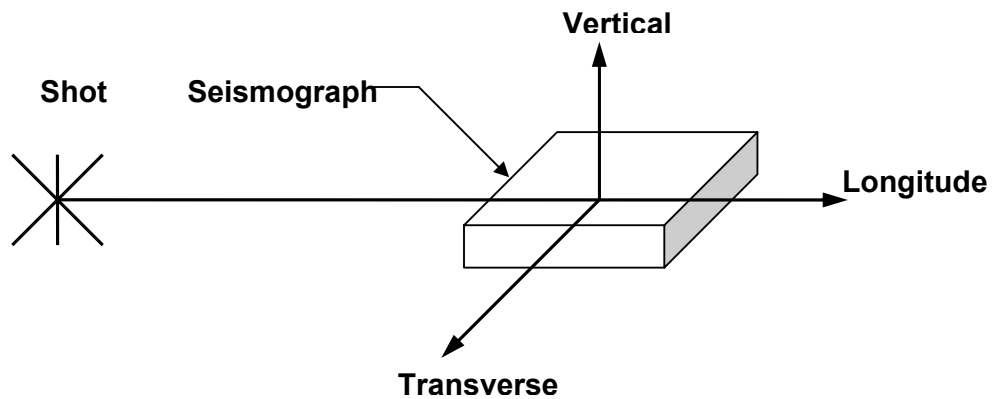


Figure 2.7 Vibration Components (Dowding 1985)

None of these vibration components, which are normal to each other, always dominates in blasting and the peak component varies with each blasting site. The peak occurs in different times and at different frequencies. The difference between the three components results from the presence of the different wave types in the blast vibration wave trains.

2.3 Peak Component and True Vector Sum

The variation of motion with each component has led to difficulty in determining which component is the most important. Is it the component with the greatest amplitude, or the peak vector sum of the components? Assume that we have the peak component of 0.9 of velocity unit recorded in longitudinal direction at time 1, and the vertical and the transverse components at the same time are 0.25 and 0.25, respectively. The true vector sum of all the components at time 1 is

$$\begin{aligned} (L^2 + V^2 + T^2)^{0.5} &= (0.9^2 + 0.25^2 + 0.25^2)^{0.5} & (2.1) \\ &= 0.96 \text{ unit} \end{aligned}$$

There may be another time when the peak true vector sum will be larger than that at the peak component and several should be checked. However, it usually occurs at the same time as the largest component peak. Peak motions should always be reported as either peak component or the peak true vector sum.

Another measure, the maximum vector sum, is frequently reported but is conservative and not directly related to a maximum velocity at a particular time. The maximum vector sum is calculated as shown in the above equation also; however, the maximum of each component is used regardless of the time when it occurs. Thus, for the same record in the example above if the peak of the vertical and transverse components are both 0.75 and occur at different time than time 1, then, the maximum vector sum is

$$(0.9^2 + 0.75^2 + 0.75^2)^{0.5} = 1.4 \text{ unit} \quad (2.2)$$

In general, the empirical observations of cracking have been made with single-component peaks; therefore, use of the maximum vector sum provides a large unaccounted safety factor. As a result of that, peak particle velocity, which is the maximum particle velocity among the radial, vertical, and transverse components recorded from the same blast event, should be taken into account instead of peak vector sum (Dowding 1985).

2.4 Frequency Properties and Durations

The frequency of ground vibration can be defined as the number of cycles executed per unit time (second). Mathematically, it can be expressed as follows:

$$F = 1/T \quad (2.3)$$

Where F is the frequency and its unit is Hertz (Hz), and T is the time in seconds required for a complete oscillation.

The amplitude (A) of ground vibration is defined as a time varying and kinematical vibration quantity of displacement, velocity or acceleration. They all have instantaneous values at any instant together with the peak or maximum at some specific moments for any vibration record.

The amplitude, frequencies, and durations of the ground vibrations change as they propagate, because of (a) interaction with various geologic media and structural interfaces, (b) spreading out the wave-train through dispersion, and/or (c) absorption, which is greater for the higher frequencies. Therefore, the vibration frequency and consequently the velocity, displacement and acceleration amplitudes depend strongly on the propagating media. For instance, thick soil overburden as well as long absolute distance creates long-duration, low-frequency wave trains. This increases the responses and damage potential of nearby structures (Siskind et. al., 1980).

The 1980 USBM's report indicates that frequencies below 10 Hz produce large ground displacement and high levels of strain, and also couple very efficiently into structures where typical resonant frequencies are 4 to 12 Hz for the corner or racking motions. It is also concluded that damage potentials for low-frequency blasts (<40 Hz) are considerably higher than those for high-frequency (>40Hz).

Other studies described the frequency character of vibration from quarry (Nicholls, 1971), and coal mine blasts. (Wiss and Linehan, 1979) The combination of large charge shots, thick soil and sedimentary rock overburdens, relatively good confinement, and long-range propagation make coal mine blast vibrations potentially more serious than quarry and construction blasts because of their low frequencies. Hard rock construction and excavation blasts tend to be shorter in duration and contain higher frequency motions than those of either coal mine or quarry. (Stagg and Engler, 1980)

2.5 Methods of Measuring Frequencies

Many researches done in the past have produced frequency-based velocity data without a clear definition of frequency or methods used to calculate frequencies. Frequency components of a vibration are equally important as the particle velocities. When the intent is to evaluate damage potential, the entire time history, or all frequency component, is an important factor to consider.

Frequency is most reliably computed by applying the Fourier frequency function, or FFT (Fast Fourier Transform), to transform the ground motion time histories (time domain) into the frequency domain. In this manner, the distribution of frequency content can be compared based on relative intensities of ground motion at specific frequencies, and predominant frequencies can be easily identified.

In contrast, the “zero-crossing” method has been widely adopted by industry for determining and reporting a single frequency value at the peak velocity of ground motions measured in three directions (radial, transverse, and vertical) or the PPV. A problem arises when the peak frequency occurs in a complex vibration time history containing a variety of frequencies and amplitudes. If the peak velocity occurs early in the time history within the high frequency components (e.g. above 20 to 30 Hz), the zero-crossing method may result in a frequency well above the natural frequency range of residential structures, even if the entire time history contains a strong low-frequency component. This may not represent the frequency at which the maximum vibration energy is transferred into the structure.

Most seismograph analysis software provides a means to plot the “zero-crossing” frequency as well as the FFT frequency for every peak contained within the time history. In this respect, the vibration energy contained over all frequencies can be evaluated with respect to potential structure response (Aimone-Martin et al., 2003).

2.6 Impact of Natural and Technological Factors on Seismic Effects of a Blast

2.6.1 Blasting conditions

In industrial blasts the wave picture is extremely complex. This is due to the prevailing geo-mining conditions on the travel path of blast induced seismic vibrations and also due to the special nature of the blast as a source of elastic waves.

In describing such a source we can only consider approximation of the models as applied to the properties of the medium in which blasting takes place. In actual conditions, various endogenous factors such as, type of explosives, weight, construction and shape of individual parts in a charge,

the total charge in the block being blasted and initiation scheme as well as external factors such as properties of rocks, availability of free face, line of least resistance and depth of charge directly or indirectly influence the blast (Arseven 2003).

2.6.2 Construction of explosive charge

The properties of explosive used in the blasts primarily influence the intensity of the source of seismic vibrations. Explosives having low velocity of detonation (VOD) are preferred for conducting blasts to produce reduced seismic effects. Explosives with higher VOD generate significant vibrations. In their spectra, higher frequencies predominate, which absorb a major part of the energy. Therefore, while selecting explosives due consideration should be given to the requirements of fragmentation and absorbing properties of surrounding rocks at different phases in the frequency spectra of oscillation.

The most effective method of reducing blast induced seismic effects as well as enhancing the quality of fragmentation is to use inactive and air gaps and also inactive stemming. It has been established that the intensity of vibrations is reduced by 1.2-2 times, depending on the properties of surrounding rocks, when charges with in-between air gaps are used. However, the use of such charges reduces the seismic effects only at specific ratios of volume of air gaps to the entire charge volume in a particular deposit. This ratio is about 0.3-0.4 (Arseven 2003).

2.6.3 Conditions of placing charges

The conditions of charge placement influence the seismic effect of a blast. Maximum seismic effects are observed in blasts conducted in a confined medium. The depth of charge placement plays a vital role since with an increase in depth the intensity of vibrations also increases. Therefore, as the

number of free faces increases, the vibration velocity of rock decreases. In such a case, seismic effects may be reduced by as much as 4-5 times compared to blasting in a confined medium. In a series of investigations the change in seismic effects of a blast due to change in bench height or length of hole charge was considered. It was established that relatively rapid growth of particle velocity is noticed when the bench height is increased from 10 to 20m. The enhanced intensity of seismic vibrations can be explained by the increased consumptions of explosives per unit time of blast and also by the lengthening of charge (Arseven 2003).

2.6.4 Properties of rocks

An important property is the acoustic rigidity of rock. Placing a charge in a medium of lower acoustic rigidity reduces the seismic effects of a blast. A blast in rocks of relatively greater acoustic rigidity produces 3 times more seismic energy at the source boundary, compared to blasts in rocks with lower acoustic rigidity.

Blasts in clays, marlstones and salts cause maximum ground movement due to the seismic wave. While blasting in hard rocks takes place, the expansion and development of existing fissuring affects the seismicity. As the specific fissuring increases, the seismic effect in large blasts reduces. At the same time, a vital role is played in not only by the number of fissures but also the expansion of their opening, filling by secondary products and spatial orientation. The spatial disposition of fissures also influences the seismic effects of a blast. By properly orienting the drill hole grid, the fragmentation and intensity of elastic vibrations can be regulated (Arseven 2003).

Change in the physicommechanical properties of rocks at the site of blasting also influences the frequency composition of blast-induced vibrations. In rocks with a low value of acoustic rigidity, lower frequencies dominate compared to rocks with higher acoustic indexes.

Ground motion dissipation in rock is attributed to three mechanisms according to Atlas, (1987):

1. Viscous damping of ground vibrations, an effect more pronounced on higher frequencies and accompanied by a trend to lower ground vibration frequencies with increasing distance from a blast.
2. Solid friction absorption of energy in the ground motion wave, which is greater for rock for coarser grain structures and extensive porosity.
3. Scattering of the ground motion wave due to reflections at discontinuities and strata inhomogeneities in the rock, in which interactions between reflected pulses are often accompanied by a trend to selectively attenuate lower ground vibration frequencies.

Since rock masses are inhomogeneous, ground motion waves travel through strata of different acoustical impedance. Scattering the ground vibration waves, initiated at boundary of discontinuities by reflections, lowers the peak vibration levels. Interactions between the reflected pulses alter the frequency composition of the wave train. High frequencies are selectively attenuated while some lower frequencies are added to the ground vibrations.

The presence of joints, fractures, faults and shear zones in the path of a ground motion wave also act to scatter the peak vibrations. Some of the lateral components of ground motion are lost as the wave crosses a discontinuity. The degree of redirection and dissipation of a ground motion wave is related to the nature and frequency of structural discontinuities in rock (Atlas, 1987).

2.7 Structure Response to Blast Excitation

Blasting can cause significant vibrations within structures even in cases where the distance between a blast and the structure is large. High levels of

vibration within structures are caused by a close match between the ground vibration frequency and the fundamental resonant frequency of the structure or some structural elements (Djordjevic et al., 1990).

2.7.1 Structure Components and Ground Vibration Parameters

Structures consist of many components, and two of most important are walls and superstructural skeletons. Superstructure response, measured at a corner, is associated with the shearing and torsional distortion of the frame, while the wall response, which measured in the middle of the wall, is associated with bending of that particular wall. The wall and superstructure continue to vibrate freely after the passage of the ground motion, according to Dowding (1985). He also indicated that the wall motion tend to be larger in amplitude than the superstructure motions and tend to occur at higher frequencies during free vibration than those of the superstructure. Detailed studies (Dowding et al., 1980; Medearis, 1976) have shown that the natural frequencies of walls range from 12 to 20 Hz and those of superstructures from 5 to 10 Hz.

The response of any structure to vibration can be calculated if its natural frequency and damping are known or can be estimated. The fundamental natural frequency F_d of the superstructure of any tall building can be estimated from compilations of work in earthquake engineering (Newmark and Hall, 1982):

$$F_d = 1 / 0.1 * N \quad (2.4)$$

where, N is the number of the stories. Substitution of 1 and 2 for residential structures for N yields F_d values that can be compared favorably with results of actual measurements (Dowding, 1992).

Damping β is a function of building construction and to some extent the intensity of vibration. Measurement reveals a wide range of damping for residential structure with an average of 5% (Dowding et al., 1981).

Excessive structural response has been separated into three categories arranged below in the order of declining severity and increasing distance of occurrence (Nothwood et al., 1963; Siskind et al., 1980). Beginning with effects that occur closest to the blast, the categories are listed here:

1. Major (Permanent Distortion). Resulting in serious weakening of the structure (e.g. large cracks or shifting of foundations or bearing walls, major settlement resulting in distortion or weakening of the superstructure, walls out of plump).
2. Minor (Displaced Cracks). Surficial, not affecting the strength of the structure (e.g. broken windows, loosened or fallen plaster), hairline cracks in masonry.
3. Threshold (Cosmetic Cracking). Opening of old cracks and formation of new plaster cracks, dislodging of loose objects (e.g. loose bricks in chimneys) (Dowding, 1992).

2.7.2 Resonance and Amplification Factor

The probability of damage in structures depends on the relationship between dominant frequency of the ground vibration and natural frequency of the structure. Most significant for blasting is that the principal frequencies of the ground motion almost always equal or exceed the gross structure natural frequencies of 4 to 10 Hz. In this case, structure resonates and it is shaken by amplified vibration a few seconds. People may still perceive and are concerned about this situation. While structure resonates, it may not be damaged but people may still complain even if particle velocity is much below the limiting vibration value. However, the damages within the structures are caused when structure resonates at a particle velocity exceeding vibration limit. Although amplitude of the exciting wave traveling in the ground is not sufficient to cause damage to structure, structure may

be damaged due to amplification during resonance. Amplification is defined as the increase in the amplitude measured in the structure with respect to ground amplitude due to the transfer of the exciting wave on the ground to the structure. The ratio of amplitude of the structure to ground amplitude is called as amplification factor (Esen and Bilgin, 2001).

Public concerns are completely due to the low-frequency and high-amplitude ground vibrations as in the case of Can Lignite Mine, Turkey (Bilgin et al., 1998, Bilgin et al., 1999) where ground vibration levels are much below 12.7 mm/sec and no damages are encountered. It may be explained by the low frequency waves that people perceive. When the frequency is high, it is hard for humans to feel and they do not react. Since frequencies below 10 Hz create great displacements and high level unit deformations on ground, they increase the damage risk (Siskind et al., 1980)

2.7.3 Distinction of blast-induced cracking from natural cracking

Control of blast-induced transient effects to prevent threshold or cosmetic cracking reduces blast-induced displacement or strains in structures to below that caused by every day activities and change in the weather (Stagg et al., 1984; Dowding, 1988).

The blast induced threshold cracks can be scientifically observed only with visual inspection immediately before and after each blast. However, the multiple origins of cracks should be taken into consideration. Several institutional references (Anon, 1977; Anon, 1956; Thoenen and Windes, 1942) summarized that cracks basically are found to be caused by the following non-blast factors:

- 1- Differential thermal expansion.
- 2- Structural overloading.

- 3- Chemical change in mortar, bricks, plaster, and stucco.
- 4- Shrinking and swelling of wood.
- 5- Fatigue and aging of wall coverings.
- 6- Differential foundation settlement.

2.8 Blast-induced Air Overpressures

Blast-induced air overpressures are the air pressure waves generated by explosion. The higher-frequency portion of the pressure waves are audible and are the sound that accompanies a blast; the lower-frequency portion not audible, but excites structures and in turn cause a secondary and audible rattle within a structure (Dowding, 1992).

Overpressure waves are of interest for three reasons. First, the audible portion produces direct noise. Second, the inaudible portion is itself or in combination with ground motion can produce structural motions that in turn produce noise. Third, they may crack windows; however, air-blast pressure alone would have to be unusually high for such cracking (Dowding, 1992).

Earlier researches (Kamperman and Nicholson, 1970; Borsky, 1965) have found that response noise within a structure (from blasting and sonic booms respectively) is the source of many complaints. It appears that structure and wall motions, which are induced by air-blasts and sonic booms, rattle loose objects within the structure, which then startle the occupants.

2.9 Human Response to Blast-induced Ground and Airborne Disturbances

Human response to blast vibrations is an important problem for mine and construction managers. Ground vibrations are occasionally blamed for house vibrations when long-range air blasts propagating under favorable weather conditions are possible. The classical study of subjective human

tolerance to vibratory motion was done by Reiher and Meister in 1931. They subjected 15 people to 5-min duration vertical and horizontal vibration in a variety of body position and established levels of perception and comfort. Responses of “slightly perceptible” occurred at 0.010 to 0.033 in/sec and the threshold of “strongly perceptible” was 0.10 in/sec, all essentially independent of frequency over the range 4 to 25 Hz.

More recent research on the effect of vibration on human has produced results similar to those of Reiher and Meister. Goldman (1948) analyzed human response to steady-state vibration in the frequency range of 2 to 50 Hz. His results were converted to particle velocities and presented in Bulletin 656 (1971), where Goldman’s “slightly perceptible” and “strongly perceptible” levels are approximately 0.0086 and 0.074 in/sec, respectively, at 10 Hz. Taking these as thresholds, they agree quite well with Reiher and Meister’s data.

Siskind (1980) in USBM report (RI 8507) indicated that human reaction to vibration is dependent on event duration as well as level. Particle velocities of 0.5 in/sec from typical blasting (1-sec vibration) should be tolerable to about 95% of the people perceiving it as “distinctly perceptible”. For people at home, the most serious blast vibration problems are house rattling, fright (fear of damage or injury), being startled, and for a few, activity interference. The 1980 report also concluded that complaints from these causes can be as high as 30 pct at 0.5 in/sec, and this is where good public relation attitudes and an educational program by the blaster are essential.

2.10 Concept of Scaled Distance

The scaled distance is a concept put forward by using the amount of explosive energy in air shock and seismic waves, and this affects the basis of distance. The scaled distance is derived by combining the distance

between source and measurement points, and the maximum charge per delay. This scaled distance is defined by equation below:

$$\mathbf{SD = D/W_d^{0.5}} \quad (2.5)$$

Where,

SD is the scaled distance (m/kg^{0.5}),

D is the absolute distance between the shot and the station (m), and W_d is the maximum explosive charge per delay (kg).

In ground vibration analysis preferably square root or rarely cube root scaling is used, whereas in air overpressure analysis cube root scaling is used.

The ground motion wave front resulting from a column charge (length to diameter ratio greater than 6:1) takes the form of an expanding cylinder. The volume of this compression cylinder varies as the square of its radius. Thus, the peak level of ground motion at any given point is inversely proportional to the square of the distance from the shot point. (Dowding 1985)

The peak particle velocity (PPV) is given by the following formula;

$$\mathbf{PPV(mm/sec) = K * (SD)^{-\beta}} \quad (2.6)$$

Where,

K is the ground transmission coefficient and,

β is a specific geological constant.

The site factors are determined from a logarithmic plot of peak particle velocity (PPV) versus scaled distance (SD). The straight line best representing the data has a negative slope β, and an intercept K at a scaled distance of 1.

2.11 Previous Investigations for Damage Criteria

Although many studies have been carried out to diminish environmental problems induced by blasting, a general reliable approach has not been established yet. The complexity of ground motions, blasting and test site factors restrict the establishment of a ground vibration criterion. Thus, experimental studies are still necessary for each site in order to minimize environmental problems, (Kahriman, 2001a). However, a number of investigators studied ground vibration induced by blasting and developed some theoretical and empirical approaches to explain the matter in detail. Therefore, a review of previous investigations for damage criteria is given below;

2.11.1 Vibration Energy as Damage Criteria

(a) Rockwell's Energy Formula, 1934.

This formula considers frequency and amplitude as parameters for estimating the potential damage (Kahriman, 2001b).

(b) United States Bureau of Mines (USBM) formula, 1942.

It was the first USBM criteria concerning the blast-induced ground vibration and was based on amplitude, quantity and distance (Kahriman, 2001b).

(c) Crandell's Energy Ratio Concept, 1949.

This damage criterion is based on pre and postblast investigations, and it has recommended that no damage can occur below 3.0 of energy ratio.

2.11.2 Peak Particle Velocity as Damage Criteria

(a) Particle Velocity Criterion of Langefors, Kihlstrom and Westerberg, 1958.

It was adopted for the first time by State of Pennsylvania to assess the damage potential of the ground vibration, and 2.0 in/sec used as an overall safe level for residential structures.

(b) Edwards Northwood's Particle Velocity, 1960.

This criterion is also based on the amplitude of particle velocity and damage type, and indicated that no damage can occur below 2.0 in/sec.

(c) USBM's Particle Velocity Criteria, 1971.

The Bureau of Mines studied various aspects of ground vibration, airblast, and seismic instrumentation, and published that in Bulletin 656 in 1971. Bulletin 656 established the use of peak particle velocity in place of displacement, and recommended to use 2.0 in/sec as an overall safe level for residential structure.

These recommendations were widely adopted by the mining and construction industry. However, soon after publication of the 2.0 in/sec safe level criterion, it became apparent that it was not practical to blast at this high vibration level. Many mining operations with nearby neighbors were designing their blast to keep velocities as low as 0.4 in/sec, and many homeowners were attributing all cracks to the blast vibration.

(d) Indian Standard Institute, 1973.

Particle velocity and rock type were the bases of this criteria.

(e) Canmet, Bauer and Calder's Particle Velocity Criterion, 1977.

The criterion considers particle velocity with connection to structure components and damage types, and adopted 0.5 mm/sec as a safe level.

2.11.3 Peak Particle Velocity and Frequency as Damage Criteria

(a) Langefors and Kihlstrom's Criterion, 1967.

Damage effects are described by peak particle velocity, and frequency, Table 2.1.

Table 2.1 Langefors and Kihlstrom's Criterion.

Damage Effects	Peak Particle Velocity					
	Sand, gravel, clay below water level; c=1,000-1,500 m/sec ¹		Moraine, slate, or soft limestone; c=2,000-3,000 m/sec		Granite, hard limestone, diabase c=4,500-6,000 m/sec	
	mm/sec	in/sec	mm/sec	in/sec	mm/sec	in/sec
No noticeable crack formation	18	0.71	35	1.4	70	2.8
Fine cracks & falling plaster...	30	1.2	55	2.2	100	3.9
Crack formation.....	40	1.6	80	3.2	150	5.9
Severe crack.....	60	2.4	115	4.5	225	8.9

¹ Propagation velocity in media is given by c.

(b) Medearis's Approach, 1976.

Particle velocity and predominant frequency were the bases of the damage criteria.

(c) USBM's Criterion, According to Siskind et al., 1980.

Safe blasting vibration criteria were developed by USBM for residential structures, involving frequency, velocity, and displacement, Figure 2.8. Safe levels of ground vibration from blasting range from 0.5 to 2.0 in/sec peak particle velocity, and having two frequency ranges and a sharp discontinuity at 40 Hz. The criteria indicated that damage potentials for low-frequency blasts (<40 Hz) are considerably higher than those for high-frequency blasts (>40 Hz), with the latter often produced by close-in construction and excavation blasts.

Moreover, practical safe criteria for blasts that generate low-frequency ground vibrations are 0.75 in/sec for modern gypsumboard houses and 0.5 in/sec for plaster on lath interiors. For frequencies above 40 Hz, a safe particle velocity maximum of 2.0 in/sec is recommended for all houses.

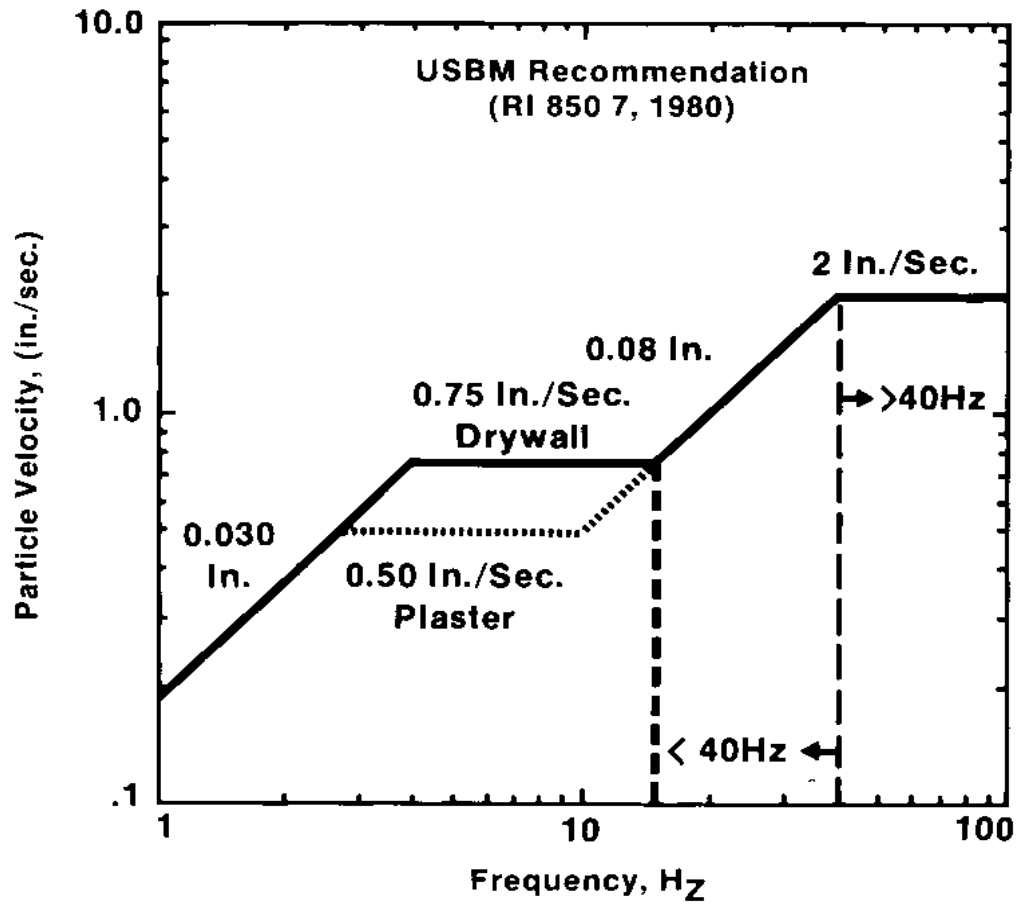


Figure 2.8 Safe levels of blasting vibration for structures, USBM's Criterion, 1980

(d) German DIN Standard 4150, 1993,

German Institute of Standard developed a criterion for vibration effects on structures based on peak particle velocity, frequency, and type of structures. This criterion is illustrated in Table 2.2 and in Figure 2.9 (Nick, 2002)

Table 2.2 Guideline value of vibration velocity, DIN 4150, 1993 (Nick, 2002)

Line	Type of Structure	Vibration Velocity (mm/sec)		
		Foundation Frequency		
		Less than 10 Hz	10 to 50 Hz	50 to 100 [*] Hz
1	Buildings used for commercial purposes, industrial buildings and buildings of similar design	20	20 to 40	40 to 50
2	Dwellings and buildings of similar design and/or use	5	5 to 15	15 to 20
3	Structures that, because of their sensitivity to vibration, do not correspond to those listed in lines 1 and 2 and are of great intrinsic value (eg buildings that are under a preservation order)	3	8 to 10	8 to 10

* For frequencies above 100 Hz, at least the values specified in this column shall be applied

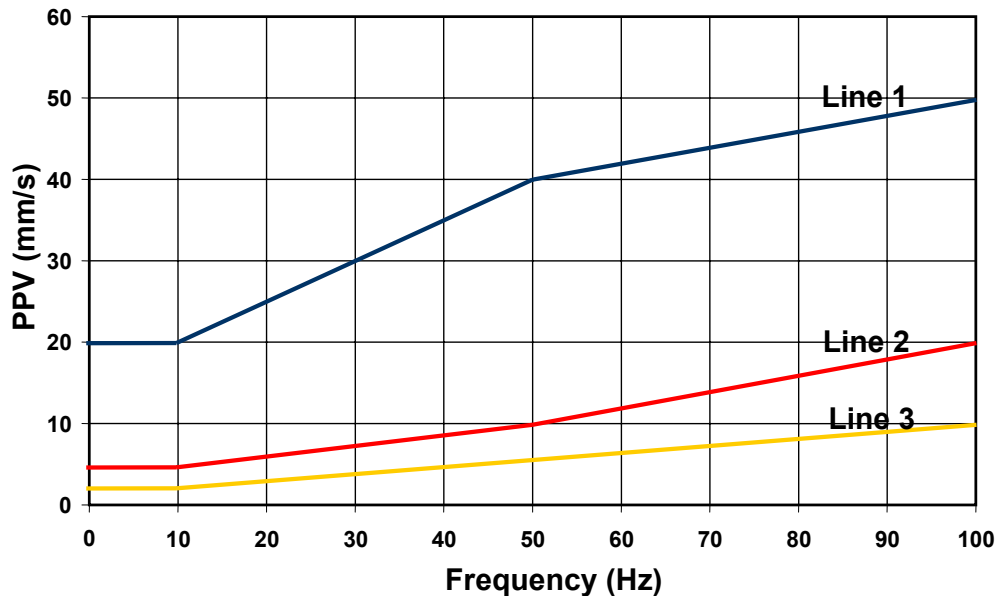


Figure 2.9 Curves Representing the Vibration Velocity as A Function of the Frequency for DIN 4150, 1993 (Nick, 2002)

(e) Indian CMRI Standard, 1987.

This criteria depending mainly on peak particle velocity and frequency associated with specification of structures (Kahriman, 2001b).

2.11.4 Peak Particle Velocity and Scaled Distance as Damage Criterion

(a) Federal Regulations of United States Office of Surface Mining (OSM), 1983.

The Office of Surface Mining (OSM) adopted a modification of the USBM's safe blasting criteria, 1980, which allows three methods for a blasting operation to demonstrate compliance, i.e. the maximum overall peak particle velocity (PPV) method, the scaled charge weight/ distance method, and the velocity-frequency chart method, Figure 2.9.

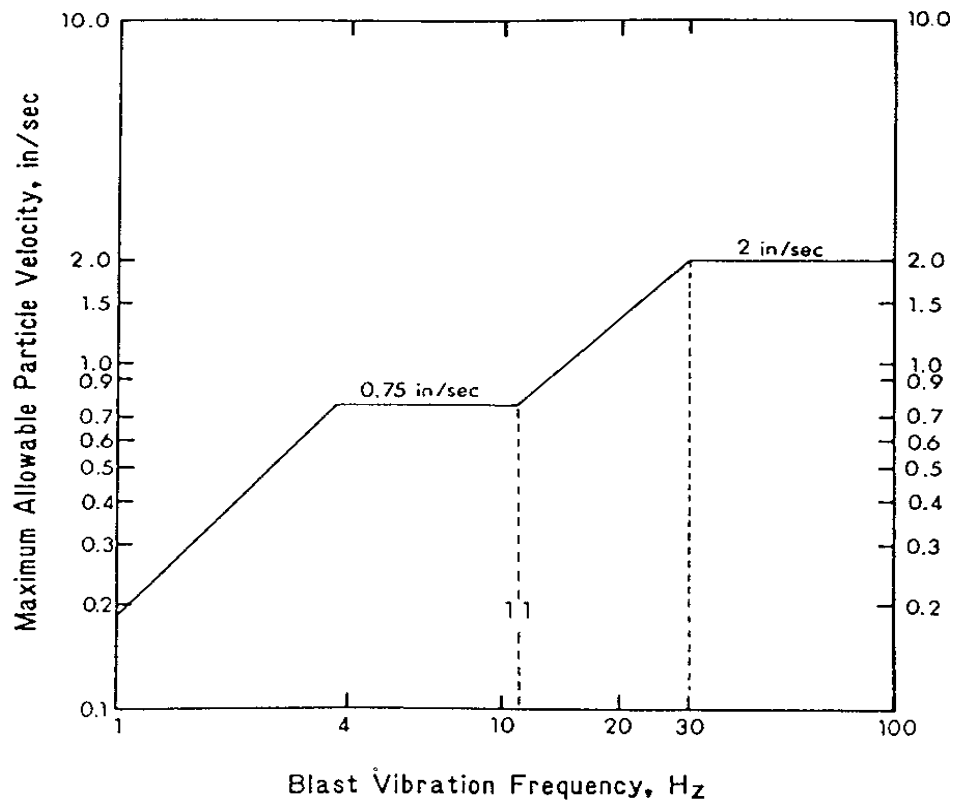


Figure 2.10 U.S. OSM's 1983 Recommendations

In this figure, note that the 2.0 in/sec range begins at 30 Hz as distinct from the USBM RI 8507 range which begins at 40 Hz. It also indicated that at large distance a lower peak particle velocity, 0.75 in/sec, and a large scaled distance, SD = 65, are mandated. At the shorter distances, a higher peak particle velocity, 1.25 in/sec and a smaller scaled distance, SD = 50, are permitted.

However, Dimitrios et al., (2001) recommended that in many projects located in urban areas, the vibration thresholds should be based more on human response than the probability of structural damage or harmful effects. The human reactions to blasting, however, was considered to be the limiting factor as shown earlier in the USBM's study in 1980.

Present regulatory control limits in many countries are below those levels at which cosmetic cracking may appear. There are two principle reasons for such tight restrictions. First, regulatory limits are influenced heavily by human response to blast-induced vibration and noise. Since humans are approximately 10 times more sensitive than structures to vibration, low regulatory limits are understandable.

Second, many regulations appear to have been adopted without the documented, scientific experimentation necessary to determine the vibration levels that cause cracking. In general, appropriate vibration thresholds, in conjunction with systematic vibration monitoring and continuous information of the residents, appease public anxiety. Hence, the mining and construction projects are protected from unjustifiable complaints, which, in some cases, can create obstacles, which are hard to overcome.

2.12 Fundamentals of Neural Networks

In 1956 the Rockefeller Foundation sponsored a conference at Dartmouth College that had as its scope:

The potential use of computers and simulation in every aspect of learning and any other feature of intelligence.

It was at this conference that the term "artificial intelligence" came into common use. Artificial intelligence can be broadly defined as:

Computer processes that attempt to emulate the human thought processes that are associated with activities that required the use of intelligence.

Neural networks technique recently has been included in this definition, so it can be accepted as a legitimate field of artificial intelligence (Tsoukalas and Uhrig, 1996).

2.12.1 Biological Basis of Neural Networks

The human brain is a very complex system capable of thinking, remembering, and problem solving. There have been many attempts to emulate brain functions with computer models, and although there have been some rather spectacular achievements coming from these efforts, all of the models developed to date pale into oblivion when compared with the complex functioning of the human brain.

A *neuron* is the fundamental cellular unit of the brain's nervous system. It is a simple processing element that receives and combines signals from other neurons through input paths called *dendrites*. If the combined input signal is strong enough, the neuron "fires," producing an output signal along the axon that connects to the dendrites of many other neurons. Figure 2.11 is a sketch of a neuron showing the various components. Each signal coming into a neuron along a dendrite passes through a *synapse* or *synaptic junction*. This

junction is an infinitesimal gap in the dendrite that is filled with neurotransmitter fluid that either accelerates or retards the flow of electrical charges (Tsoukalas and Uhrig, 1996).

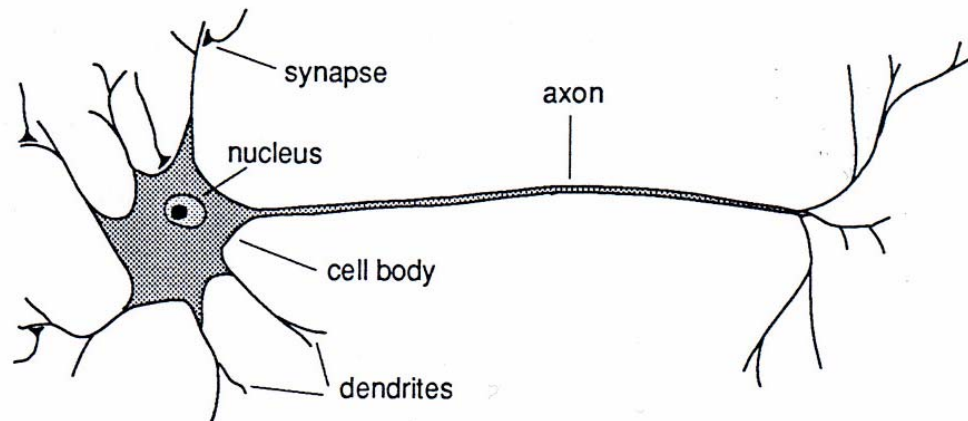


Figure 2.11 Schematic drawing of a typical neuron.

The fundamental actions of the neuron are chemical in nature, and this neurotransmitter fluid produces electrical signals that go to the nucleus or *soma* of the neuron. The adjustment of the impedance or conductance of the synaptic gap is a critically important process. Indeed, these adjustments lead to memory and learning. As the synaptic strengths of the neurons are adjusted, the brain "learns" and stores information.

When a person is born, the cerebral cortex portion of his or her brain contains approximately 100 billion neurons. The outputs of each of these neurons are connected through their respective *axons* (output paths) to about 1000 other neurons. Each of these 1000 paths contains a synaptic junction by which the flow of electrical charges can be controlled by a neurochemical process. Hence, there are about 100 trillion synaptic junctions that are capable of having influence on the behaviour of the brain.

It is readily apparent that in our attempts to emulate the processes of the human brain, it cannot be thought of billions of neurons and trillions of synaptic junctions. Indeed, the largest of our neural networks typically contain a few thousand artificial neurons and less than a million artificial synaptic junctions. (Tsoukalas and Uhrig, 1996).

2.12.2 Artificial Neurons

An artificial neuron is a model whose components have direct analogs to components of an actual neuron. Figure 2.12 shows the schematic representation of an artificial neuron. This artificial neuron was first presented by McCulloch and Pitts in 1943. The input signals are represented by $x_0, x_1, x_2, \dots, x_n$. These signals are continuous variables, not the discrete electrical pulses that occur in the brain. Each of these inputs is modified by a *weight* (sometimes called the *synaptic weight*) whose function is analogous to that of the synaptic junction in a biological neuron. These weights can be either positive or negative, corresponding to acceleration or inhibition of the flow of electrical signals.

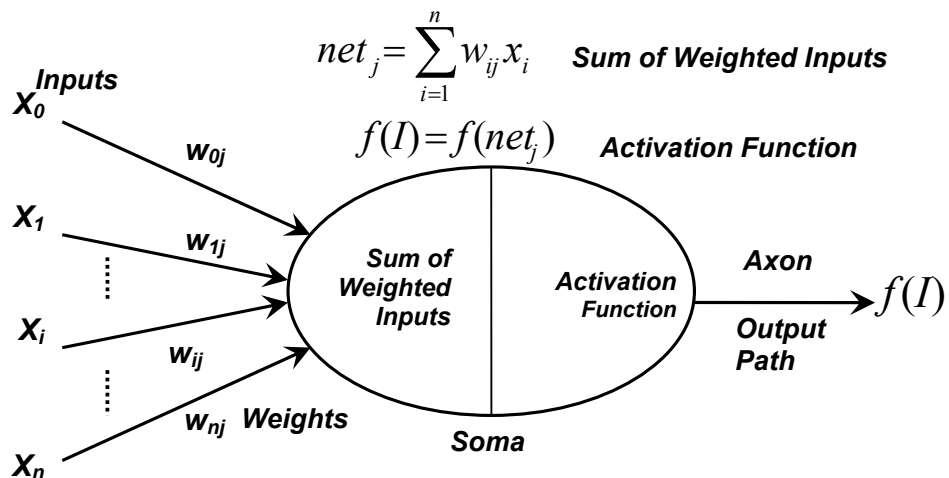


Figure 2.12 Schematic representation of an artificial neuron (Tsoukalas and Uhrig, 1996).

This processing element consists of two parts. The first part simply aggregates (sums) the weighted inputs resulting in a quantity, $I = (\sum_{i=1}^n w_{ij} x_i)$; the second part is effectively a nonlinear filter, usually called the *activation function*, through which the combined signal flows (Tsoukalas and Uhrig, 1996).

More commonly, the activation function is a continuous function that varies gradually between two asymptotic values, typically 0 and 1 or -1 and $+1$, called the *sigmoidal function*. The most widely used activation function is the logistic function, which is shown in Figure 2.13 and represented by the equation.

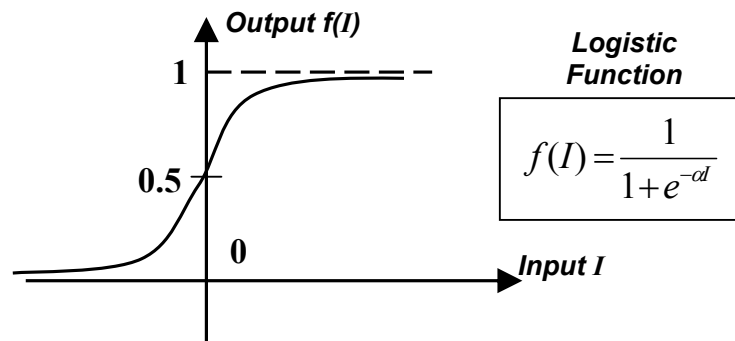


Figure 2.13 Activation function for neurons (Tsoukalas and Uhrig, 1996)

$$f(I) = \frac{1}{1 + e^{-\alpha I}} \quad (2.7)$$

Where α is a coefficient that adjusts the abruptness of this function as it changes between the two asymptotic values.

2.12.3 Artificial Neural Network

An artificial neural network can be defined as:

A data processing system consisting of a large number of simple, highly interconnected processing elements (artificial neurons) in an architecture inspired by the structure of the cerebral cortex of the brain (Tsoukalas and Uhrig, 1996).

These processing elements are usually organized into a sequence of layers or slabs with full or random connections between the layers. This arrangement is shown in Figure 2.14, where the input layer is a buffer that presents data to the network.

The following layer(s) is called the hidden layer(s) because it usually has no connection to the outside world. The output layer is the following layer in the network, which presents the output response to a given input. Typically the input, hidden, and output layers are designated the i th, j th, and k th layers, respectively.

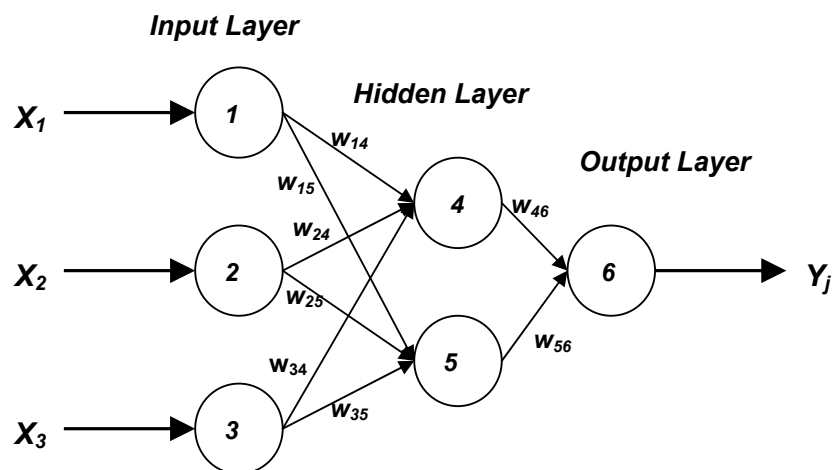


Figure 2.14 Scheme of an artificial neural network.

A typical neural network is “fully connected,” which means that there is a connection between each of the neurons in any given layer with each of the neurons in the next layer as shown in Figure 5.4. When there are no lateral connections between neurons in a given layer and none back to previous layers, the network is said to be a feedforward network (Tsoukalas and Uhrig, 1996). This network is said to be trained until the Least-mean-square (LMS) is minimized. The LMS is defined by the equation

$$E_p = \frac{1}{2} \sum_j^N (t_{pj} - o_{pj})^2 \quad (2.8)$$

Where t_{pj} and o_{pj} are the target and actual outputs for pattern p on node j , respectively.

2.13 Backpropagation Neural Network

Backpropagation is a systematic method for training multiple (three or more)-layer artificial neural networks. The clarification of this training algorithm by Rumelhart, Hinton, and Williams (1986) was the key step in making neural networks practical in many real-world situations². However, Rumelhart, Hinton, and Williams were not the first to develop the backpropagation algorithm. It was developed independently by Parker (1982) in 1982 and earlier by Werbos (1974) in 1974. Nevertheless, the backpropagation algorithm was critical to the advances in neural networks because of the limitations of the one- and two-layer networks discussed previously. Indeed, backpropagation played a critically important role in the resurgence of the neural network field in the mid-1980s.

Today, it is estimated that 80% of all applications utilize this backpropagation algorithm in one form or another. In spite of its limitations, backpropagation has dramatically expanded the range of problems to which neural network can be applied, perhaps because it has a strong mathematical foundation (Tsoukalas and Uhrig, 1996).

2.14 Error Back-propagation Algorithm

Error back-propagation is a learning scheme in which the error is back-propagated and used to update the weights. The algorithm employs a gradient descent method that minimizes the error between the desired and actual outputs calculated by the multilayer perceptron (Rumelhart and Hinton, 1986). Back-propagation and error adjustment continue until all examples from the training set are learnt within an acceptable overall error.

The following is the scenario for the p th pattern in a feedforward network with hidden layers.

1. The i th node in the input layer holds a value of x_{pi} for the p th pattern.
2. The net input to the j th node in the hidden layer for pattern p is

$$net_{pj} = \sum_i^N w_{ij} o_{pi} \quad (2.9)$$

Where w_{ij} is the weight from node i to node j . the output from each unit j is the threshold function, f_j , which acts on the weighted sum. In this multilayer perceptron f_j is the sigmoid function, defined as

$$f(net) = \frac{1}{(1 + e^{-knet})}; (0 < f(net) < 1) \quad (2.10)$$

Where k is a positive constant that controls the spread of the function.

3. The output of the i th node in the hidden layer can also defined as

$$o_{pj} = f_j(net_{pj}) \quad (2.11)$$

4. The net input to the k th node of the output layer is

$$net_k = \sum_j w_{kj} x_{pj} \quad (2.12)$$

Where w_{kj} is the weight values between the i th hidden layer and the k th output layer node.

5. Output of the k th node of the output layer can also be defined as

$$o_{pk} = f_k(\text{net}_k) \quad (2.13)$$

6. If E_p is the error function for a pattern, p , that is proportional to the square of difference between the actual and desired outputs for all the patterns to be learnt

$$E_p = \frac{1}{2} \sum_k^N (t_{pk} - o_{pk})^2 \quad (2.14)$$

Where t_{pk} and o_{pk} are the target and actual outputs for pattern p on node k , respectively.

In more general setting, with more than one hidden layer, weight $w_{kj}^{(i+1,i)}$ denotes the weight assigned to the link from node j in the i th layer to node k in the $(i+1)$ th layer, and x_{pj}^i denotes output of the j th node in the i th layer for the p th pattern (Mehrotra et. al., 1996).

Now it is needed to discover w , the vector consisting of all weights in the network, such that the value of E_p is minimized. One way to minimize E is based on the gradient decent method. According to this method, the direction of weight change of w should be in the same direction as $-\partial E/\partial w$.

To simplify the calculation of $-\partial E/\partial w$, the weight change in a single weight is examined. the value of $\partial E/\partial w_{kj}$ is calculated for each connection from the hidden layer to the output layer. Similarly, the value of $\partial E/\partial w_{ji}$ is calculated for each connection from the input layer to the hidden layer. The connection weights are then changed by using the value so obtained; this method is also known as the *generalized delta rule*. In brief, the following two equations describe the suggested weight changes.

$$\Delta w_{kj} \propto \left(\frac{-\partial E}{\partial w_{kj}} \right) \quad (2.15)$$

$$\Delta w_{ji} \propto \left(\frac{-\partial E}{\partial w_{ji}} \right) \quad (2.16)$$

The derivative of E with respect to a weight w_{kj} associated with the link from node j of the hidden layer to the k th node of the output layer is easier to calculate than for a weight w_{ji} connecting the i th node of the input layer to the j th node of the hidden layer. But both calculations use the same general idea—the chain rule of derivatives.

The error depends on w_{kj} only through o_{pk} , hence, for the calculations that follow, it is sufficient to restrict attention to the partial derivative of E with respect to o_{pk} and then differentiate o_{pk} with respect to w_{kj} . From equation (2.14), the following equation is obtained

$$\frac{\partial E}{\partial o_{pk}} = -2(t_{pk} - o_{pk}). \quad (2.17)$$

Since equation (2.12) represents the total input to a node k in the output layer, and equation (2.13) gives the output, o_{pk} , hence;

$$\frac{\partial o_{pk}}{\partial net_k} = S'(net_k) \quad (2.18)$$

and,

$$\frac{\partial net_k}{\partial w_{kj}} = x_j \quad (2.19)$$

Consequently, the chain rule is

$$\frac{\partial E}{\partial w_{kj}} = \frac{\partial E}{\partial o_{pk}} \frac{\partial o_{pk}}{\partial net_k} \frac{\partial net_k}{\partial w_{kj}} \quad (2.20)$$

Which gives

$$\frac{\partial E}{\partial w_{kj}} = -2(t_{pk} - o_{pk})S'(net_k)x_j \quad (2.21)$$

Next, consider the derivative of $(\partial E / \partial w_{ji})$. The error E depends on w_{ji} through net_j , also, $o_{pk} = S(net_k)$, $x_j = S(net_j)$ and

$$net_j = \sum_i w_{ji} \times x_i \quad (2.22)$$

Therefore, using the chain rule of derivatives, the following equation is obtained

$$\frac{\partial E}{\partial w_{ji}} = \sum_{k=1}^K \frac{\partial E}{\partial o_{pk}} \frac{\partial o_{pk}}{\partial net_k} \frac{\partial net_k}{\partial x_j} \frac{\partial x_j}{\partial net_j} \frac{\partial net}{\partial w_{ji}} \quad (2.23)$$

$$= \sum_{k=1}^K \left\{ -2(t_{pk} - o_{pk}) S'(net_k) w_{kj} S'(net_j) x_i \right\} \quad (2.24)$$

From equations 2.15 and 2.21, the weight changes at the outer layer of weights can be summarized as

$$\Delta w_{kj} = \eta \times \delta_k \times x_j \quad (2.25)$$

and from equation 2.13 and 2.24, weight changes at the inner layer of weights are

$$\Delta w_{ji} = \eta \times \mu_j \times x_i \quad (2.26)$$

Where η is an independent parameter known as the “learning rate,” and its value ranges between 0 and 1, and

$$\delta_k = (t_{pk} - o_{pk}) S'(net_k) \quad (2.27)$$

and

$$\mu_j = \left(\sum_k \delta_k w_{kj} \right) S'(net_j) \quad (2.28)$$

Thus, similar equations determine the change in both layers of weights proportional to the product of the input to the weight in the forward direction (x_j or x_i) and a generalized error term (δ_k or μ_j).

- The value of δ_k is proportional to the amount of error ($t_{pk} - o_{pk}$) multiplied by the derivative of the output node with respect to the net input to the output node.
- The value of μ_j is proportional to the amount of weighted error $\sum_k \delta_k w_{kj}$ (using the previous layer's δ values) multiplied by the derivative of the output of the hidden node with respect to the net input of the hidden node.

The above analysis does not make any assumption about the node activation function except that it should be differentiable. For the sigmoid function

$$S(x) = \frac{1}{(1 + e^{-x})} \quad (2.29)$$

, the derivative $S'(x) = \partial S(x) / \partial x$ is equal to

$$= S(x)(1 - S(x)) \quad (2.30)$$

Hence, if every node uses this node function, then

$$\delta_k = (t_{pk} - o_{pk})o_{pk}(1 - o_{pk}) \quad (2.31)$$

and

$$\mu_j = \sum_k \delta_k w_{kj} x_j (1 - x_j) \quad (2.32)$$

Thus, the weight updating for every individual weight w_{ij} , between the output layer and hidden layer, can be done using the following formula

$$w_{new} = w_{old} + \eta * (\delta_k * x_j)_{w_{old}} \quad (2.33)$$

and, for the weights between the hidden layer and the input layer, the following formula can be used

$$w_{new} = w_{old} + \eta * (\mu_j * x_j)_{w_{old}} \quad (2.34)$$

In brief, there are two phases of back-propagation algorithm;

1. Present input patterns, propagate activation through output to generate o_{pk} for each output unit. Then compare the output against the desired output, to calculate the error signals.
2. Pass error backwards through the network so as to recursively compute error signals, and use them to update weights of the previous layers.

However, back-propagation may lead the weights in a neural network to a local minimum of the mean-square-error (MSE), possibly substantially different from the global minimum that corresponds to the best choice of weights. This problem can be particularly bothersome if the “error surface” (plotting MSE against network weights) is highly uneven or jagged, Figure 2.15.

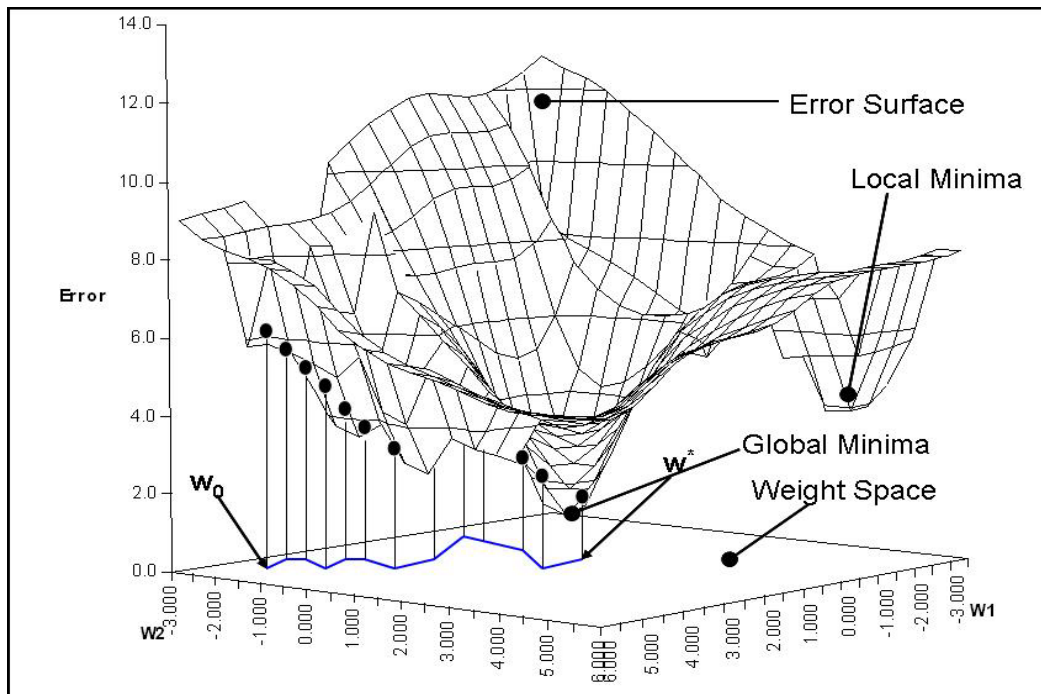


Figure 2.15 Graph of jagged error surface of error vs. weights (Saha, 2003)

To avoid getting stuck in the local minimum, another term can be added to the weight updation formula; this term is called the “*momentum*”.

$$w_{n+1} = w_n + \eta * (\delta_k * x_j)_{w_n} + \alpha * (w_n - w_{n-1}) \quad (2.35)$$

Where, α is the momentum coefficient and its value ranges between 0 and 1 (typically about 0.9).

2.15 Neural Network Design and Architecture

Many important issues, such as determining how large a neural network is required for a specific task, and how many nodes and layers should be included in the network design, are solved in practice by trial and error. For instance, with too few number of nodes, the network may not be powerful enough for a given learning task. With a large number of nodes (and connections), computation is too expansive. Neural learning is considered successful only if the model can perform well on test data on which the network has not been trained.

2.15.1 Training Parameters

The training parameters, the learning rate and the momentum (typical values between 0 and 1) have a significant effect on the training process. A large value of learning rate will lead to rapid learning but the weight may then oscillate, while low values imply slow learning and it takes long time to converge to global minima. A high value of a momentum coefficient allows one to choose higher value of learning rate. In fact, there is no clear consensus on any fixed strategy in choosing the proper values of the training parameters. However, in practice, the best choice can be achieved by trial and error, which leads to the minimum prediction error (Tsoukalas and Uhrig, 1996).

2.15.2 Data Scaling and Representation and Weight Initialization

Scaling has the advantage of mapping the desired range of a variable (with range between the minimum and maximum values) to the full “working” range of the network input and output. Scaling of the variable between 0.1 and 0.9 is often used to limit the amount of the sigmoid activation function used in the representation of the variables in order to avoid “network paralysis” in the training process.

In addition to that, the data is represented randomly to the neural network for each training cycle, which means the data is fedforward to the network in different order for each epoch. This randomization of the input patterns helps in speeding up the training process and takes less time to converge to global minima.

Moreover, training is generally commenced with randomly chosen weight values. Typically, the weight chosen are (between -1.0 and 1.0 or -0.5 to +0.5), since large weight magnitudes may drive the output of layer 1 nodes to saturation, requiring large amounts of training time to emerge from the saturated state (Mehrotra et. al., 1996).

CHAPTER 3

RESEARCH OBJECTIVES, SITE DESCRIPTION AND FIELD WORK

3.1 Research Objectives

The scope of the current study conducted at Tunçbilek coal mine covers the following aims:

1. Assessment of the present situation by monitoring the ground vibrations induced by bench blasting performed at the mine site in order to evaluate the risk of structural damage at Tunçbilek Township.
2. Establishment of, statistically, a reliable empirical formula from the relationship between the scaled distance and the recorded peak particle velocity and determine the slope of the attenuation curve for this site, so that the PPV can be predicted at any desired location using this formula.
3. Determination of maximum allowable charge weights per delay with respect to distances to the Tunçbilek Township based on USBM criteria.
4. Investigation the potential use of neural networks approach in predicting the peak particle velocity induced from Panel BYH.
5. Comparison between prediction of peak particle velocity by statistical and neural networks approaches.

3.2 Test Site Description

Tunçbilek open-pit coal mine is operating by Western Lignite's Co., which is a subsidiary of the state-owned Turkish Coal Enterprise (TKI). Western Lignite's BYH Panel is operating approximately 3750 m away from Tunçbilek township of Tavşanlı county of Kütahya Province in western region of Turkey, Figure 3.1.



Figure 3.1 Map of Turkey shows Tunçbilek township of Tavşanlı county of Kütahya Province.

The removal of the overburden at BYH panel is carried out by a contractor. The mine operation of stripping the overburden will continue for two years period of time in order to reach the coal layers.

The contractor uses the drilling and blasting means so as to loosen the rock material, and the power shovels and trucks to remove the blasted material to dumping area. These operations are carried out in two shifts a day, 11 hours for each. The present extent of the BYH working area is 700 m long by 600 m wide of overburden being removed in two benches, Figure 3.2.



Figure 3.2 General view of the mine's working area, BYH Panel.

3.3 Regional Geological Settings

The regional geological setting of Tunçbilek Coal Region, can be divided into three main groups. These are:

- 1) Pre-Neogene basement rocks,
- 2) Neogene sequences, and
- 3) Quaternary units.

- 1) Basement rocks are exposed extensively in the western, south-eastern and northern parts of the area and surround the Neogene sequences. The dominant lithology of the basement rocks is serpentinite. The age of the basement rocks is assigned as pre-Cretaceous.
- 2) The Neogene sequences are composed of four formations; these are, from bottom to top, Beke formation, Tunçbilek formation, Saruhanlar formation and Karaköy volcanics;
 - Beke formation is represented by dark green marls with intersections of black, thin coal measures of no economic value. The age of the Beke formation is assigned as Middle Miocene based on the determination of the pollen analysis from coal layers.
 - Tunçbilek formation conformably overlies the Beke formation. The formation is divided into two units as Demirbilek and Gurağaç members. Demirbilek member mainly consists of clay, marl and coal with some siltstone, conglomerate and limestone interbeddings. The coal seam, reaching to 14m, is exposed either as single bed or exists as intercalations within clay-marl layers.

The marl layers above the coal contain considerable amount of Ostracpoda. The age of the formation based on ostracpoda and other pollens is assigned as Late Miocene. Gurağaç formation is exposed around Gurağaç village. The member consists of conglomerates, sandstone, siltstone and clay. Maximum observable thickness of the member is about 75 meters. The age of Late Miocene is assigned to the Gurağaç member considering the relative position of the member.

- Saruhanlar Formation is exposed in a wide area between Tunçbilek, Domaniç, Karaköy and Ömerler, and west of Saruhanlar village. The formation consists basically of conglomerates, sandstones, marls and tuff.

Thin limestone intercalations are also common. Total thickness of the formation is about 300 m. An early Pliocene age is assigned considering the age of underlying Upper Miocene sequences.

- Karaköy volcanics are extensively exposed around Karaköy village. These volcanics are basaltic and andesitic in composition. Microscopic analysis of thin section prepared from these volcanics revealed the presence of orthopyroxene, clinopyroxene and plagioclase. Olivine also exists in minor amount.

- 3) Quarternary Units are the youngest units exposed in the area. They are formed along the major streams and their tributaries. Beke River is the main stream along which Quarternary deposits are accumulated.

3.4 Rock Characterizations and Geological Observations at BYH Panel

Intensive geomechanical studies on the basis of field and laboratory tests were conducted by the Department of Mining Engineering at the Middle East Technical University in Ankara, Turkey (Paşamehmetoğlu, et. al., 1988). In these studies, some of the mechanical and physical properties of rock units were determined, Table 3.1, and Table 3.2.

In-situ measurements of P-wave (propagation wave) velocity also were carried out by the same university (METU), and the results are shown in Table 3.3.

Table 3.1 Physical and mechanical properties of Marl of Tunçbilek BYH Panel, from core samples (Paşamehmetoğlu, et. al., 1988)

Rock Type	Uniaxial Compressive Strength (MPa)	Young's Modulus (10^3 MPa)	Poisson's Ratio	Cohesion (MPa)	Internal Friction Angle (degree)	Natural Density (g/cm^3)	Moisture %	Hardness	Core Indenter Index	Indirect Tensile Strength (MPa)	Slake Durability Index %	Toughness ($N-cm/cm^3$)
Marl	(16.18-24.32) 18.92	4.835	0.28	5.88	37	2.043	7.970	38	2.38	5.23	0.994 0.991	1.13

50

Table 3.2 Rock mass properties of Tunçbilek BYH Panel (Paşamehmetoğlu, et. al., 1988)

Discontinuity Type	Position	Continuity (average)(m)	Spacing (m)	Roughness	Filling Material	Rebound Hardness	Notes
Bedding	Horizontal	–	0.7	–	–	–	–
First Joint Set	Perpendicular to Bedding	Horizontal 0.6 Vertical 0.7	0.6	Smooth Planar	No	Average 44.88 St. Deviation 3.44	1 st Joint Set is dominant compared to 2 nd Joint Set
Second Joint Set	Perpendicular to Bedding	Horizontal 0.6 Vertical 0.7	0.5	Smooth Planar	No	Average 44.88 St. Deviation 3.44	

Geotechnical description: Gray coloured, fresh marl, occasionally slightly to moderately weathered zone are present. Bedding plane thickness varies between 0.3 to 0.6m. After blasting, the average size boulders in the much pile is $0.3m \times 0.4m \times 0.55m$ ($0.07m^3$), and the maximum size of boulders is $1.2m \times 1.2m \times 1m$ ($1.44m^3$).

Table 3.3 In-situ measurements of P-wave velocity, Tunçbilek BYH Panel (Paşamehmetoğlu, et. al., 1988)

Rock Type	Formation Description	P-wave Velocity (m/sec)	Thickness (m)
Marl	- Fresh, occasionally slightly weathered. - Bedding thickness 30-150cm (Average 70cm)	V₁ = 703	3.0
	- 1 st Joint Set Spacing 40-80cm, continuity 30cm to few meters. - 2 nd Joint Set Spacing 100cm, continuity 0.3-100cm	V₂ = 1900 - 2027	>3.0

These rock properties were taken into account, together with observations on actual blasting activities, to determine the excavation class of encountered rock units in the mine. These values confirm that drilling and blasting is an unavoidable operation for the rock units.

Integrated columnar section of rock units existing in the Tunçbilek coal mine BYH Panel provided from TKI-GLI Company, Figure 3.3.

Many faults, joint sets, and bedding planes are existing in the blasting area and in the area between Panel BYH and Tunçbilek township. Most of the faults are dipping to the north and some others dipping to the east. Existence of the fault planes may cause some reflection and refraction in seismic wave propagation.

Age	Thickness (m)	Lithology	Description
Neogene	2.00		Soil and Planted-Cover
	50 – 60		Marl: Gray coloured, fresh marl, with limestone interactions.
	10 – 15		Coal: Brown-black Lignite, clayey with some siltstone.
Pre-Cretaceous	>3.00		Basement Rock: Green, altered serpentine.

Figure 3.3 Integrated columnar section of rock units existing in The Tunçbilek coal mine BYH Panel

3.5 Blasting Parameters

The blast design that is currently being used for bench blasting at the mine site is based on the classical blast parameters. These parameters are setup

by the firing crew members of the contractor firm. The parameters are including; bench height, hole diameter, hole depth, burden, spacing, and stemming. Type of explosives, firing pattern and sequences, and amount of charge per delay are also taken into account. Table 3.4 shows the blasting design parameters followed in practice for the blasts in removal of overburden rock materials.

Table 3.4 Blast design parameters applied at the mine.

No.	Parameter	Value
1	Bench Height (m)	6 – 8
2	Hole Diameter (mm)	152.4
3	Subdrilling (m)	1
4	Hole Length (m)	7 – 9
5	Burden (m)	4 – 6
6	Spacing (m)	4 – 6
7	Stemming (m)	3 – 3.5
8	Type of Explosive	ANFO
9	Charge/hole (kg/hole)	25 - 75
10	Hole Inclination	Vertical
11	Initiation System	Electric Delay Detonator

Moreover, the blasting geometry applied in the mine is shown in Figure 3.4.

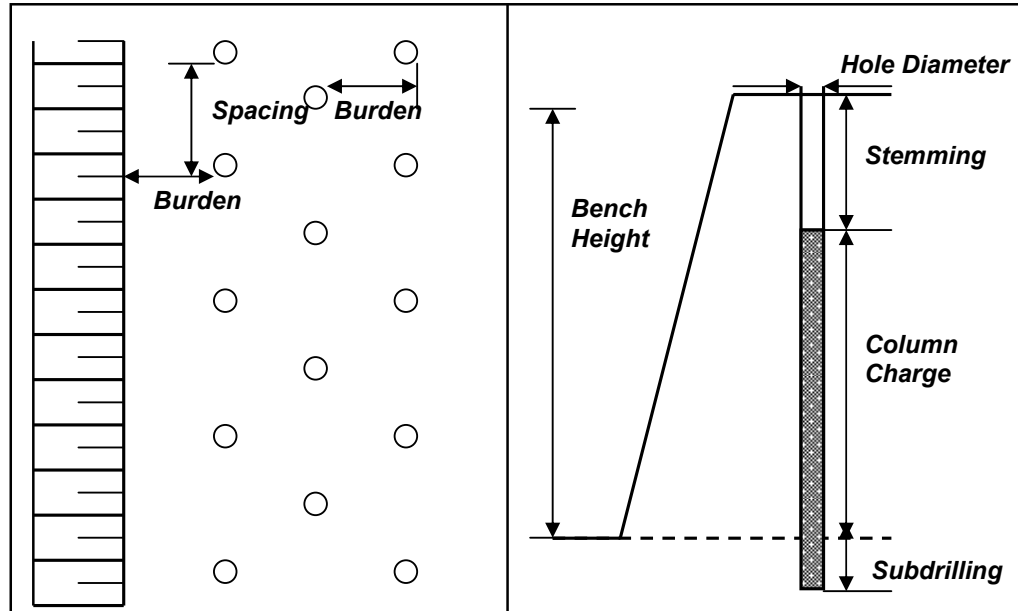


Figure 3.4 Blasting geometry applied at Tunçbilek Coal Mine, Panel BYH.

3.6 The Field Work

Within the scope of the current study, ground vibrations induced by bench blasting were measured to estimate the damage risk and site-specific attenuation. In order to produce a site-specific propagation equation and then to predict peak particle velocity as well as to find the maximum allowable charge for this site, bench blasting field studies were conducted over a period of four months.

In Tunçbilek coal mine, Panel BYH, the removal of the overburden is being done by a contractor. The blasting operations are performed as a round-blast, and it will continue for two years period of time to reach the coal layer.

After exploring the situation at the mine site, two paths toward Tunçbilek township were determined. The blasting events were monitored along two parallel lines, A and B, toward the township. Along the first line (A), which was established in the beginning stage of monitoring, the vibration components were recorded at arbitrary chosen locations (stations; T2, T3, T4, T5, T6). As the stripping operation advanced in a direction perpendicular to the path toward the township, a second line (B), parallel to the first one, was needed in order to monitor the blasting events. For this line the blasting events were recorded at; T3A and T6A stations, Figure 3.5.

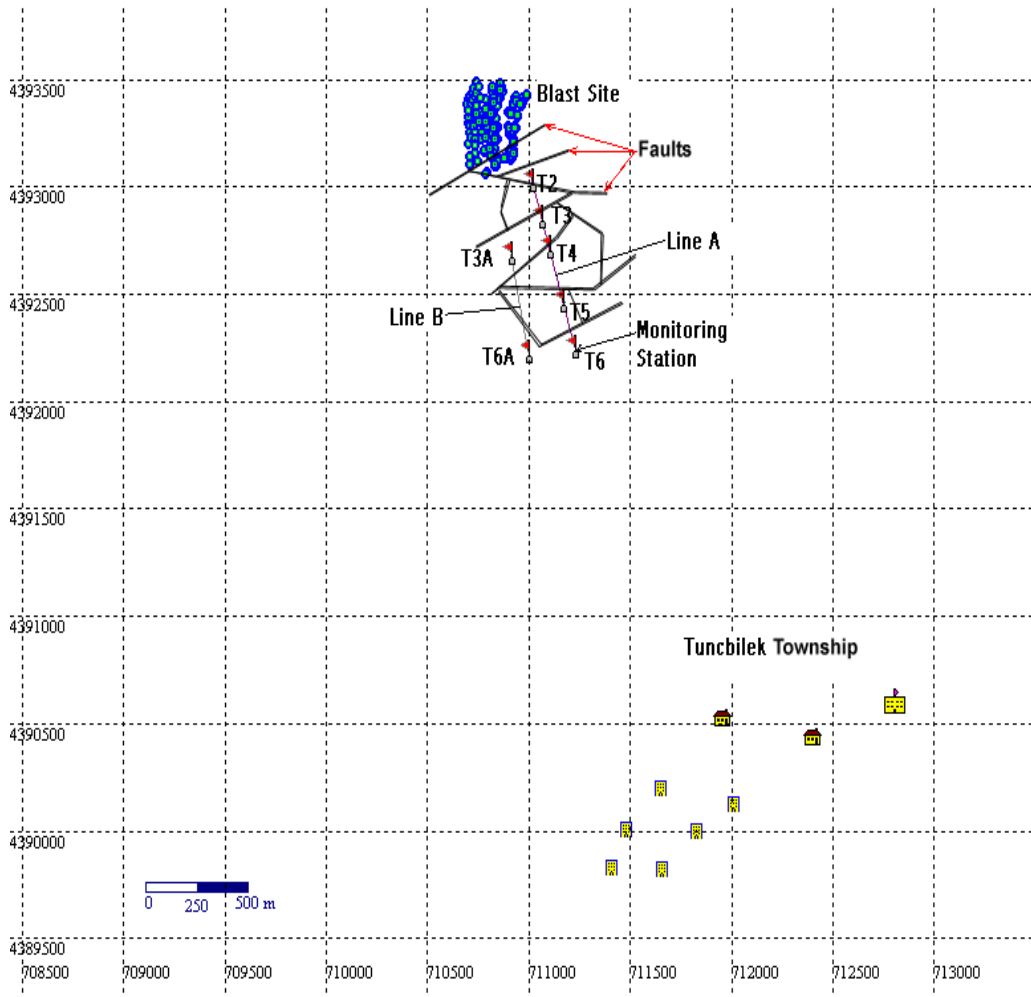


Figure 3.5 Map of blast site, monitoring stations, and the Tunçbilek township.

The distances from the blasting site to the monitoring stations were measured carefully by means of hand-held GPS (Global Positioning System) instrument, whereas, the ground vibration components were recorded by using the White Mini-Seis II Model vibration instrument, as shown in Figure 3.6.

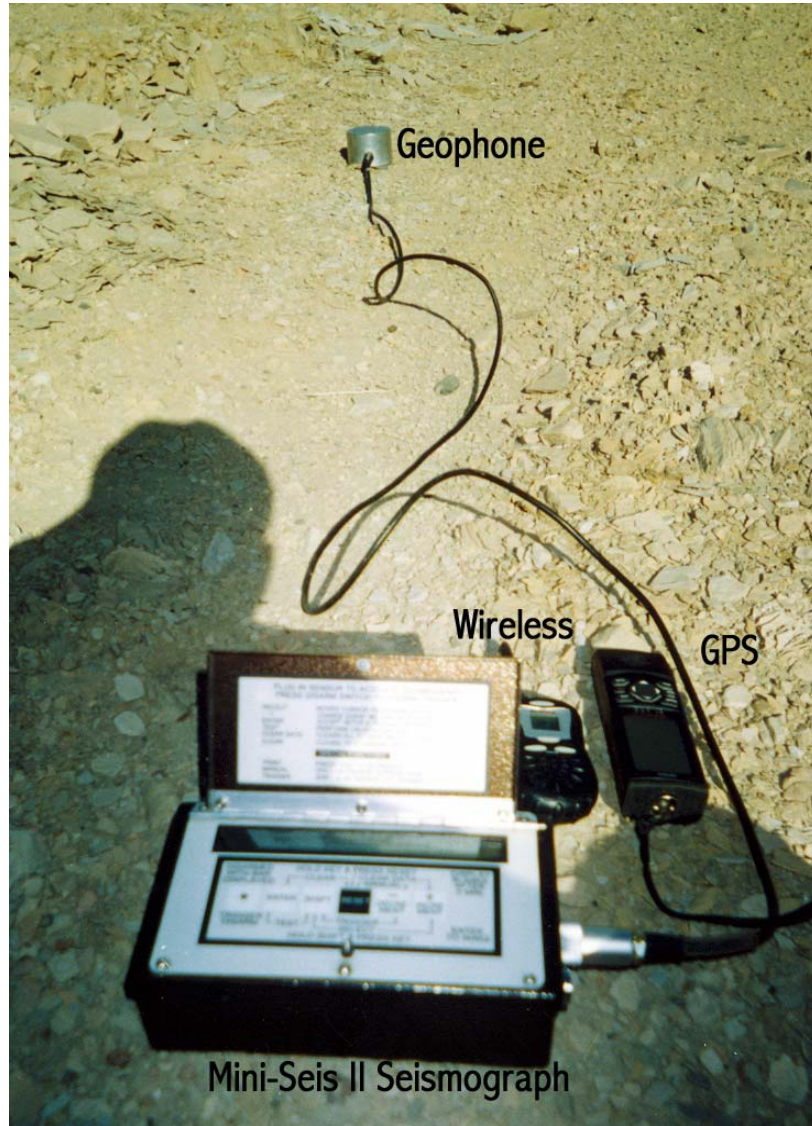


Figure 3.6 Instruments used in ground vibration measurements.

The specifications of the seismograph are summarized below.

- 1- The model is portable seismograph for monitoring and recording seismic and sound signals produced from blasting.
- 2- It can be used for a single shot or a continuous mode.
- 3- It basically consists of three geophones (transversal, vertical and longitudinal) positioned perpendicular to one another.
- 4- A microphone rated to at least 160 dB can be connected to the seismograph.
- 5- Mini-Seis II can record frequencies from 2 to 250 Hz.
- 6- The full waveform signature is stored in solid state memory for up to 341 events.
- 7- Seismic recording range selected is from 0.125 to 64 mm/sec.
- 8- With a full charged battery, the instrument will operate from 7 to 10 days.
- 9- Maximum record duration is 9 seconds.

The instrument records peak values of particle velocity in three directions, transverse, vertical and longitudinal (radial) as well as the time-histories of seismic vibrations. The seismograph also has its own data analysis software, which provides the easiest way to access and analyze recorded data. This program was installed in a portable computer brought to the mine site, so the recorded data could be downloaded to the computer and analyzed day by day. An example of the waveform time-history of a blasting event is given in Figure 3.7.

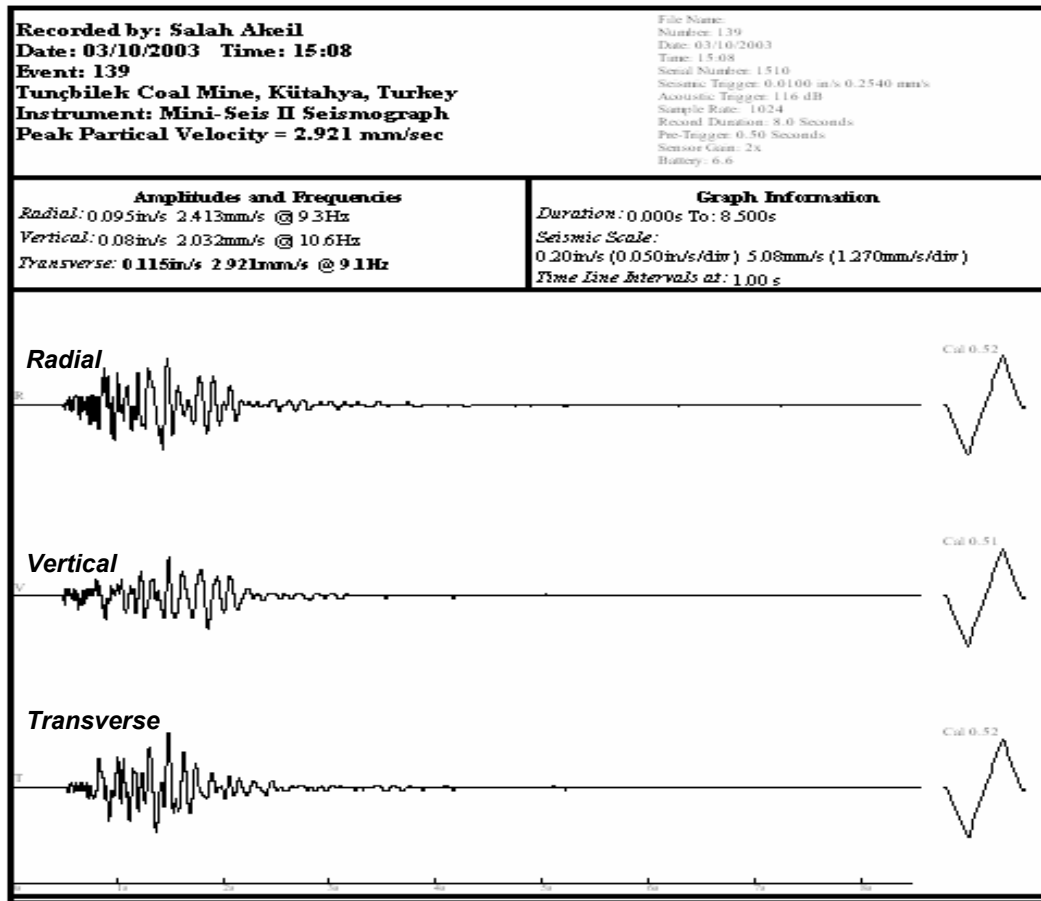


Figure 3.7 Waveforms of a round-blast event.

The blasting geometry applied in the mine and the charging process was designed by blasters from the company, and the vibration measurements were applied to this blasting geometry. In other words, the blasting pattern (borehole length, spacing and burden) as well as the amount of charge to be fired at the same delay period, were the only data obtained from the blast site, which would be the basis of monitoring. However, these data were measured carefully for each blast, Figure 3.8.



Figure 3.8 Measurement of the blasting parameters applied at the mine.

CHAPTER 4

STATISTICAL ANALYSES AND DISCUSSIONS

4.1 Measurement Results

The data pairs obtained from the round blast operations performed at the mine, which were recorded along two parallel lines A and B from the blasting site toward the village, are presented in Table A.1 (Appendix A). In this table, events codes, dates of monitoring, stations codes, amount of charge per delay (W_d , kg), absolute distance (D , m), calculated scaled distance (SD , $m/kg^{0.5}$), amplitudes of vibration components for radial (RPV, mm/sec), vertical (VPV, mm/sec), and transverse (TPV, mm/sec) directions as well as the peak particle velocity (PPV, mm/sec) are given respectively. The peak vector sum (PVS, mm/sec) is also presented in this table. The last three columns show the dominant frequency values (F_R , F_V , F_T , Hz) calculated by FFT analysis for radial, transverse, and vertical vibration components, respectively.

During the trips to the mine site at different dates totally 74 blasting events were monitored, 64 events were recorded along Line A and 10 events along Line B. Among these events, 60 were round-blasts and 14 were single-hole blasts (performed under request).

The data pairs for single hole blasts are presented in Table A.2 (Appendix A). The absolute measurement distances ranges between 100 and 1250 meters. The maximum amount of charge per delay used was found to be 402.5 kg at

30 milliseconds delay interval. Note that, in determining the maximum charge per delay, the amount of dynamite used as priming has been taken into consideration, and this added to the amount of ANFO. The scaled distance ranges between 13.235 to 143.858 m/kg^{0.5}.

In addition to that, the lowest peak particle velocity recorded was 0.381 mm/sec at absolute distance equal to 1210 m, whereas, the highest recorded value was 23.876 mm/sec at absolute distance of 100 m.

4.2 The Adopted Site-specific Criterion

In the predictions of ground vibration, although a lot of empirical relationships have been established and used by different researchers in the past, the site-specific technique is still implemented for each different site. The most reliable relationships are those that accept the scaled distance and particle velocity as a basis. The scaled distance is defined by equation below:

$$\mathbf{SD = D/W_d^{0.5}} \quad (4.1)$$

where SD is the scaled distance and D is the absolute distance between the shot and the station (m), and W_d is the maximum charge per delay (kg).

The peak particle velocity (PPV) is determined from the following formula;

$$\mathbf{PPV(mm/sec) = K * (SD)^{-\beta}} \quad (4.2)$$

which has extensively been used in practice, and where K is the ground transmission coefficient and β is a specific geological constant.

On the other hand, in order to establish a best fit relationship between the peak particle velocity and the scaled distance, simple regression analysis has to be performed using the obtained data pairs from the blasting events.

4.3 Statistical Analysis of Results

4.3.1 Round Blasts Events

When statistical analyses techniques are applied to the measured round blasts vibration data pairs, peak particle velocity, and scaled distance will give a site-specific velocity attenuation equation. The relationships between peak particle velocity and the scaled distance for the pairs of data for all velocity components are shown by the Figures 4.1, 4.2, 4.3, and 4.4. These figures were plotted by means of Excel program from Microsoft.

The regression analysis was done individually for all particle velocity components, and it was found that the highest correlation coefficient was determined from the relation between peak particle velocity (PPV) and scaled distance (SD), ($R^2 = 0.8056$); Whereas the lowest correlation coefficient was determined from the relation between the transverse particle velocity and scaled distance as ($R^2 = 0.7218$).

Since the peak particle velocity (PPV) is the most critical velocity to structural damage, then it should be taken into account. The attenuation equation of the relation between the PPV and the scaled distance (SD), and the correlation coefficient, which determined from Figure 4.4, are as follows:

$$\text{PPV(mm/sec)} = 300.87 * (\text{SD})^{-1.2539} \quad (R^2 = 0.8056) \quad (4.3)$$

The R-square quantity is a basic measure of the quality of fit. In this case, a value of 0.8056 indicates that 80.56% of the PPV variability is explained by the linear regression. The ground transmission coefficient (the intercept) ($K=300.87$), and the specific geological constant ($\beta=-1.2539$) (the slope) are obtained from the linear regression in the log-log transformed space.

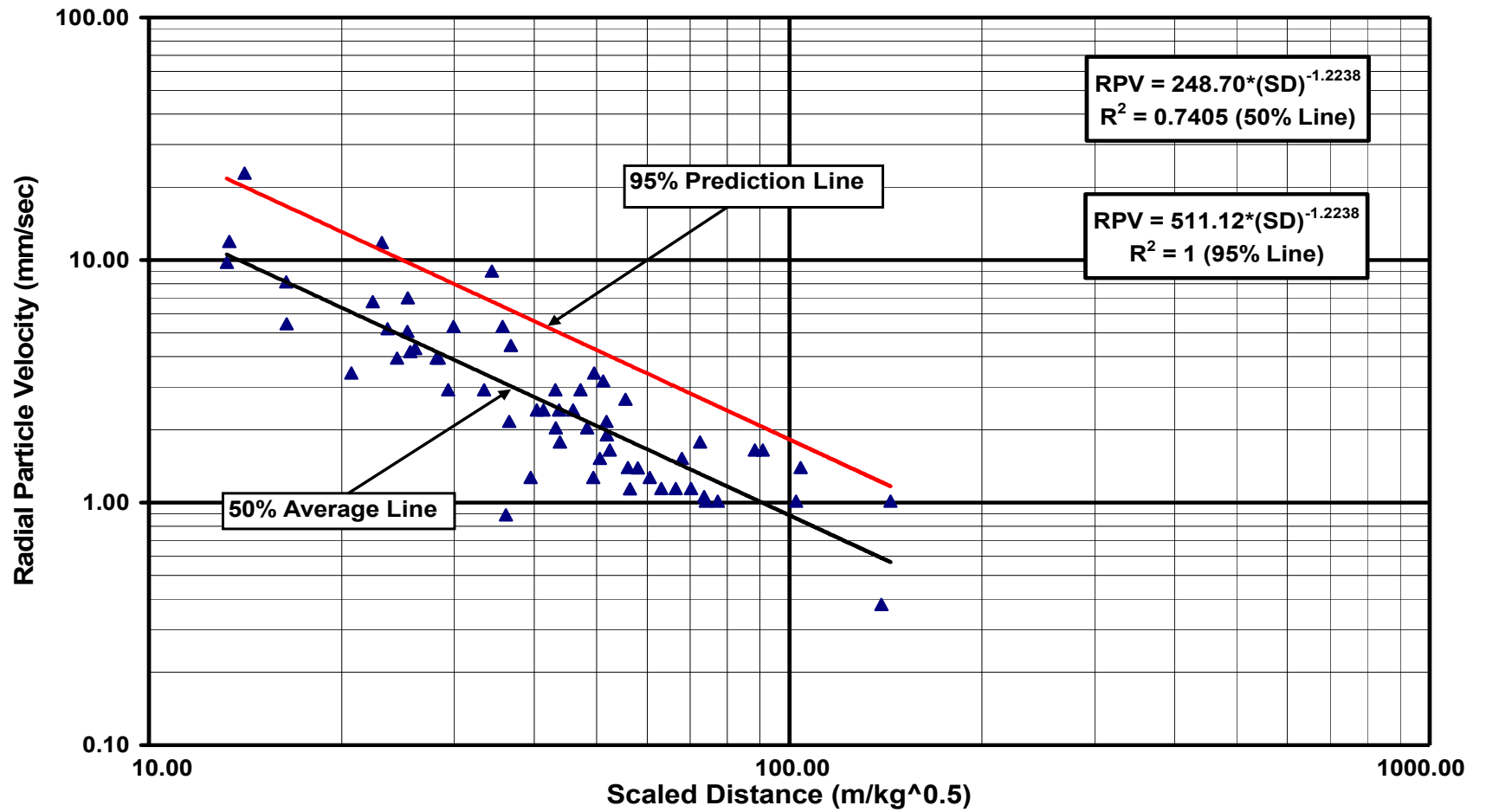


Figure 4.1 Radial particle velocity versus scaled distance, round-blast (at 50% and upper 95% prediction limits)

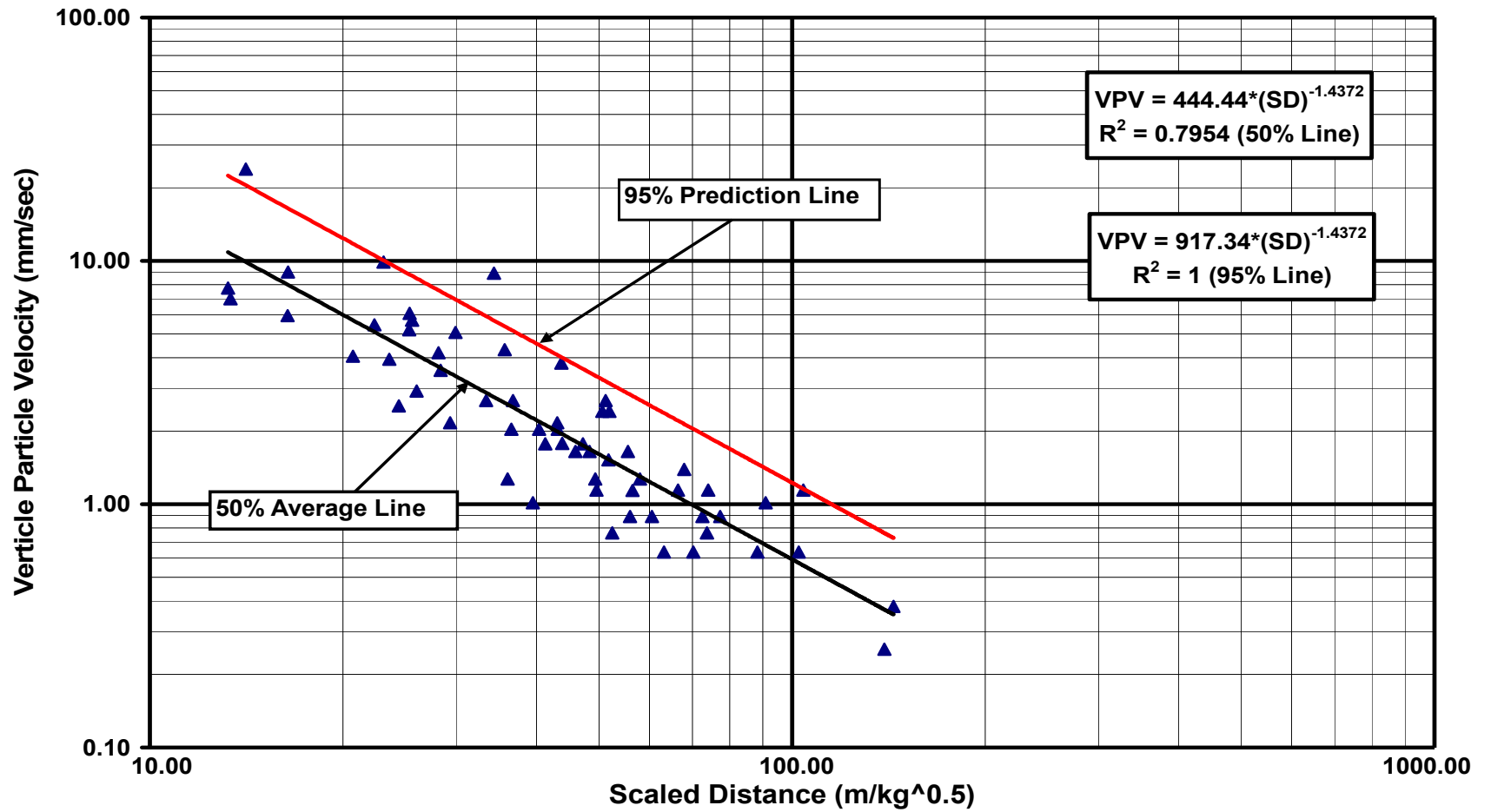


Figure 4.2 Vertical particle velocity versus scaled distance, round-blast (at 50% and upper 95% prediction limit)

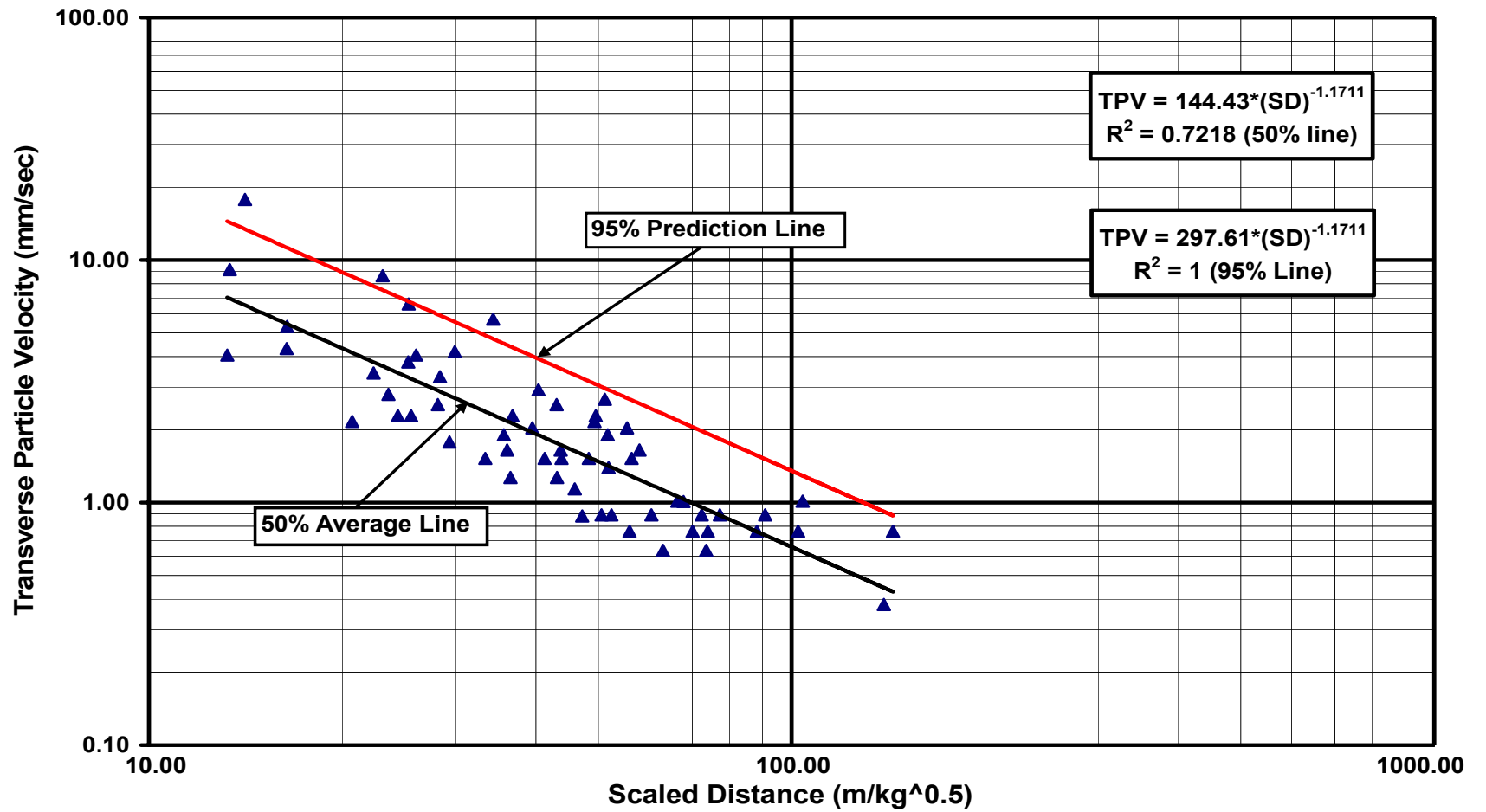


Figure 4.3 Transverse particle velocity versus scaled distance, round-blast (at 50% and upper 95% prediction limit).

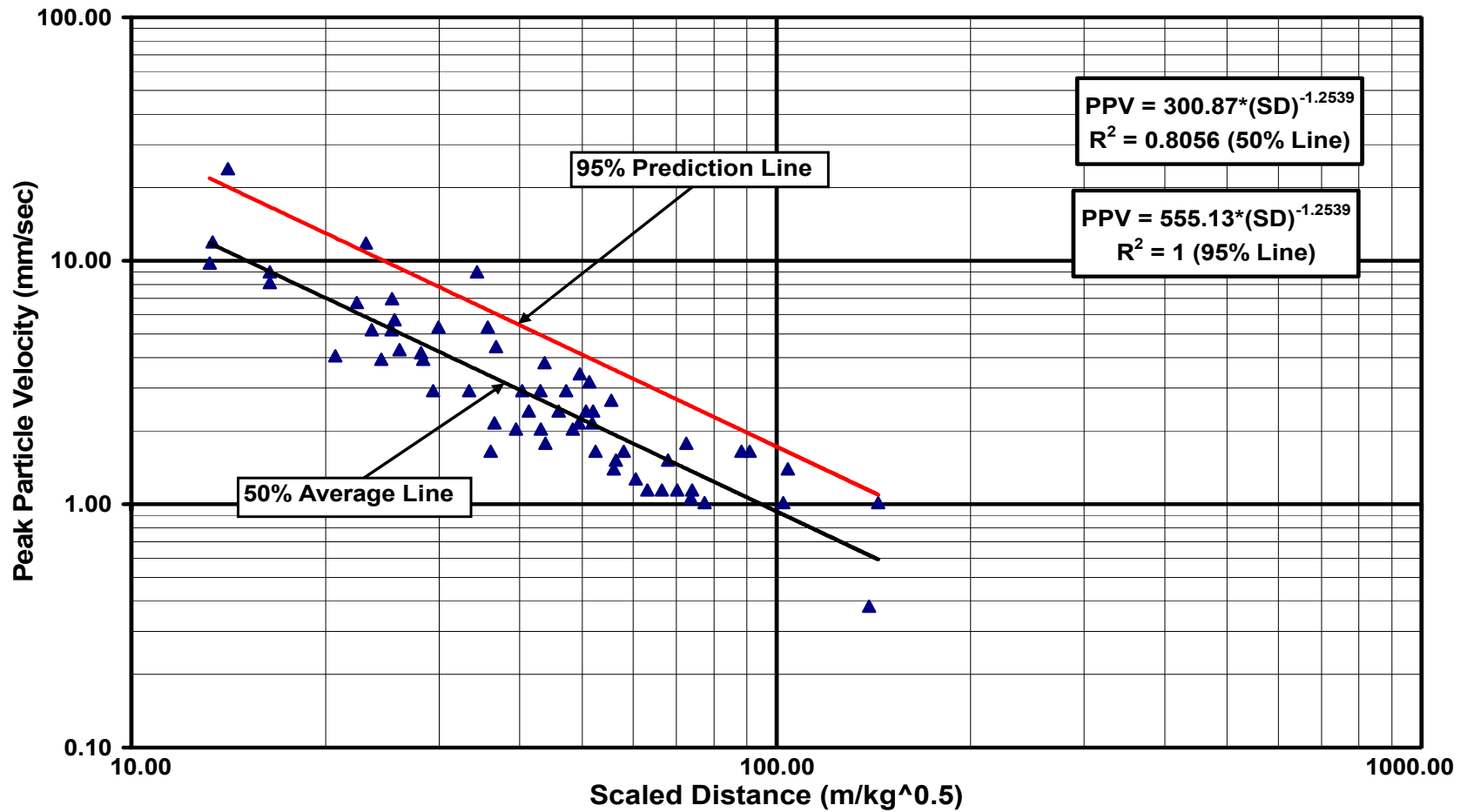


Figure 4.4 Peak particle velocity versus scaled distance, round-blast (at 50% and upper 95% prediction limit)

The relations between the particle velocity and the scaled distance for all particle velocities, RPV, VPV, TPV, and PPV are presented in Table 4.1.

Table 4.1 Coefficients of attenuation equation for all vibration components, round blasts.

Site factors	RPV	VPV	TPV	PPV
K (intercept)	248.70	444.44	144.43	300.87
β (slope)	-1.2238	-1.4372	-1.1711	-1.2539
R-Sq, %	74.05	79.54	72.18	80.56

Moreover, when a plot of the peak particle velocity against the absolute distance is drawn for the data recorded at the recording stations, it can be observed that the particle velocity components attenuated gradually with the distance as shown in Figure 4.5.

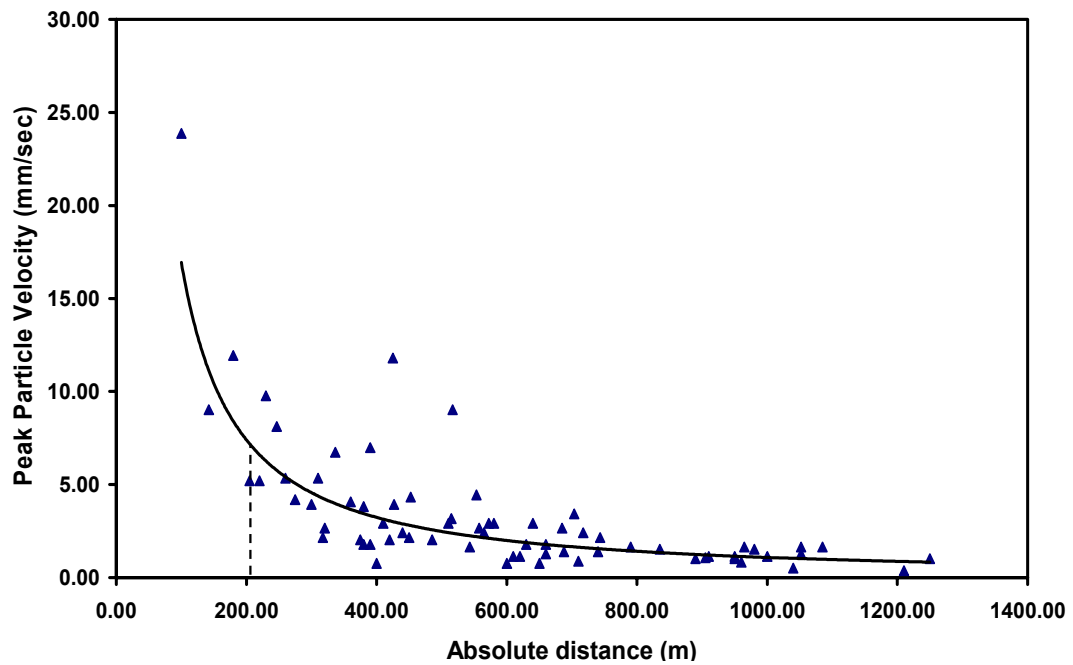


Figure 4.5 Peak particle velocity versus distance

This graph also shows that beyond 200 m, peak particle velocity falls well below the limit of 12.70 mm/sec (0.5 in/sec) as recommended by USBM in RI 8507 report, 1980. However, there may occur other type of hazard due to flyrock beyond 200 m.

4.3.2 Single Hole Events

The attenuation relationships between the peak particle velocity and the scaled distance for the single hole blasts were determined. These relationships are plotted in Figures 4.6, 4.7, 4.8, and 4.9. The regression analysis showed that the correlation coefficient, determined from the relation between peak particle velocity (PPV) and scaled distance (SD), is found to be 0.7754. The attenuation equation of the relation between the PPV and the scaled distance (SD), and the correlation coefficient, which determined from Figure 4.13, are as follows:

$$\text{PPV(mm/sec)} = 346.45 * (\text{SD})^{-1.3105} \quad (\text{R}^2 = 0.7754) \quad (4.4)$$

The R-square quantity is a basic measure of the quality of fit. In this case, a value of 0.7754 indicates that 77.54% of the PPV variability is explained by the linear regression. The ground transmission coefficient (the intercept) (**K=346.45**), and the specific geological constant (**β=-1.3105**) (the slope) are obtained from the linear regression in the log-log transformed space. The relations between the particle velocity components and the scaled distance for all particle velocities, RPV, VPV, TPV, and PPV are presented in Table 4.2.

Table 4.2 Coefficients of attenuation equation for all vibration components, single hole blasts

Site factors	RPV	VPV	TPV	PPV
K (intercept)	228.80	1114.90	66.24	346.45
β (slope)	-1.2341	-1.6621	-1.036	-1.3105
R-Sq, %	69.42	87.90	77.79	77.54

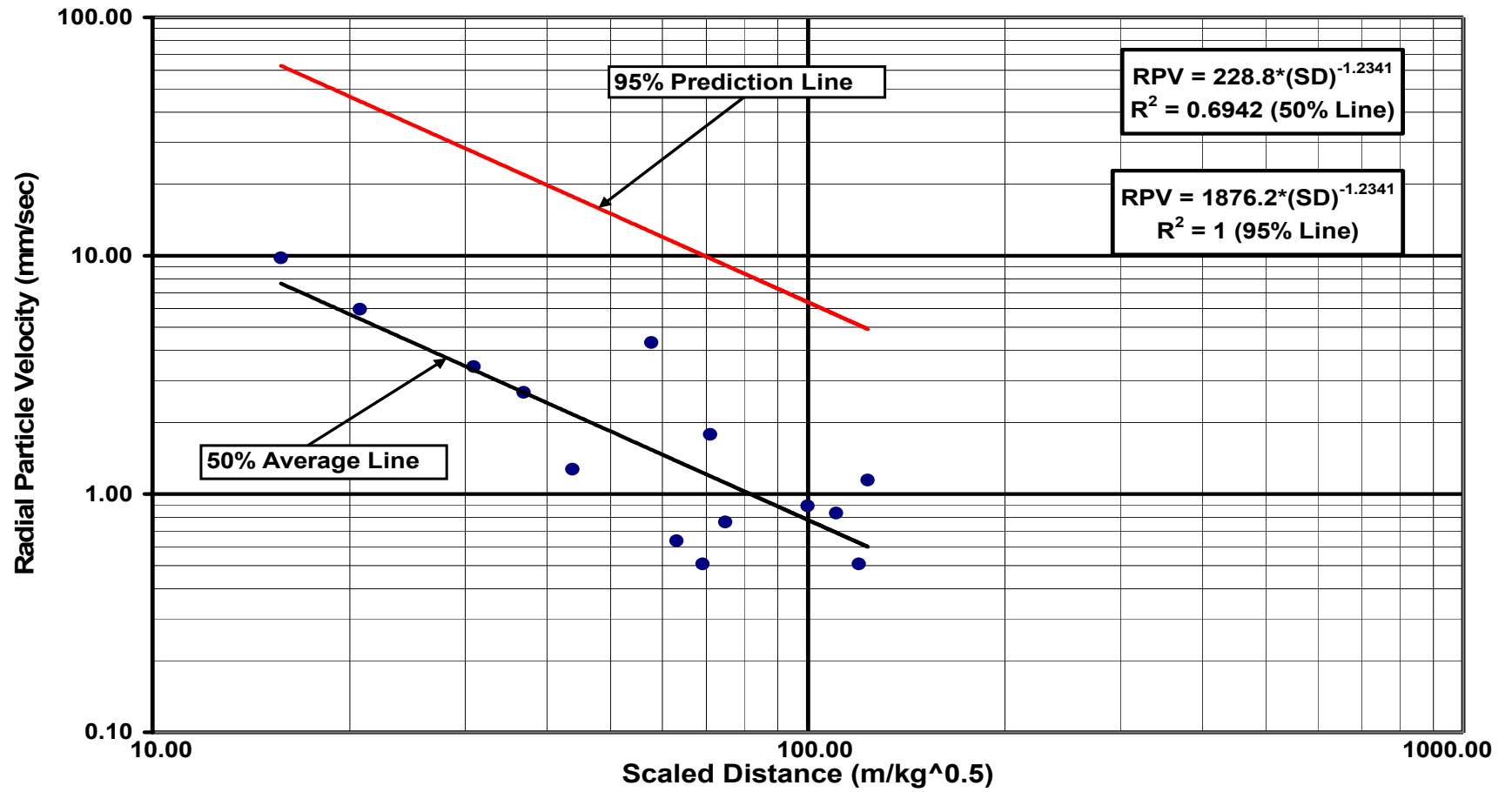


Figure 4.6 Radial particle velocity versus scaled distance, single-hole blast (at 50% and upper 95% prediction limits)

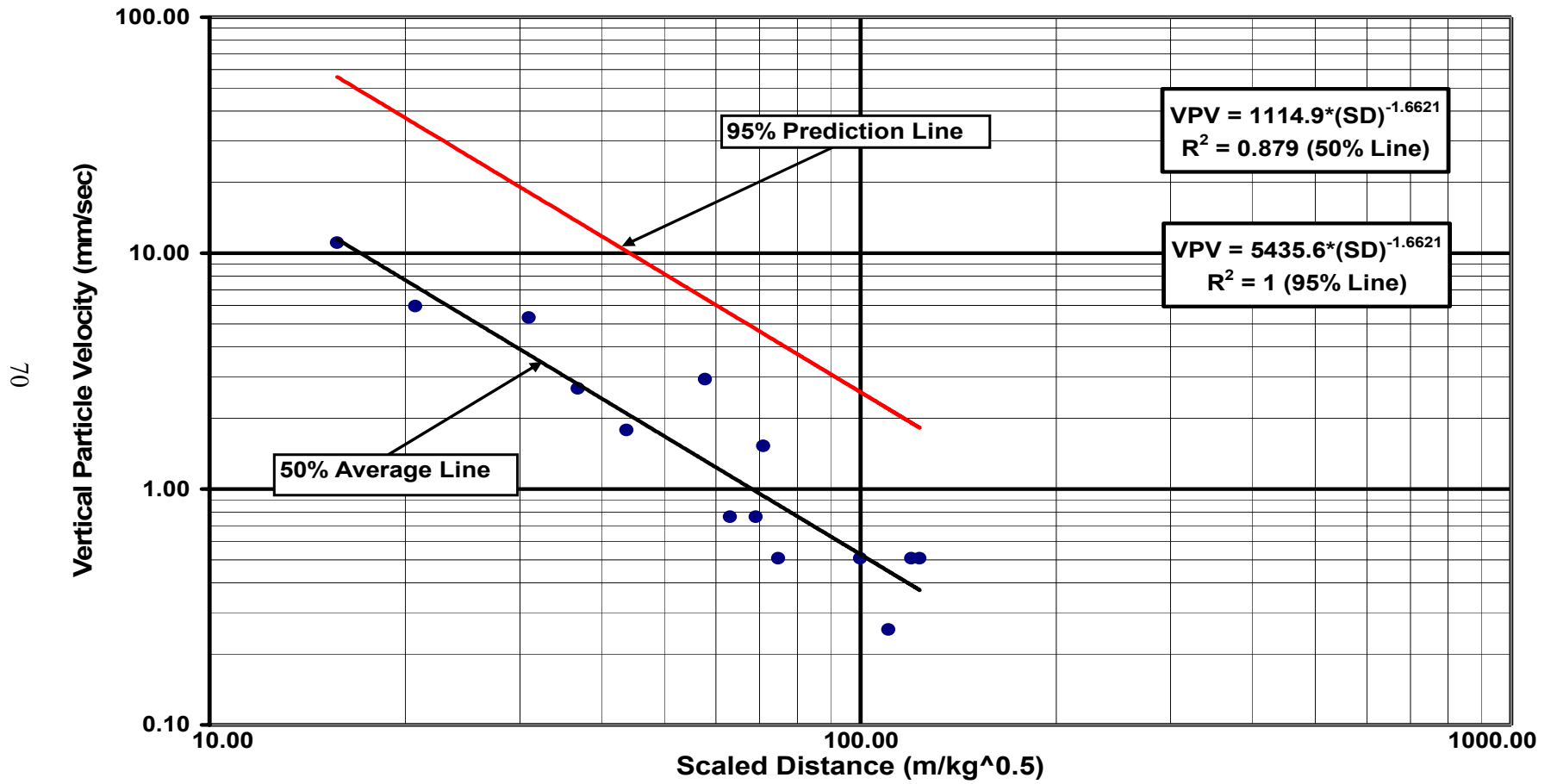


Figure 4.7 Vertical particle velocity versus scaled distance, single-hole blast (at 50% and upper 95% prediction limits)

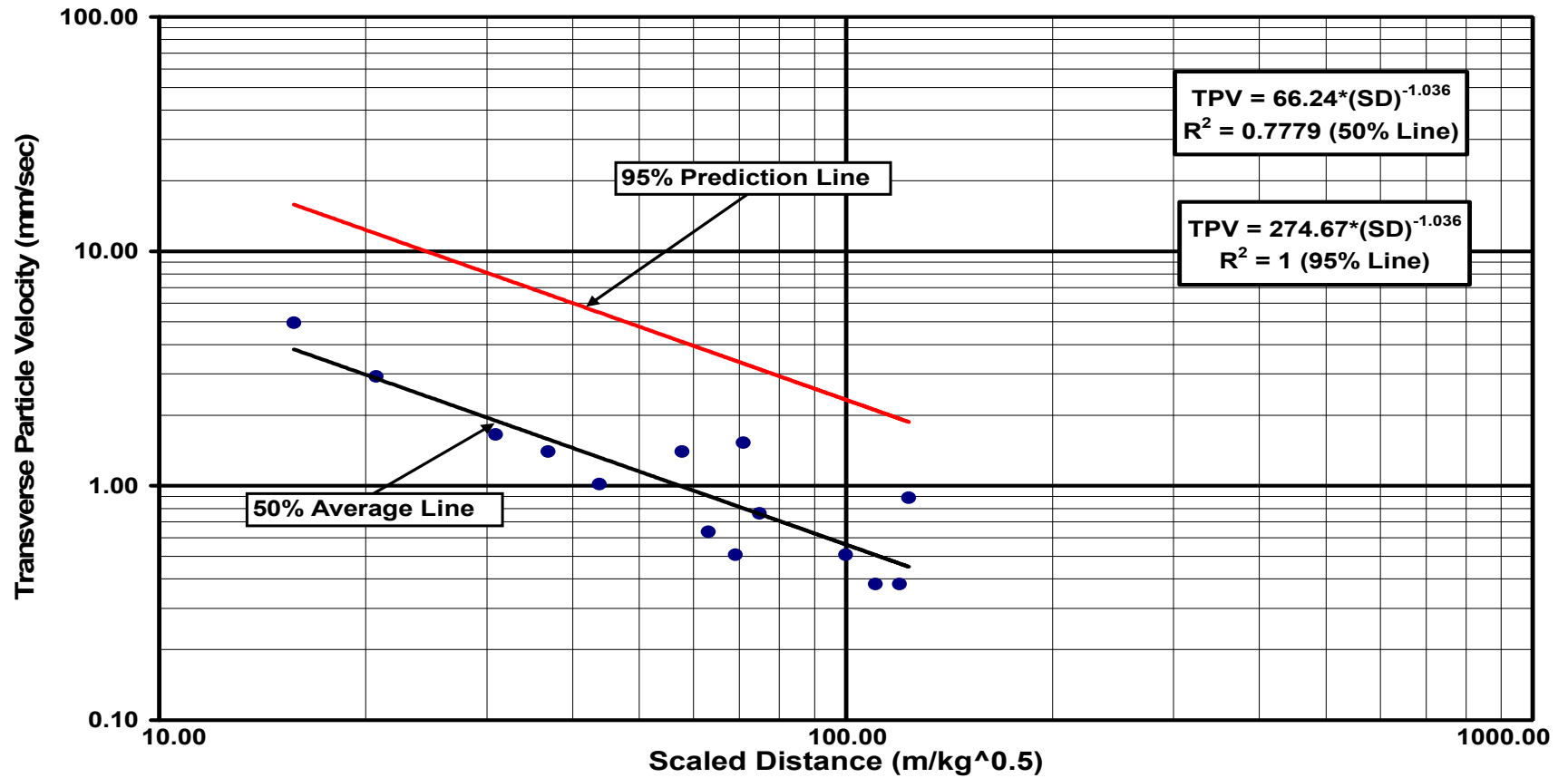


Figure 4.8 Transverse particle velocity versus scaled distance, single-hole blast (at 50% and upper 95% prediction limits)

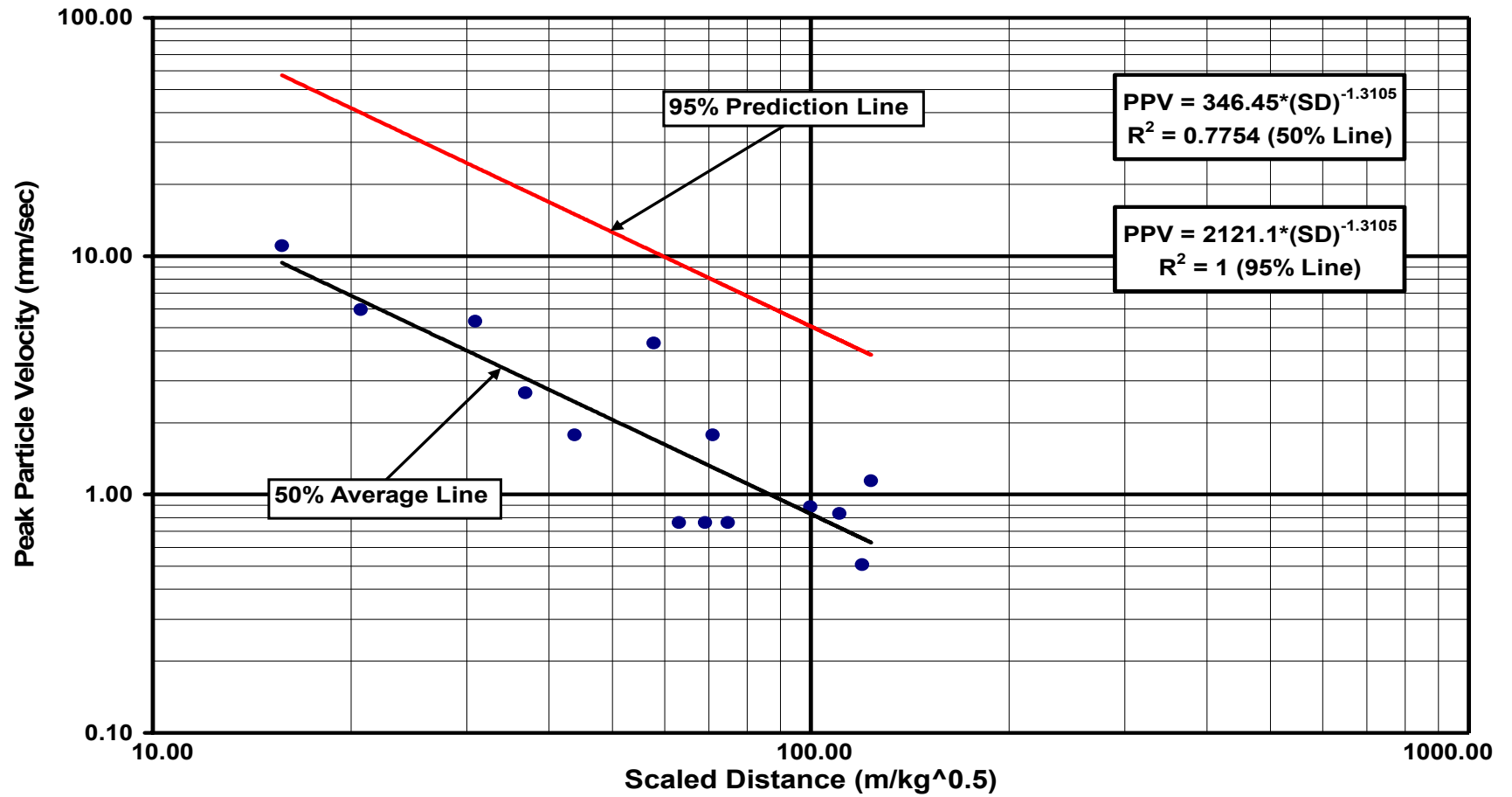


Figure 4.9 Peak particle velocity versus scaled distance, single-hole blast (at 50% and upper 95% prediction limits)

4.4 Predictions of PPV at 50% and 95% Levels for Round Blasts

The prediction of particle velocity requires that the average and upper bound values be well known. The 50% average line is the line about which the recorded data is gathered. The 95% prediction limit line is a line generated from the standard error and data distribution curve by means of Excel program from Microsoft to give upper bound values, as shown in the attenuation charts. Therefore, given a particular scaled distance, we can find the best estimate for PPV at 50% average line as well as the 95% prediction limit below which it is expected future blasts will occur. Table 4.3 shows these results.

Table 4.3 Prediction of peak particle velocity at 50% and 95% levels

Given (W_d) (kg)	D (m)	SD ($m/kg^{0.5}$)	Predicted (PPV) (mm/sec) 50%	Predicted (PPV) (mm/sec) 95%
75.50	100	11.51	14.059	25.940
75.50	150	17.26	8.456	15.602
75.50	275	31.65	3.954	7.296
75.50	360	41.43	2.821	5.205
75.50	450	51.79	2.133	3.935
75.50	590	67.90	1.518	2.802
75.50	710	81.71	1.204	2.221
75.50	800	92.07	1.037	1.912
75.50	925	106.46	0.864	1.594
75.50	990	113.94	0.793	1.464
75.50	1050	120.84	0.737	1.360
75.50	1115	128.32	0.684	1.261
75.50	1220	140.41	0.611	1.127
75.50	1280	147.31	0.575	1.061
75.50	1350	155.37	0.538	0.992
75.50	1675	192.77	0.410	0.757
75.50	2000	230.17	0.329	0.606
75.50	2625	302.10	0.234	0.431
75.50	3000	345.26	0.198	0.365
75.50	3750	431.58	0.149	0.276

The above table, indicates that by utilizing 75.5 kg of explosive per delay time at a maximum distance of 3750 m, the peak particle velocity predicted using the attenuation equation will not exceed 0.149 (mm/sec) for 50% average line. At 95% prediction level and at the same distance (3750m), the predicted peak particle velocity also will not go beyond 0.276 (mm/sec). In addition to that, at distance of 710 m with 75 kg of explosive, the predicted peak particle velocity at 50% and 95% levels are 1.204 and 2.221 (mm/sec), respectively. These values are lower than the USBM safe level (12.7mm/sec) of structural damage. Moreover, the nearest buildings belonging to the mine management in the path towards Tunçbilek township is 2625m distant. Therefore, there is no damage risk to those buildings from the blasting operation that is carried out at BYH panel since the predicted PPV are 0.234 and 0.431 mm/sec at 50% and 95% lines, respectively.

Furthermore, the established relationship at the 95% prediction level was tested using five new shots. The recorded values of PPV for the new events were below the 95% prediction level. The empirical formula was also tested using these new shots with different scaled distance, as can be seen in Table 4.4, the recorded and the predicted values of PPV are close to each other. This indicates that 60 vibration records from which the attenuation equation is extracted are statistically meaningful, and the equation can be used safely and reliably for vibration prediction.

Table 4.4 Predicted and recorded values of peak particle velocity (PPV) at 50% average line and 95% upper bound line.

No.	Given W_d (kg)	D (m)	SD ($m/kg^{0.5}$)	Recorded (PPV) (mm/sec)	Predicted (PPV) (mm/sec) (50%)	Predicted (PPV) (mm/sec) (95%)
1	226.5	685	45.52	2.667	2.507	4.626
2	75.50	660	75.96	1.270	1.319	2.434
3	75.50	350	40.28	2.286	2.922	5.392
4	75.50	450	51.79	2.877	2.133	3.935
5	151.00	320	26.04	4.699	5.050	9.317

4.5 Maximum Allowable Charge for the Blasting Site

In order to estimate the maximum allowable charge amounts for the blasting site, attenuation equations for 50% and 95% levels can be used. These estimations are calculated based on the USBM peak particle velocity limit in RI 8507 report, with different absolute distance, Table 4.5, and 4.6. These tables can be used to limit the amount of charge fired at 30 seconds delay time interval.

Table 4.5 Maximum allowable charge weight based on a given peak particle velocity at a given absolute distance for 50% average line.

D (m)	Given (PPV) (mm/sec)	SD (m/kg ^{0.5})	Maximum (W _d) Allowable (kg)
100	12.7	12.48	64.20
150	12.7	12.48	144.45
275	12.7	12.48	485.33
360	12.7	12.48	832.00
450	12.7	12.48	1448.46
590	12.7	12.48	2234.73
710	12.7	12.48	3236.21
800	12.7	12.48	4108.66
925	12.7	12.48	5492.93
990	12.7	12.48	6292.03
1050	12.7	12.48	7077.81
1115	12.7	12.48	7981.23
1220	12.7	12.48	9555.20
1280	12.7	12.48	10518.17
1350	12.7	12.48	11700.05
1675	12.7	12.48	18011.50
2000	12.7	12.48	25679.13
2625	12.7	12.48	44236.31
3000	12.7	12.48	57778.04
3750	12.7	12.48	90278.18

From Table 4.5, it can be noticed that the amount of charge per delay should not exceed 64.2 kg at an absolute distance of 100 m if the peak particle velocity value set to 12.7 (mm/sec) as a safe level to structural damage. For the same safe level of structural damage, the maximum amount of charge per delay could be as much as 3236.21 kg per delay at an absolute distance of 710, where the nearest mine buildings are located. Therefore, for Tunçbilek township, which is 3750 m distant to the mine, there is no risk.

Table 4.6 Maximum allowable charge based on a given peak particle velocity at a given absolute distance for 95% limit line

D (m)	Given (PPV) (mm/sec)	SD (m/kg^{0.5})	Maximum (W_d) Allowable (kg)
100	12.7	20.34	24.17
150	12.7	20.34	54.37
275	12.7	20.34	182.76
360	12.7	20.34	313.20
450	12.7	20.34	545.26
590	12.7	20.34	841.24
710	12.7	20.34	1218.24
800	12.7	20.34	1546.66
925	12.7	20.34	2067.75
990	12.7	20.34	2368.57
1050	12.7	20.34	2664.36
1115	12.7	20.34	3004.45
1220	12.7	20.34	3596.95
1280	12.7	20.34	3959.45
1350	12.7	20.34	4404.36
1675	12.7	20.34	6780.29
2000	12.7	20.34	9666.63
2625	12.7	20.34	16652.28
3000	12.7	20.34	21749.91
3750	12.7	20.34	33984.24

From Table 4.6, it can be noticed that the amount of charge per delay should not exceed 1218.24 kg for a distance of 710 m, at which the mine buildings are distant from Panel BYH.

On the other hand, the previous blasts conducted at the Panel No. 6, exploited before, which lies in the same path and is nearer to Tunçbilek township than Panel BYH, should also be evaluated in terms of ground vibration magnitude. Since the Panel No. 6 lies in the same path, the empirical attenuation relations established for the Panel BYH can be used. The absolute distances between the Panel No. 6 and other buildings belonging to the mine and those at Tunçbilek township are 275 m and 1675 m, respectively.

From Table 4.6, the maximum allowable charge per delay is found as 182.76 kg for the mine buildings located at 275 m from Panel No.6. On the other hand, the maximum allowable charge per delay is 6780.29 kg (Table 4.6) for a distance of 1675 m, not to result even cosmetic cracking of the plaster of buildings at Tunçbilek township. It is clear that the detonation of about 6.78 tonnes of explosives is impractical. Besides this, the allowable charge of 6780.29 kg per delay for Tunçbilek township creates a 66.33 mm/sec of PPV at a distance of 275 m, so that the buildings belonging to the mine will certainly experience sever damage. Since, no damage is observed in mine buildings, it is concluded that, even the previous blasting operations did not cause any damage in the buildings at Tunçbilek township. Therefore, it is also concluded that the damage claims put forward by the inhabitants of Tunçbilek township were not true.

At last, It should be noted that the empirical attenuation equation that are used to calculate the maximum allowable charge weights as well as to predict the PPV is valid only for the rock type and the structural geology prevailing at this site, which are given in section 3.4.

4.6 Frequencies Analysis

Peak particle velocity (PPV) data versus frequency are plotted in Figure 4.10 and 4.11. The upper bound is shown for safe level blasting criteria recommendations reported in USBM RI 8507 (Siskind, et al, 1980) as well as the OSM regulation limit, 1983.

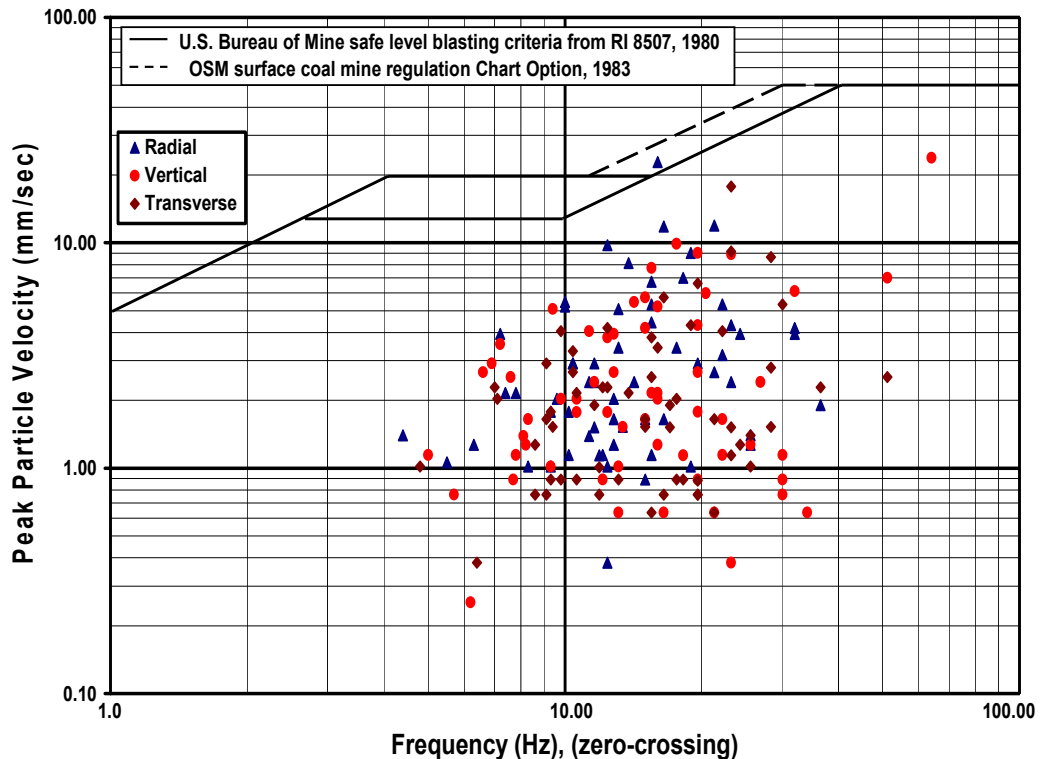


Figure 4.10 Peak Particle Velocities versus Frequency (Zero-Crossing)

Frequencies given in Figure 4.10 are the peak frequencies at zero-crossing for peaks of radial, vertical, and transverse components. While in Figure 4.11, they are the predominant frequencies calculated from the power spectrum of the Fast Fourier Transform (FFT) using Mini-Seis II data analysis software, 2003. In both figures the ground vibration components fall below

the safe level of blasting vibration for structures as recommended by USBM in report, RI 8507, as well as the OSM regulation, 1983.

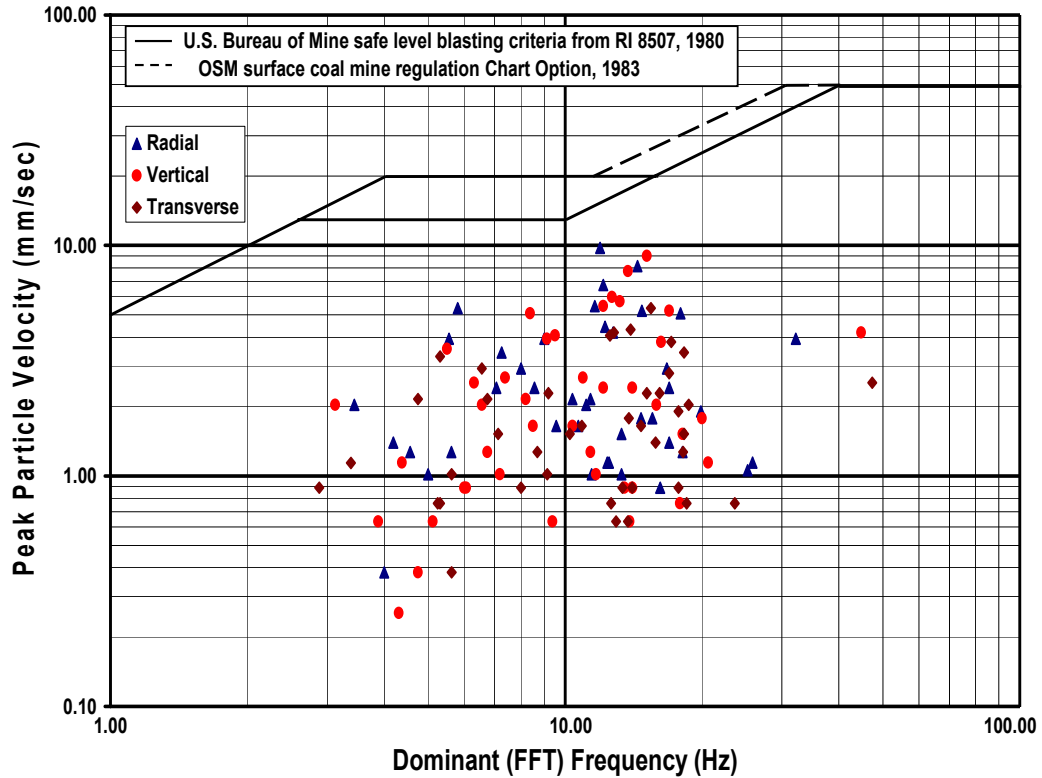


Figure 4.11 Peak Particle Velocities versus Dominant (FFT) Frequency

Table 4.7 summarizes differences in frequency range calculated by the “zero-crossing” (Z.C.) and FFT methods. In this table, Z.C. frequencies are higher particularly at the upper end of the range compared with the FFT method for all vibration components. Average values of frequency ranges also prove that the Z.C. average values are higher than the average values of FFT method. These results prove that calculating a frequency using the “zero-crossing” method results in a frequency well above the natural frequency range of residential structures (5–15 Hz), even if the entire time history contains a strong low-frequency component. The Z.C. frequency values may not represent the frequency at which the maximum vibration energy is

transferred into the structure. Therefore, damage risk assessment based on zero crossing frequency gives unreliable results.

Table 4.7 Comparisons of two methods used to determine frequencies: Zero-crossing and FFT methods

Component	Range of Frequencies (Hz)			
	Measured using zero-crossing method	Ave.	Calculated using FFT method	Ave.
Radial	4.4 - 36.5	15.08	3.44 - 32.19	12.39
Vertical	5.0 - 64.0	17.02	3.12 - 44.81	11.42
Transverse	4.8 - 51.2	16.75	2.88 - 47.38	12.96

4.7 Frequency Distributions

The distributions of frequency values for all vibration components calculated using FFT are shown in Figures 4.12, 4.13 and 4.14.

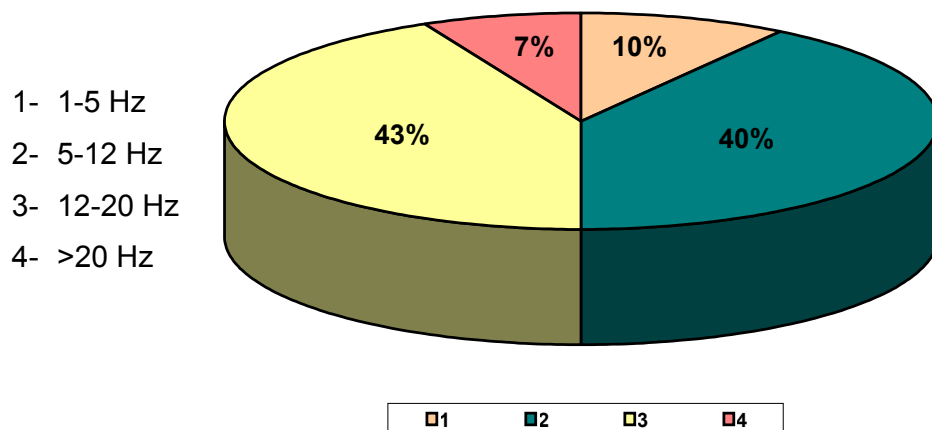


Figure 4.12 Frequency distribution for radial component.

From Figure 4.12, it can be determined that for radial particle velocity component, 10% of frequency values are between 1-5 Hz, 40% are between 5-12 Hz, 43% are between 12-20 Hz, and 7% greater than 20 Hz.

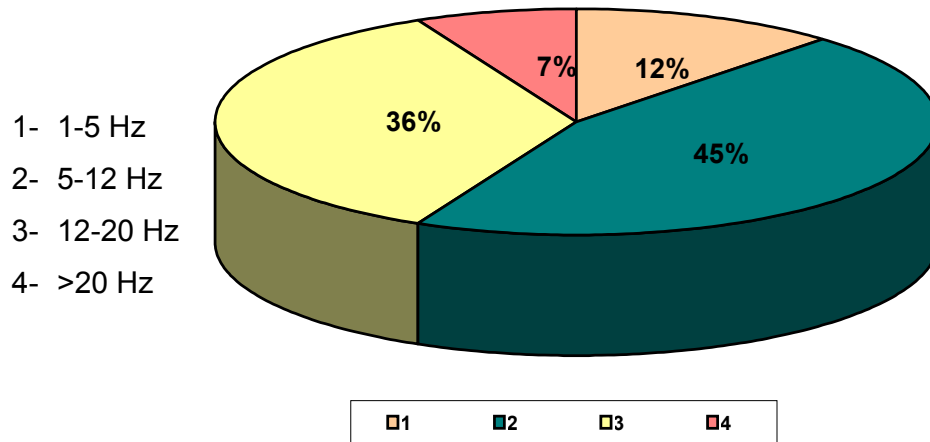


Figure 4.13 Frequency distribution for vertical component.

Figure 4.13 shows that for vertical particle velocity component, 12% of frequency values are between 1-5 Hz, 45% are between 5-12 Hz, 36% are between 12-20 Hz, and 7% greater than 20 Hz.

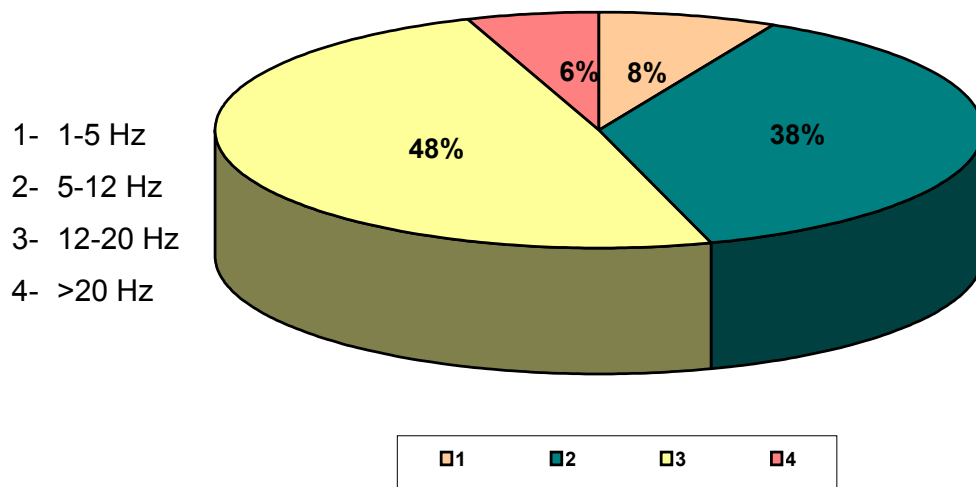


Figure 4.14 Frequency distribution for transverse component.

From Figure 4.14, it can be determined that for transverse particle velocity component, 8% of frequency values are between 1-5 Hz, 38% are between 5-12 Hz, 48% are between 12-20 Hz, and 6% greater than 20 Hz.

These results prove that the measured frequency values at this site are quite low. It is well known that low-frequency vibrations have a greater potential for damage than high-frequency vibrations. Since the self-structural frequencies of buildings range between 4–12 Hz for the superstructure and 10–20 Hz for the wall in general, and then the damage risk can be quite high if the amplitude of vibration is greater than 12.70 mm/sec when the frequency of the exciting ground wave is in the range of 3–10 Hz (USBM, 1890). This most probably results in cosmetic cracking. Moreover, if the measured frequency of the exciting ground wave is equal to or greater than the natural frequency of the building, and even if the amplitude of vibration, measured at the ground outside the building, is lower than 12.70 mm/sec, the building will resonate. The resonance, therefore, will increase the vibration amplitude due to the amplification, which means cosmetic cracking can also occur. Consequently, the low-frequency values determined show that it is important for the blaster and mine authority to record and evaluate all blast events.

4.8 The Optimum Delay Interval

In addition, the millisecond delay interval can be found from the average value of predominant frequency calculated using FFT method. However, it is well known that pyrotechnic detonators have a certain scatter in their nominal detonation time. Furthermore, blast design parameters certainly affect vibration levels. Therefore, it is not possible to use a ground vibration record obtained from a production blast in finding a proper delay interval. Ground vibration records from signature blasts should be used to determine an optimum delay time.

Since;

$$F = 1/ T \quad (4.5)$$

then,

$$T = 1 / F \quad (4.6)$$

since the average of FFT frequencies of signature blasts is calculated as $F = 15.24$ Hz.

then,

$$T = 1 / 15.42 = 64.85 \text{ ms} \quad (4.7)$$

So the recommended delay time will be half of the above calculated time, and is equal to **32.43** ms. However, this period of time is close to the delay interval used at the mine site (30 ms) by the contractor firm. As a result of that, the contractor can keep using the 30 ms delay interval for the rest of the blasting operation in order to minimize the vibration magnitude induced by production blasts.

CHAPTER 5

APPLICATION OF A NEURAL NETWORKS APPROACH IN PREDICTION OF PEAK PARTICLE VELOCITY

5.1 Introduction

Traditionally, in modeling of ground vibration induced by bench blasting, statistical algorithms that take an advantage of computer programs that rely on mathematics are used, and are generally not portable to other sites. Additionally, if an unusual noise or uncertainties exist in the collected data, those models have difficulty in making accurate predictions. An alternative to traditional models is through the use of neural networks (NN), from a branch of artificial intelligence. The Neural networks are computer algorithms that have the ability to learn patterns by experience. Basically, the neural network is a biologically inspiration from the human brain.

5.2 Neural Network Methodology

Neural network study gives information, examines the data and the maps for the interrelationships. It uses the derived interrelationships to become an 'expert' in the field. The neural network 'expert' can then be given new data to incorporate, analyse and assess to make new predictions. The neural network accepts 'fuzzy' data similarly to the humans do, organizing the data and modifying the analysis as more data are obtained. This adaptability is one of the major advantages of neural networks.

Neural networks use a trial-and-error method to establish connections and analyse applied input and output data. An input data is used by the 'expert' to arrive at a solution, prediction or decision; whereas an output is the solution, prediction or decision that the neural network will be learning to produce. The neural network determines the relationship between inputs and outputs by calculating their relative importance. It calculates and compares calculated results with the actual answer in the database.

Initially, a neural network makes mistakes just as a human does. It corrects mistakes by modifying the weight applied to each of the input items. The network then evaluates the data again. This process continues until the network converges on the used-defined accuracy. A well-trained 'expert' neural network is obtained once the network is sufficiently adapted at analysing the given data. Users can then provide new data for the 'expert' to analyse and make predictions based on the knowledge gained from the initial database.

5.3 The Neural Network Models for predicting the Peak Particle Velocity

The artificial neural network model used to predict the peak particle velocity (PPV) is based on the backpropagation algorithm. The appropriate choice of neural network type for this model is the multilayer supervised learning network, which requires pair of data consisting of input patterns and the correct output. The used model has many identical nodes with computational features that enable them to transform perceiving signals into new transmittable signals.

The network learning is based on repeated representations of the training samples. In the current study, two different models were established in order to predict the peak particle velocity depending on two different inputs. The first model uses the scaled distance as the only input to the neural network,

whereas the amount of charge per delay and the absolute distance are the two inputs to the second neural network model.

5.4 Database for the Neural Network Model

The data used in training the first neural network model is consisting of the scaled distance as the only input to the model and the peak particle velocity as output, which needs to be predicted. As illustrated in the literature, the scaled distance is derived by dividing the absolute distance, between source and measurement points, by the square root of and the maximum amount of charge per delay. The data collected from the mine site were the amount of charge per delay, the distance between the blasting site and the monitoring stations, and the recorded peak particle velocity. The amount of charge per delay and the distance are combined in single input, the scaled distance. However, the second neural network model is based on the maximum amount of charge per delay and the absolute distance as inputs to the model. The total number of the data pairs used in training the network for both models was from 60 blasting shots. This pair of data is given in Table A.1 in the Appendix A.

5.5 Training Backpropagation Neural Network Model

Backpropagation is a gradient descent system that tries to minimize the mean squared error (MSE) of the system by moving down the gradient of the error curve. In order to achieve this goal a training algorithm was written and implemented. This backpropagation algorithm is defined as follows;

Decide the neural network architecture

(# Hidden layers, #Neurons in each Hidden Layer)

Decide the learning parameter and momentum

Initialize the network with random weights

While MSE is unsatisfactory

and computational bounds are not exceeded

Do for each input pattern

Compute First hidden layer's nodes inputs;

Compute First hidden layer's nodes outputs;

Compute Second hidden layer's nodes inputs;

Compute Second hidden layer's nodes outputs;

Compute inputs to the output nodes

Compute the network outputs

Compute the MSE between the desired and actual outputs

Back propagate the error and adjust the weights

(weights adjustment between output layer and second hidden layer, then weight adjustment between second hidden layer and first hidden layer, and then weight adjustment between first hidden layer and input layer)

End-Do

Check MSE error for convergence

End-While

The Visual Basic programming language was used in writing a code for the above backpropagation training algorithm. The powerful and flexible environment of Visual Basic enhances the capability of the neural network. Application of the Visual Basic Code includes the following steps:

- (1) Initializing the weights, and scaling and representing the data patterns to the network randomly.
- (2) Training the network for certain epochs until the prediction error is minimized.
- (3) Testing the trained network with data set that the network has never encountered before.
- (4) Saving the trained network in a file that can be recalled for any further predictions, this includes weights, training parameters, and error values for each epoch.

5.6 Results and Discussions of Neural Network Models

A well-trained, satisfactory model used to predict the peak particle velocity was obtained after a series of neural network training and testing sessions had been conducted using combinations of different settings.

5.6.1 One-Single Input Neural Network Model

In this model, five different designs of neural network sessions were trained based on one input (the scaled distance) and one output (the PPV). A different number of nodes in the hidden layers, and training cycles, as well as different learning rates were selected. Then, these parameters were being changed and modified until satisfactory network design and training parameters were reached. An exception was made for the momentum coefficient, where it was set fixed to the value of 0.9 for all training sessions, as recommended in the literature. Table 5.1 represents the best neural network architectures and training parameters for all the sessions that give a satisfactory prediction to the peak particle velocity.

Table 5.1 Neural network design and training parameters for all sessions, one input model.

Session	# of Nodes in Input Layer	# of Nodes in First Hidden Layer	# of Nodes in Second Hidden Layer	# of Nodes in output Layer	Learning Rate	Momentum Coefficient	# of Examples Used in Training	# of Epoch	Mean Square Error (MSE)
1	1	7	5	1	0.4	0.9	60	7000	0.0285580
2	1	5	5	1	0.3	0.9	60	7000	0.0284184
3	1	5	3	1	0.2	0.9	60	8000	0.0295946
4	1	4	4	1	0.5	0.9	60	7000	0.0280383
5	1	6	4	1	0.3	0.9	60	7000	0.0276006

Furthermore, a plot was drawn for the error values for each training cycle against the number of epochs for the training sessions as shown in Figure 5.1. This plot indicates that in the beginning stage of training, the prediction error decreases rapidly up to 1400 epochs. Then, the error minimization slows down to the end of training cycles.

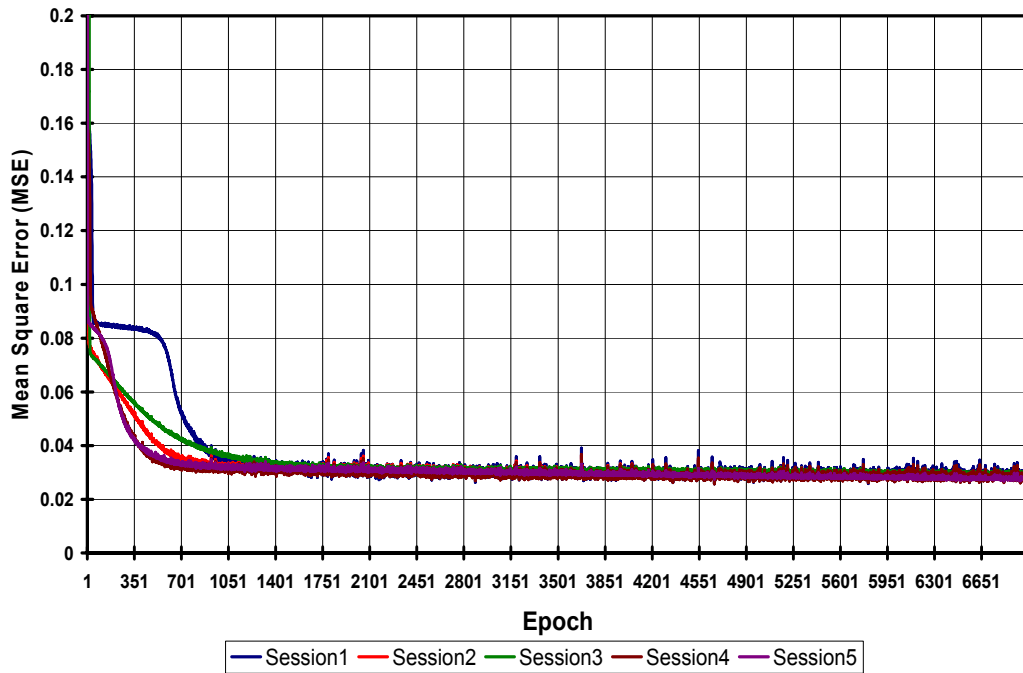


Figure 5.1 Mean-square-error versus epochs for all training sessions, for one input NN model.

The predicted peak particle velocity values using one-single input neural network model are tested and compared to the recorded values obtained from the mine site. Testing the training sessions is illustrated in Table 5.2, where the set of data used in testing, the model has never encountered during the training process. Table 5.2 is including the input (scaled distance), the recorded PPV values, the predicted PPV using the five neural network training sessions, and the standard deviation values of the predicted PPV from the recorded values. The average of standard deviation was also calculated in order to choose the best training session for prediction of peak particle velocity.

Table 5.2 Comparison between recorded peak particle velocities and predicted ones using one single input neural network model

Data No.	SD (m/kg ^{0.5})	Recorded PPV (mm/sec)	Predicted PPV, NN Session1	Standard Deviation	Predicted PPV, NN Session2	Standard Deviation	Predicted PPV, NN Session3	Standard Deviation	Predicted PPV, NN Session4	Standard Deviation	Predicted PPV, NN Session5	Standard Deviation
1	45.515	2.667	2.428	0.169	2.381	0.202	2.365	0.214	2.358	0.218	2.427	0.170
2	75.957	1.27	1.551	0.199	1.053	0.153	1.223	0.033	0.727	0.384	1.38	0.078
3	40.281	2.286	2.865	0.409	2.969	0.483	2.922	0.450	3.065	0.551	2.903	0.436
4	51.789	2.877	2.084	0.561	1.889	0.699	1.919	0.677	1.754	0.794	2.039	0.593
5	26.04	4.699	5.596	0.634	6.115	1.001	6.094	0.986	6.427	1.222	5.736	0.733
Average of Standard Deviation				0.394		0.508		0.472		0.634		0.402

The best training session to be used for predicting the peak particle velocity was selected among the aforementioned training sessions based on the lowest average of standard deviation. The selected training session was session number one, where the average of the standard deviation value is 0.394. The neural network architecture that gives the best predicted (PPV) values is shown in Figure 5.2.

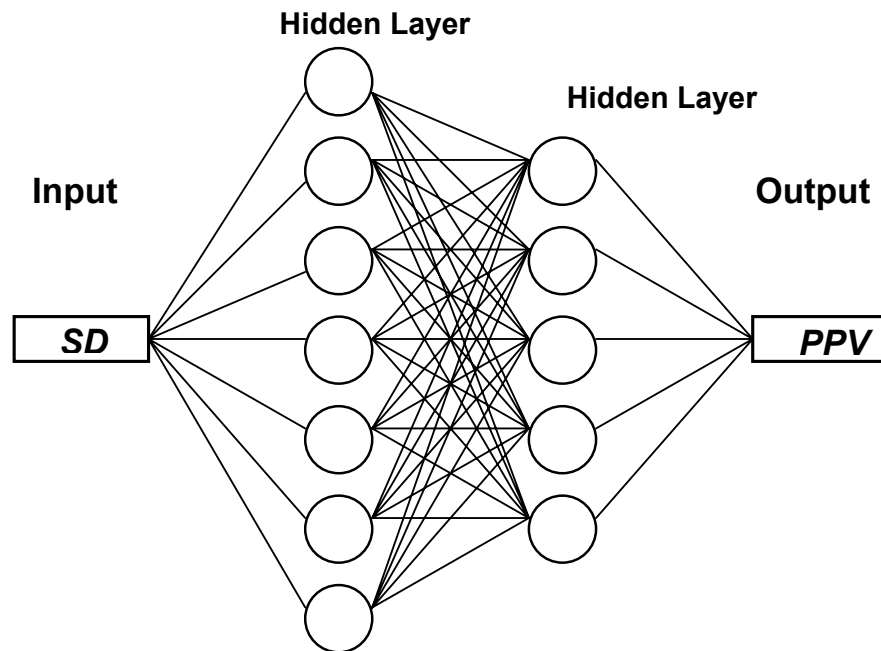


Figure 5.2 Neural network architecture for the best training model with single input.

This network is consisted of four layers, one input layer, two hidden layers, and one output layer. Since there are one input and one output, then the number of neurons in the input layer and the output layer is one for each. The number of neurons in the first hidden layer is different from the second layer.

In the first hidden layer, number of neurons was found to be seven neurons, whereas in the second layer were five neurons.

The comparison between the predicted (PPV) values and the recorded values for session number 1 indicates that some predicted (PPV) values are close to the recorded ones in data number 1 and number 2, where the standard deviation is 0.169 and 0.199, respectively. For the data number 3, 4, and 5, the standard deviation is higher; it is 0.409, 0.561, and 0.634, respectively. This error in predicting some values of peak particle velocity is probably due to the scatter in the data involved in training the neural network model.

5.6.2 Two Inputs Neural Network Model

Due to the deviation between the predicted peak particle velocity and the recorded ones using the single input neural network model, another neural network model based on two individual inputs is established in order to obtain a better prediction of PPV. These inputs are the amount of explosive charge per delay (W_d , kg) and the absolute distance between the blasting site and the recording stations (D , m).

In this model, five different designs of neural network sessions were trained based on two aforementioned inputs and one output (the PPV). A different number of nodes in the hidden layers, and training cycles, as well as different learning rates were selected. Then, these parameters were being changed and modified as it has been done in the first model until satisfactory network design and training parameters were reached. Table 5.3 represents the best neural network architectures and training parameters for all the sessions.

A plot was constructed for the error values for each training cycle against the number of epochs for the training sessions as shown in Figure 5.3. This plot indicates that in the beginning stage of training, the prediction error

decreases rapidly up to 1400 epochs. Then, the error minimization slows down to the end of training cycles.

Table 5.3 Neural network design and training parameters for all sessions, two input model

Session	# of Nodes in Input Layer	# of Nodes in First Hidden Layer	# of Nodes in Second Hidden Layer	# of Nodes in output Layer	Learning Rate	Momentum Coefficient	# of Examples Used in Training	# of Epoch	Mean Square Error (MSE)
1	2	5	5	1	0.4	0.9	60	7000	0.0114323
2	2	7	5	1	0.3	0.9	60	7000	0.0117511
3	2	5	6	1	0.4	0.9	60	8000	0.0117950
4	2	4	4	1	0.2	0.9	60	7000	0.0161122
5	2	6	4	1	0.1	0.9	60	7000	0.0202868

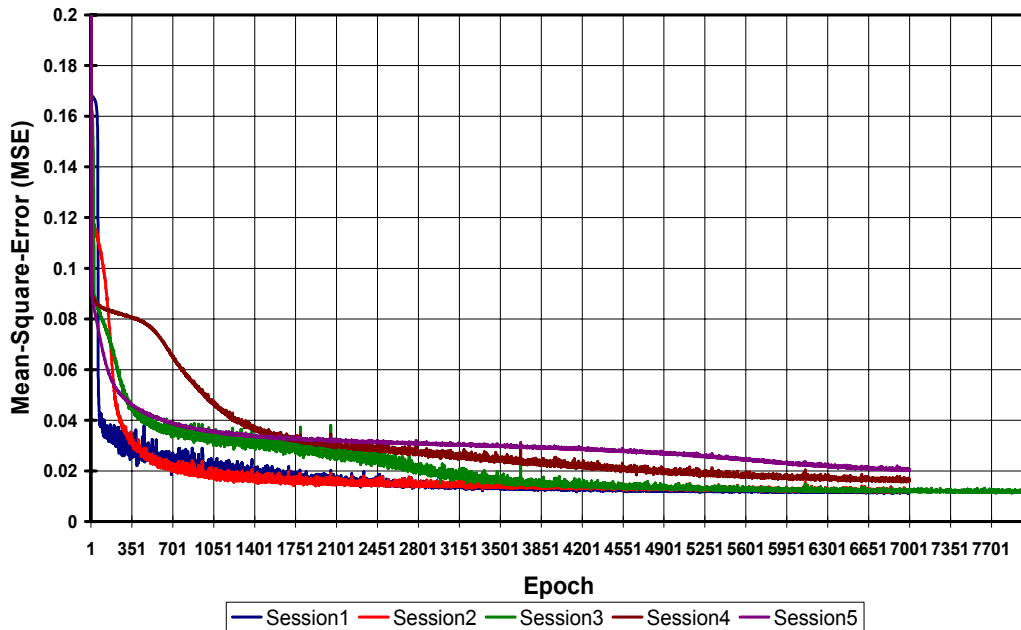


Figure 5.3 Mean-square-error versus epochs for all training sessions, for two inputs NN model.

Testing the training sessions is illustrated in Table 5.4, where the set of data used in testing, the model has never encountered during the training process. Table 5.4 is including the two inputs (the amount of charge, W_d and the absolute distance, D), the recorded PPV values from the blasting shots, the predicted PPV using the five neural network training sessions, and the standard deviation values of the predicted PPV from the recorded values. The average of standard deviation was also calculated in order to choose the best training session for prediction of peak particle velocity.

The best training session to be used for predicting the peak particle velocity was selected among the aforementioned training sessions based on the lowest average of standard deviation. The selected training session was session number two, where the average of the standard deviation value is 0.245. The neural network architecture that gives the best predicted (PPV) values is shown in Figure 5.4.

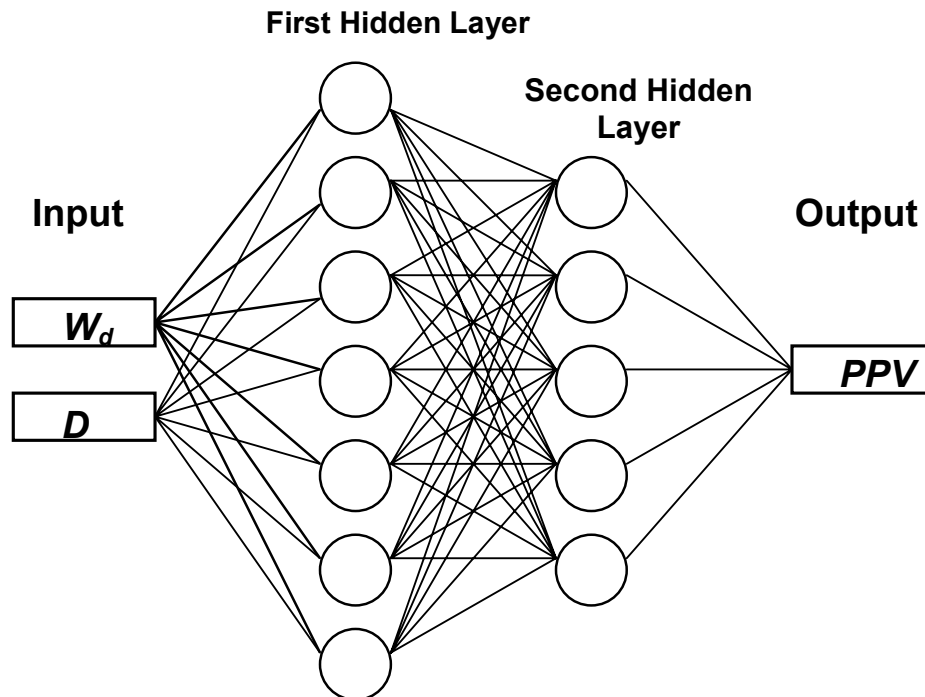


Figure 5.4 Neural network architecture for the best training session with two inputs.

Table 5.4 Comparison between recorded peak particle velocities and predicted ones using two inputs neural network model

No.	W _d (kg)	D (m)	Recorded PPV (mm/sec)	Predicted PPV NN Session1	Standard Deviation	Predicted PPV NN Session2	Standard Deviation	Predicted PPV NN Session3	Standard Deviation	Predicted PPV NN Session4	Standard Deviation	Predicted PPV NN Session5	Standard Deviation
1	226.5	685	2.667	2.507	0.113	2.649	0.013	2.909	0.171	2.299	0.260	2.253	0.293
2	75.5	660	1.27	1.144	0.089	1.283	0.009	1.304	0.024	1.176	0.066	1.07	0.141
3	75.5	350	2.286	3.038	0.532	2.783	0.351	2.928	0.454	3.433	0.811	3.566	0.905
4	75.5	450	2.877	2.029	0.600	1.947	0.658	2.028	0.600	2.184	0.490	2.149	0.515
5	151	320	4.699	4.667	0.023	4.423	0.195	4.928	0.162	4.347	0.249	4.917	0.154
Average of Standard Deviation					0.271		0.245		0.282		0.375		0.402

This network is consisted of four layers, one input layer, two hidden layers, and one output layer. Since there are two inputs and one output, then the number of neurons in the input layer is two and in the output layer is one. The number of neurons in the first hidden layer is different from the second layer. In the first hidden layer, number of neurons was found to be seven neurons, whereas in the second layer were five neurons.

The comparison between the predicted (PPV) values and the recorded values for session number 2 indicates that some predicted (PPV) values are almost the same as the recorded ones particularly in data number 1, 2, and 5, where the standard deviation is 0.013, 0.009, and 0.195, respectively. For the data number 3, and 4, the standard deviation is a bit higher; it is 0.351, and 0.658, respectively. This much deviation in predicting some values of peak particle velocity using two input model is still lower than the deviation when using one input model. In that sense, it can be concluded that the neural network model with two inputs, the amount of charge per delay and the absolute distance, gives a better prediction for the peak particle velocity compared to using one-single input model. In the two input neural network model, the deviation in prediction of the PPV still due to the scatter existing in the data pairs involved in training the neural network models. Nevertheless, the predicted peak particle velocity values are too close to the recorded PPV values.

5.7 Neural Network Approach versus Statistical Approach

The results obtained from the neural network prediction models can be compared to that of the statistical model illustrated in chapter four. Table 5.5 shows this comparison between the predicted peak particle velocity using the statistical model and the two neural network models with the recorded PPV values.

Table 5.5 Comparison between the predicted PPV's using statistical and neural network models and a set of recorded PPV.

No.	Wd(kg)	D (m)	SD (m/kg ^{0.5})	Recorded PPV (mm/sec)	Predicted PPV from Statistical Model	Standard Deviation	Predicted PPV from One input Neural Network Model Session1	Standard Deviation	Predicted PPV from Two Input Neural Network Model Session2	Standard Deviation
1	226.5	685	45.515	2.667	2.507	0.113	2.428	0.169	2.649	0.013
2	75.5	660	75.957	1.27	1.319	0.035	1.551	0.199	1.283	0.009
3	75.5	350	40.281	2.286	2.922	0.450	2.865	0.409	2.783	0.351
4	75.5	450	51.789	2.877	2.133	0.526	2.084	0.561	1.947	0.658
5	151	320	26.04	4.699	5.050	0.248	5.596	0.634	4.423	0.195
<i>Average of Standard Deviation</i>						0.274		0.394		0.245

When studying Table 5.5, the predicted peak particle velocity values using both the statistical model and the two neural network models can be compared with respect to the recorded PPV values. In terms of standard deviation, the neural network model with two inputs gives the lowest value of overall standard deviation, 0.245, followed by the statistical model, 0.274, and then the one-single input neural network model, 0.394. For the two-input neural network model, all the predicted peak particle velocities are very close to the recorded ones except shot number 4, where the predicted PPV value deviates from the recorded one. However, from shot number 4, the predicted peak particle velocity from the statistical model is closer to the recorded PPV value than the one predicted using two-input neural network. The deviation in predicting PPV from the recorded value in shot number 4 from both models is probably associated with the scatter in the pairs of data collected from the mine site, which can be attributed to the existence of several faults at the mine site.

From the above comparison, it can be inferred that the empirical statistical technique is not the only acceptable approach that can be taken into account in predicting the peak particle velocity. An alternative and interesting neural network approach can also be taken into consideration. One advantage with the neural network approach is the ability to predict without knowing the relationship between the input data and the output data. The application of the neural network can improve the analysis and interpretation of peak particle velocity prediction. However, due to the uncertainty attached to geological conditions at the mine site, the empirical statistical model should not be expected to predict accurately in all cases. The reliability of the neural network, like the empirical approach, depends on the data collection and complexity of the geological environment. Nevertheless, this is an attempt to bring the neural network technique to the field of ground vibration prediction and it can open the door for the gain from the advantages of this technique.

CHAPTER 6

CONCLUSIONS AND RECOMMENDATION

6.1 Conclusions

1. From the data pairs collected from the Tunçbilek Coal Mine, Panel BYH, it was found that the radial particle velocity dominates and the dominant wave type is Rayleigh wave.
2. The maximum charge per delay utilized by the contractor in Panel BYH is determined to be 402.5 kg and highest peak particle velocity value recorded was found to be 23.876 mm/sec at absolute distance of 100 m.
3. For the Panel BYH, taking into account the distance to the nearest buildings belonging to the mine, which is 710 m, the maximum allowable charge per delay is determined to be 1218 kg.
4. Since the absolute distance from the blasting site toward the Tuncbilek township is about 3750m, the predicted PPV using the established attenuation equation is found to be 0.149 mm/sec at this distance when 75.5 kg of charge per delay, as usual, is utilized. Therefore, there is no damage risk to the buildings in the township due to the blasting operations conducted at BYH Panel.
5. The safe scaled distance to eliminate the risk of structural damage was determined to be 25 for round blasts and 15 for single hole blasts.

6. When the recorded frequencies were analyzed, it was found that the predominant frequencies of ground motion time histories, as estimated from the Fast Fourier Transform (FFT) power spectrum tend to be smaller than those computed using the zero-crossing (Z.C.) method computed at the PPV. The average of frequency range with zero-crossing at PPV was 15.08 to 17.02 Hz compared to an 11.42 to 12.96 Hz from the FFT method.
7. Even though most of the recorded frequencies are low, there will be no damage risk at distances greater than 710 m, provided that the allowable charge per delay of 1218 kg is not exceeded at Panel BYH. Therefore, the claims of structural damages made by the inhabitants of Tunçbilek township appear to be unjustifiable.
8. When the recorded ground vibration components compared to the previous damage criteria based on peak particle velocity and frequency by USBM and OSM, whole results seem to occur below damage limits.
9. The proper delay time interval to be used in round-blast performed at the mine site was found to be 32.43 milliseconds, which is close to 30 milliseconds used currently by the contractor. As a result of that, the contractor can keep using the 30 ms delay interval for the rest of the blasting operation in order to minimize the vibration magnitude induced by production blasts.
10. The statistical technique is not the only acceptable approach that can be taken into account in predicting the peak particle velocity. An application of an alternative and interesting neural network approach in predicting the PPV was put forward in this thesis.
11. Two different models of neural networks were used in predicting the peak particle velocity. It was found that the NN model that is based on the

amount of charge per delay and the absolute distance as the two inputs gives better prediction of PPV over the NN model that uses the scaled distance as the only one input to the neural network.

12. Comparisons between the predicted PPV using the empirical statistical approach and the neural networks approach are made with respect to an additional data set of recorded PPV values. It was found that the neural network model with two inputs gives a better prediction of PPV than the statistical model.

6.2 Recommendation

In this thesis study, the neural network has shown the ability to predict the peak particle velocity with a satisfactory accuracy, hence, for further study, it is recommended that other parameters affecting the ground vibrations should be designated and included in the training neural network model.

REFERENCES

Aimone-Martin C. T., Martell M. A., McKenna L. M., Siskind D. E., Dowding C. H., (2003) Comparative Study of Structure Response to Coal Mine Blasting. *U.S. Office of Surface Mining*.

<http://www.osmre.gov/blastingindex.htm>

Anon., 1956. "Blasting Claims, A Guide to Adjusters," *Association of Casualty and Surety Companies, New York*.

Anon., 1977, "Cracking in Buildings," *Building Research Establishment Digest*, Vol. 75, Building Research Station, Garston, UK, 8 pp.

Arseven B. 2003, "Blasting Optimization for the Assessment of Ground Vibrations at Demirbilek Panel of Tunçbilek Mine. Msc. Thesis, the Middle East Technical University, Ankara, Turkey, pp. 12-14.

Atlas Powder Company (1987), "Explosive and Rock Blasting", pp. 321-406.

Bilgin, H. A., Esen, S. and Kiliç, M., 1999, *Effect of Blasting Induced Ground Vibrations on Buildings and the Importance of the Amplification Factor*, 16th Mining Congress, Ankara, Turkey, pp. 25-32, in Turkish.

Bilgin, H. A., Esen, S. and Kiliç, M., 1998, *A Research for Solving the Environmental Problems due to Blasting at TKI Çan Lignite Mine*, Project No: 97-03-05-01-08, ODTÜ, Ankara, Turkey, 100 pages, in Turkish.

Borsky, P. N., 1965, "Community Reactions to Sonic Booms in the Oklahoma Area," Final Report, *Aerospace Medical Research Laboratory*, AMRL-TR-65-37, Vol. II, Wright-Patterson Air Force Base.

Crandell, F. J. (1949), "Ground Vibrations Due to Blasting and Its Effects upon Structures," *Journal of the Boston Society of Civil Engineers*, Vol. 36, No. 2.

Dimitrios C. Kaliamparkos and Dimitrios G. Damigos, (2001) Blasting Vibration Limits to Prevent Human Annoyance Remarks from some Case Studies. *Mineral Resources Engineering*, Vol. 10, No. 1, pp.71-82.

Djordjevic N., Kavetsky A., and Scott A. Blast Design Optimization to Minimize Induced Vibrations of Structures. *International Journal of Blasting and Fragmentation*. (1990), pp. 373-380.

Dowding, C. H., W. K. Beck, and D. K. Atmatzidis. Blast Vibration Implications of Cyclic Shear Behavior of Model Plaster Panels. *Geotechnical Testing J., ASTM*, v. 3, No. 2, June 1980.

Dowding, C. H., Murray, P. D., and Atmatzidis, D. K., 1981, "Dynamic Response Properties of Residential Structures Subjected to Blasting Vibrations," *Journal of Structural Engineering*. Vol. 107, No. ST2, pp. 1233-1249.

Dowding, C.H., (1985). *Blast Vibration Monitoring and Control*. Prentice-Hall, Englewood Cliffs, 297 pp.

Dowding, C. H., 1988, "Comparison of Environmental and Blast Induced Effects through Computerized Surveillance," *The Art and Science of Geotechnical Engineering at the Dawn of the 21st Century*, R. B. Peck Honorary Volume, W. J. Hall, ed., Prentice-Hall Englewood Cliffs, NJ, pp. 143-160.

Dowding, C. H., Aimone C. T., Rock Breakage, Explosives. *Mining Engineering Handbook*, Chapter 9.2, pp. 722-746, 1992.

Dowding, C. H., 1992, "Monitoring and Control of Blast Effects". *Mining Engineering Handbook*, Vol. 1, pp. 746-760.

Duvall W. I., *Empirical Approach to Problems in Blasting, Failure and Breakage of Rocks.*, Ch 28., pp 500-523, 1966.

Edwards, A. T., and Northwood, T. D. (1960), "Experimental Studies of the Effects of Blasting on Structures," *The Engineer*, Vol. 210, 40 pp.

Esen, S. and Bilgin H. A., Evaluation of Blast Vibrations from Sekköy Surface Coal Mine in Turkey, *Proceedings of the Twenty-Seventh Annual Conference on Explosives and Blasting Technique*. Orlando, Florida, USA, Jan., 2001, Vol. 1, pp. 313-327.

Goldman, D. E. A Review of Subjective Responses of Vibration Motion of the Human Body in the Frequency Range, 1 to 70 Cycles per Second. *Naval Medical Res. Inst. Proj. NM 004001, Rept. 1*, Mar. 16, 1948, 17 pp.

Kahriman A., (2001a), Prediction of Particle Velocity Caused by Blasting for an Infrastructure Excavation Covering Granite Bedrock. *Mineral Resources Engineering*, Vol. 10, No. 2, pp. 205-218.

Kahriman A., (2001b), Analysis of Ground Vibrations Caused by Bench Blasting at Can Open-pit Lignite Mine in Turkey. *Environmental Geology*, Vol. 41, pp. 653-661.

Kamperman, G., and Nicholson, M. A., 1970, "The Transfer Function of Quarry Blast Noise and Vibration into Typical Residential Structures," *Report EPA 55/9-77-351, US Environmental Protection Agency, Washington, DC*.

Konya C. J., Walter E. J. (1991), "Rock Blasting and Overbreak Control", National Highway Institute, 415 pp.

Kutter H.K. & Fairhurst C., On the Fracture Process in Blasting. *International Journal of Rock Mech. Min. Sci. & Geomech Abstr.* Vol. 8, p 181-202, Pergamon Press, 1971.

Langefors, U., and B. Kihlstrom, and H. Westerberg. Ground Vibrations in Blasting. *Water Power*, February 1958, pp. 421-424.

Langefors U. & Kihstrom B., The Modern Technique of Rock Blasting. Almquist and Wiksell. Upsalla, Sweden, (*John Wiley and Sons, New York, 405 p*) 1967.

Medearis, K. The Development of Rational Damage Criteria for Low-Rise Structures Subjected to Blasting Vibrations. *Kenneth Medearis Associates, Final Rept. to National Crushed Stone Assn.*, Washington, D. C., August 1976, 93 pp.

Mehrotra, K. G., Mohan, C. K., and Ranka, S.. Elements of Artificial Neural Networks. MIT Press, Cambridge, 1996, pp 65-156.

Newmark, N. M. and Hall, W. J., 1982, *Earthquake Spectra and Design*, Earthquake Engineering Research Institute, Berkeley, CA, 103 pp.

Nicholls, H. R., Johnson, C. F., and Duvall, W. I. Blasting Vibrations and Their Effects on Structures. *BuMines Bull.* 656, 1971.

Nick, S., Preliminary Vibration Assessment - Tahiri Street, Mapua, Nelson. Report Prepared for *TONKIN & TAYLOR LTD.*, (2002).
<http://www.tdc.govt.nz/pdfs/394.pdf>

Parker, D. Learning Logic, Invention Report, S81-64, File 1, Office of Technology Licensing, Stanford University, Palo Alto, CA, 1982.

Northwood, T. D., Crawford, R., and Edwards, A. T., 1963, "Blasting Vibrations and Building Damage," *Engineer*, Vol. 215, No. 5601, May.

Olofsson S. O., Applied Explosives Technology for Construction and Mining, *Applex, Arla, Sweden*, 304 p. 1988.

Paşamehmetoğlu A. G., Karpuz C., Müftüoğlu Y., Özgenoğlu A., Bilgin A., Ceylanoğlu A., Bozdağ T., Toper Z., Dinçer T., 1988, Cost Analysis, Determination of Unit Cost and Equipment Selection for Turkish Coal Enterprise, Vol. 2, Determination of Geotechnical and Performance Parameters, METU, Ankara, pp. 37-50.

Persson P. A., The Basic Mechanisms in Rock Blasting. Proc. 2. *International Congress on Rock Mechanics*. Vol. 111b., Belgrade, 1978.

Reiher, H., and F. J. Meister. (The Effect of Vibration on People.) *Forschung auf dem Gebiete des Ingenieurwesens (Germany)*, v. 2, No. 11, 1931, p. 381.

Rumelhart, D. E., Hinton, G. R., and Williams, R. J., Learning Internal Representations by Error Propagation, in *Parallel Distributed Processing*, Vol. 1, D. E. Rumelhart, and J. L. McClelland, eds., MIT Press, Cambridge, MA, 1986.

Saha, A., A Tutorial on Neural Network Based Modeling - for beginners. <http://www.geocities.com/adotsaha/index.html>

Singh S. P., The Effects of Shock and Gas Energies on Fracturing Process. *Proceedings of the 25th Annual Conference of Explosives and Blasting Technique.*, p397-406, Tennessee, USA, February, 1999.

Siskind DE., Stagg MS., Kopp JW., Dowding C.H., (1980) Structure Response and Damage Produced by Ground Vibration from Surface Mine Blasting. *United States Bureau of Mines, Report of Investigation 8507.*

Stagg, M. S., and A. J. Engler. Ground Vibration Measurement and Seismograph Calibration. *BuMines RI. 8506*, 1980.

Stagg, M. S., Siskind, D. E., Stevens, M. G., and Dowding, C. H., 1984. "Effects of Repeated Blasting on a Wood-Frame House," *Report of Investigations 8896, US Bureau of Mines*, Washington, DC, 82 pp.

Thonen, J. R., and Windes, S. L., 1942, "Seismic Effects of Quarry Blasting," *Bulletin 441, US Bureau of Mines*, Washington, DC. 83 pp.

Tsoukalas L. H., Uhrig R. E. (1996). *Fuzzy and Neural Approaches in Engineering*. John Wiley Publishing Company.

USBM Bulletin, OSM Bulletin, USA, 1983.

Werbos, J. P., Beyond Regression: New Tools for Prediction and Analysis in the Behavioral Sciences, Ph.D. Dissertation, Harvard University, Boston, MA, 1974.

Wiss, J. F., and P. Linehan (Wiss, Janneyr, Elstner and Associates, Inc.). Control of Vibration and Blast Noise from Surface Coal Mining. *BuMines Open File Rept.* 1979.

APPENDIX A

Table Showing the ground vibration measurements results from blasting operations conducted at Tunçbilek Coal Mine, Panel BYH.

Table A.1 Vibration Data Pairs for round blasts measured at the mine site

Event Code	Date	Station Code	W_d (kg)	D (m)	SD (m/kg ^{0.5})	RPV (mm/sec)	VPV (mm/sec)	TPV (mm/sec)	PPV (mm/sec)	PVS (mm/sec)	F_R (Hz)	F_V (Hz)	F_T (Hz)
26o1	26/06/2003	T4	151.0	687.5	55.9479	1.3970	0.8890	0.7620	1.3970	1.454	16.94	14.06	18.50
26o2	26/06/2003	T5	151.0	905.0	73.6478	1.0600	0.7620	0.6350	1.0600	1.078	25.19	17.88	12.94
26o3	26/06/2003	T6	302.0	1052.	60.5358	1.2700	0.8890	0.8890	1.2700	1.497	5.62	6.06	2.88
26o8	26/06/2003	T2	151.0	300.0	24.4136	3.9370	2.5400	2.2860	3.9370	3.978	9.00	6.31	9.19
26o6	26/06/2003	T3	75.50	317.5	36.5401	2.1590	2.0320	1.2700	2.1590	2.440	11.38	15.88	18.19
26o7	26/06/2003	T4	75.50	450.0	51.7891	2.1590	1.5240	1.9050	2.1590	2.456	10.38	18.12	17.75
26o9	26/06/2003	T5	75.50	890.0	102.427	1.0160	0.6350	0.7620	1.0160	1.085	5.00	5.12	5.25
27o3	27/06/2003	T5	151.0	950.0	77.3099	1.0160	0.8890	0.8890	1.0160	1.332	13.31	13.50	13.38
27o4	27/06/2003	T4	75.50	630.0	72.5048	1.7780	0.8890	0.8890	1.7780	1.823	14.69	6.00	17.75
27o1	27/06/2003	T3	75.50	375.0	43.1576	2.0320	2.0320	1.2700	2.0320	2.252	3.44	3.12	8.69
27o2	27/06/2003	T2	75.50	142.5	16.3999	5.461	9.017	5.334	9.017	9.275	11.62	15.12	15.44
28o1	28/06/2003	T2	75.50	205.0	23.5928	5.2070	3.9370	2.7940	5.2070	5.252	14.75	9.12	16.94
28o2	28/06/2003	T4	226.5	660.0	43.8540	1.7780	1.7780	1.5240	1.7780	2.349	15.56	20.00	18.25
28o3	28/06/2003	T6	226.5	950.0	63.1232	1.143	0.635	0.635	1.143	1.212	12.38	13.88	13.75
28o4	28/06/2003	T3	151.0	410.0	33.3653	2.9210	2.6670	1.5240	2.9210	3.441	8.00	7.38	7.12
02o1	02/07/2003	T3	302.0	510.0	29.3472	2.921	2.159	1.778	2.921	3.358	16.75	8.19	13.81

W_d = charge weight per delay, D = absolute distance, SD = Scaled Distance, RPV = Radial Particle Velocity, VPV = Vertical Particle Velocity, TPV = Transverse Particle Velocity, PPV = Peak Particle Velocity, PVS = Peak Vector Sum, F_R = Radial dominant frequency, F_V = Vertical dominant frequency, F_T = Transverse dominant frequency.

Table A.1 (cont'd)

Event Code	Date	Station Code	W _d (kg)	D (m)	SD (m/kg ^{0.5})	RPV (mm/sec)	VPV (mm/sec)	TPV (mm/sec)	PPV (mm/sec)	PVS (mm/sec)	F _R (Hz)	F _V (Hz)	F _T (Hz)
02o3	02/07/2003	T4	151.00	565.00	45.9790	2.413	1.651	1.14	2.413	2.899	8.56	8.50	3.38
03o1	03/07/2003	T5	277.00	965.00	57.9812	1.390	1.270	1.650	1.650	1.900	*	*	*
03o2	03/07/2003	T5	151.00	835.00	67.9513	1.520	1.390	1.010	1.520	1.650	*	*	*
04o1	04/07/2003	T4	302.00	717.50	41.2874	2.410	1.770	1.520	2.410	2.540	*	*	*
04o2	04/07/2003	T4	151.00	580.00	47.1997	2.920	1.770	0.880	2.920	3.300	*	*	*
05o1	05/07/2003	T5	302.00	980.00	56.3926	1.140	1.140	1.520	1.520	1.520	*	*	*
05o2	05/07/2003	T4	75.50	610.00	70.2031	1.143	0.635	0.762	1.143	1.454	25.83	3.88	23.63
06o1	06/07/2003	T2	302.00	230.00	13.2350	9.772	7.747	4.064	9.772	10.697	11.94	13.75	12.56
07o1	07/07/2003	T6	75.50	1250.0	143.858	1.016	0.381	0.762	1.016	1.047	11.44	4.75	5.31
07o3	07/07/2003	T6	75.50	1210.0	139.255	0.381	0.254	0.381	0.381	0.458	4.00	4.31	5.63
07o2	07/07/2003	T4	75.50	790.00	90.9187	1.651	1.016	0.889	1.651	1.858	9.56	11.69	8.00
07o5	07/07/2003	T3	75.50	420.00	48.3365	2.032	1.651	1.524	2.032	2.129	11.13	10.38	10.25
07o4	07/07/2003	T3	151.00	485.00	39.4687	1.270	1.016	2.032	2.032	2.362	18.13	7.19	18.69
07o6	07/07/2003	T2	75.50	220.00	25.3191	5.080	5.207	3.810	5.207	6.447	17.94	16.94	17.13
07o7	07/07/2003	T2	302.00	360.00	20.7156	3.429	4.064	2.159	4.064	4.121	7.25	9.5	6.75
07o8	07/07/2003	T2	75.50	440.00	50.6383	1.524	2.413	0.889	2.413	2.443	13.31	12.13	14.06
08o2	08/07/2003	T2	226.50	246.50	16.3788	8.128	5.969	4.318	8.128	9.639	14.44	12.69	13.94

Table A.1 (cont'd)

Event Code	Date	Station Code	W_d (kg)	D (m)	SD ($m/kg^{0.5}$)	RPV (mm/sec)	VPV (mm/sec)	TPV (mm/sec)	PPV (mm/sec)	PVS (mm/sec)	F_R (Hz)	F_V (Hz)	F_T (Hz)
08o1	08/07/2003	T2	75.50	380.00	43.7330	2.413	3.810	1.651	3.810	4.088	16.94	16.25	14.69
09o1	09/07/2003	T6	151.00	1085.0	88.2960	1.651	0.635	0.762	1.651	1.661	10.69	9.38	12.63
09o2	09/07/2003	T3	226.50	543.00	36.0799	0.889	1.270	1.651	1.651	1.694	16.19	11.38	10.88
10o1	10/07/2003	T5	226.50	1000.0	66.4455	1.143	1.143	1.016	1.143	1.690	12.5	20.63	9.13
10o2	10/07/2003	T4	226.50	553.30	36.7643	4.445	2.667	2.286	4.445	4.799	12.25	10.94	15.13
11o2	11/07/2003	T2	226.50	336.60	22.3655	6.731	5.461	3.429	6.731	7.018	12.13	12.13	18.25
11o1	11/07/2003	T2	75.50	260.00	29.9226	5.334	5.080	4.191	5.334	5.766	5.81	8.38	12.81
26A1	26/09/2003	T3A	50.25	100.00	14.1069	22.86	23.876	17.78	23.876	31.125	*	*	*
26A3	26/09/2003	T6	402.50	1052.0	52.4363	1.651	0.762	0.889	1.651	1.661	*	*	*
26A2	26/09/2003	T5	338.00	425.00	23.1169	11.811	9.906	8.636	11.811	14.359	*	*	*
27A2	27/09/2003	T6	201.50	703.50	49.5594	3.429	1.143	2.286	3.429	3.755	*	*	*
27A3	27/09/2003	T5	236.50	390.00	25.3599	6.985	6.096	6.604	6.985	8.419	*	*	*
28A1	28/09/2003	T5	226.50	516.50	34.3191	9.017	8.89	5.715	9.017	11.322	*	*	*
28A3	28/09/2003	T6	176.50	572.50	43.0926	2.921	2.159	2.54	2.921	3.892	*	*	*
28A2	28/09/2003	T5	151.00	910.00	74.0547	1.016	1.143	0.762	1.143	1.164	*	*	*

Table A.1 (cont'd)

Event Code	Date	Station Code	W_d (kg)	D (m)	SD (m/kg ^{0.5})	RPV (mm/sec)	VPV (mm/sec)	TPV (mm/sec)	PPV (mm/sec)	PVS (mm/sec)	F_R (Hz)	F_V (Hz)	F_T (Hz)
29A1	29/09/2003	T3A	181.50	180.00	13.3608	11.938	6.985	9.144	11.938	13.412	*	*	*
01A3	01/10/2003	T6	101.00	557.50	55.4733	2.667	1.651	2.032	2.667	2.820	*	*	*
01A4	01/10/2003	T6	101.00	515.00	51.2444	3.175	2.667	2.667	3.175	3.542	*	*	*
02A2	02/10/2003	T3A	75.50	310.00	35.6769	5.334	4.318	1.905	5.334	6.122	*	*	*
02A3	02/10/2003	T6A	302.00	452.50	26.0384	4.318	2.921	4.064	4.318	4.410	*	*	*
03A1	03/10/2003	T6A	251.50	640.00	40.3562	2.413	2.032	2.921	2.921	4.060	7.06	6.56	6.56
04A1	04/10/2003	T6A	226.50	426.70	28.3523	3.937	3.556	3.302	3.937	4.154	5.56	5.50	5.31
04A3	04/10/2003	T6A	50.50	740.00	104.132	1.397	1.143	1.016	1.397	1.540	4.19	4.38	5.63
05A1	05/10/2003	T6A	226.50	743.30	49.3889	1.270	1.270	2.159	2.159	2.376	4.56	6.75	4.75
05A3	05/10/2003	T3	95.50	275.00	28.1404	3.937	4.191	2.54	4.191	5.236	32.19	44.81	47.38
05A4	05/10/2003	T3	95.50	250.00	25.5822	4.191	5.715	2.286	5.715	6.083	12.75	13.19	16.13
06A1	06/10/2003	T5	176.50	690.00	51.9369	1.905	2.413	1.397	2.413	2.697	19.88	14.06	15.81

Table A.2 Vibration Data Pairs for single hole blasts measured at the mine site

Event Code	Date	Station Code	W_d (kg)	D (m)	SD ($m/kg^{0.5}$)	RPV (mm/sec)	VPV (mm/sec)	TPV (mm/sec)	PPV (mm/sec)	PVS (mm/sec)	F_R (Hz)	F_V (Hz)	F_T (Hz)
27(S. H)	27/06/2003	T5	75.50	960.00	110.483	0.3810	0.2540	0.3810	0.3810	0.554	13.50	9.75	7.56
28(S. H)	28/06/2003	T4	50.50	710.00	99.9108	0.889	0.508	0.508	0.889	1.000	14.5	14.62	10.56
02(S. H)	02/07/2003	T3	75.50	600.00	69.0522	0.508	0.762	0.508	0.762	0.950	17.94	8.44	22.62
5/7(S. H)	05/07/2003	T5	75.50	1040.0	119.690	0.508	0.508	0.381	0.508	0.596	9.13	10.13	13.81
8/7(S.H)	08/07/2003	T2	75.50	380.00	43.7330	1.270	1.778	1.016	1.778	1.814	11.44	9.31	12.69
26A(SH)	26/09/2003	T5	30.25	390.00	70.9090	1.778	1.524	1.524	1.778	2.063	*	*	*
27A(SH)	27/09/2003	T5	40.25	400.00	63.0488	0.635	0.762	0.635	0.762	0.823	*	*	*
28A(SH)	28/09/2003	T6	25.25	620.00	123.384	1.143	0.508	0.889	1.143	1.231	*	*	*
2/10(S.H)	02/10/2003	T3A	75.50	320.00	36.8278	2.667	2.667	1.397	2.667	3.365	*	*	*
5/10(S.H)	05/10/2003	T6A	75.50	650.00	74.8065	0.762	0.508	0.762	0.762	0.950	6.88	7.38	9.06
7/3(S.H)	07/10/2003	T3	50.50	410.00	57.695	4.314	2.921	1.397	4.314	4.856	6.88	7.38	9.06
7/4(S.H)	07/10/2003	T2	40.50	100.00	15.7135	9.779	11.049	4.953	11.049	11.860	11.38	13.88	11.62
7/5(S.H)	07/10/2003	T2	75.50	180.00	20.7157	5.969	5.969	2.921	5.969	6.953	24.12	21.88	59.31
7/6(S.H)	07/10/2003	T3	100.50	310.00	30.9228	3.429	5.334	1.651	5.334	5.9406	15.44	13.25	22.31

W_d = charge weight per delay, D = absolute distance, SD = Scaled Distance, RPV = Radial Particle Velocity, VPV = Vertical Particle Velocity, TPV = Transverse Particle Velocity, PPV = Peak Particle Velocity, PVS = Peak Vector Sum, F_R = Radial dominant frequency, F_V = Vertical dominant frequency, F_T = Transverse dominant frequency.